Analysis of loads encountered during a single lift operation of offshore wind turbines.

Master Thesis

Ana Nusa Versnik

TU Delft
Delft University of Technology
NTNU
MARINE CONTRACTORS
EWEM

Analysis of loads encountered during a single lift operation of offshore wind turbines.

Master Thesis

by

Ana Nusa Versnik

to obtain the degrees

Master of Science
in Offshore and Dredging Engineering
at the Delft University of Technology,

Master of Science
in Technology - Wind Energy
at the Norwegian University of Science and Technology

to be defended publicly on Monday 24th of July, 2023.

Student number TU Delft:	4814142	
Student number NTNU:	582210	
Project duration:	January 2023 – July, 2023	
Thesis committee:	Prof. Dr. Ir. J. Jovanova,	TU Delft supervisor
	Dr. A. Grammatikopoulos,	TU Delft supervisor
	Prof Dr. M. Greco,	NTNU supervisor
	Ing. J.A. de Jong,	Heerema MC supervisor

TU Delft
Delft University of Technology
NTNU
MARINE CONTRACTORS
EWEM

Preface

This thesis is written as a part of the European Wind Energy Master and serves as a final deliverable in order to obtain the degree in Offshore and Dredging Engineering from the Delft University of Technology (TU Delft) and the degree in Technology - Wind Energy from the Norwegian University of Science and Technology (NTNU). The master thesis, in which the objective was to investigate the single lift wind turbine installation with the use of the Upper Stabiliser Frame, was proposed by and written in cooperation with Heerema Marine Contractors.

Heerema Marine Contractors presented me with interesting potential thesis topics, from which I decided to focus on the single lift installation using the Upper Stabiliser Frame. Single lift wind turbine installation has not been utilised on a wide scale yet and only a few demonstration projects have been done using this installation strategy so far, as there are still many aspects of the method that need to be improved until the method becomes viable, technologically and economically, on a large scale. However, with the right improvements and developments of the strategy, the single lift strategy could offer a faster and more efficient way of installing wind turbines offshore. The upper stabiliser frame, which is a concept developed by Heerema Marine Contractors, offers the possibility to increase workability as it decreases the yaw motions caused by the environmental loads working on the wind turbine during installation. The environmental loads acting on the USF during the free-hanging stage of operation, along with physical solutions for the USF concept are investigated in this thesis.

I would like to thank all my supervisors for guiding me, helping me and believing in me throughout the whole project. Apostolos Grammatikopoulos from TU Delft, thank you for supporting me throughout the thesis and making time to listen to my weekly updates. You always managed to find a new perspective for me to consider in my work and improve. Marilena Greco from NTNU, even though you were not in The Netherlands while I was writing the thesis, I am very thankful for your support from the beginning stages in Trondheim, when I was still developing my topic, up until the very end when I was making last minute adjustments. I could not have done it without your technical (and moral) support. Jovana Jovanova from TU Delft, thank you for being the chair of my committee and for making time and attending all the milestone meetings of my thesis. I greatly appreciated your feedback and suggestions. Jurgen de Jong from Heerema Marine Contractors, thank you for assisting me whenever I needed it but also for letting me be independent and solving problems on my own. Also, I would like to thank everyone at Heerema Marine Contractors, who welcomed me to their team and were always willing to help me with any issue or question I had, no matter how big or small. Additionally, I would like to thank my fellow EWEM students for keeping me company while studying at different universities throughout Europe and making every place feel like home. Last but definitely not least, I would like to thank my family for being my biggest supporters, always.

Ana Nusa Versnik
Leiden, July 2023

Abstract

The success of offshore wind farm installations is often related to the costs and time taken to be completed. Current installation strategies require several critical offshore lifts for the completion of a single wind turbine, as in most cases each component gets installed separately. This is time-consuming and has a direct link to the cost of the operation. Therefore trying to find more efficient methods of offshore wind turbine installation should be one of the main focuses in the industry. A possible solution to the problem involves the single-lift wind turbine installation. For this method, the whole wind turbine is pre-assembled and lifted onto the offshore foundation with one lift. This way the number of critical lifts offshore is reduced, which has the potential to reduce overall installation time and cost. The downside of this method is that, for the lifting of a whole wind turbine, very calm environmental conditions are required, leading to low workability. Calm environmental conditions do not often occur at offshore wind farm locations, and hence, solutions to improving the workability of this particular method are required to make it competitive with current installation methods.

The solution proposed in this thesis is to utilise the Upper Stabiliser Frame (USF), a Heerema Marine Contractors concept, which helps to eliminate unwanted motions of the wind turbine while in the air. The frame gets mounted at a height on the tower above the combined centre of gravity of the whole wind turbine. Since this frame is only a concept, its exact effect on the installation has not yet been studied in detail, and the actual design of the frame has not yet been fully developed. Therefore, the aim of this thesis was to analyse the loads experienced by the whole system (floating vessel and wind turbine) during such an installation and to investigate how the USF frame could be designed to constrain the relative rotation between the tower and the USF.

To reach the objective of the thesis, various analyses were conducted in LiftDyn, an in-house Heerema software, and OrcaFlex, where the whole system, or parts of the system, were investigated. A modal analysis and frequency domain analysis were done in LiftDyn while time domain analyses of different environmental loads were performed in OrcaFlex. The response of the system was examined, and based on the results, the maximum yaw moment acting on the tower under limiting environmental conditions was determined.

The results of the investigation showed that the WTG motions are limiting for safe operation and lead to very low acceptable environmental conditions compared to other installation methods. Based on these conditions, the maximum tower yaw-moment recorded was 2100 kNm. This moment was transformed into a tangential force acting on the tower, which the frame had to counteract. Two possible designs of the USF, both utilising friction, were created. The first design consisted of friction pads spaced around the circumference of the tower, while the second used a band brake to deliver the necessary friction. A multi-criteria analysis with weighted factors was conducted to evaluate which design performed better. Based on this analysis, the band brake design showed better performance, making it the most suitable design for the USF.

The novel concept of the single lift installation strategy with the USF is still not ready to be used yet for real projects and will require further development to become competitive with currently used strategies. This thesis has formed the basis for further research in the field by identifying key problems that must be resolved and suggesting innovative solutions for the USF design. This installation strategy has the potential to revolutionise wind turbine installation by decreasing installation time, increasing operational efficiency, and in general, streamlining the whole process.

Key words: Crane operation, Floating vessel, Offshore wind, Offshore wind turbine, Offshore wind turbine installation, OrcaFlex, Semi-submersible vessel, Single lift installation

Contents

Preface i

Abstract ii

Nomenclature v

List of Figures vi

List of Tables viii

1 Introduction 1
- 1.1 Offshore wind . . . 1
- 1.2 Offshore wind turbine installation . . . 2
  - 1.2.1 Offshore wind installation vessels . . . 2
  - 1.2.2 Offshore wind installation strategies . . . 3
- 1.3 Problem statement . . . 6
- 1.4 Research objective and questions . . . 7
  - 1.4.1 Research objective . . . 7
  - 1.4.2 Research questions . . . 8
- 1.5 Thesis outline . . . 8

2 Theoretical Background 9
- 2.1 Operability . . . 9
  - 2.1.1 Operating conditions . . . 9
  - 2.1.2 Weather Operating Window . . . 10
- 2.2 Wind . . . 10
  - 2.2.1 Wind profile . . . 11
  - 2.2.2 Wind spectrum . . . 11
  - 2.2.3 Aerodynamic Theory . . . 11
- 2.3 Waves . . . 12
  - 2.3.1 Wave characteristics . . . 13
  - 2.3.2 Wave spectrum . . . 13
  - 2.3.3 Motions . . . 14
  - 2.3.4 Potential flow theory . . . 14
  - 2.3.5 Linear wave theory . . . 15
  - 2.3.6 Response in linear waves . . . 16
  - 2.3.7 Deep-water floating system: Semi-submersible . . . 16
- 2.4 Friction . . . 17
- 2.5 Thin-walled cylinders . . . 18
  - 2.5.1 Stresses . . . 18
  - 2.5.2 Buckling . . . 20
- 2.6 Software . . . 21
  - 2.6.1 LiftDyn . . . 21
  - 2.6.2 OrcaFlex . . . 22
  - 2.6.3 Software comparison . . . 24

3 System and scenario 25
- 3.1 Scenario . . . 25
  - 3.1.1 Location . . . 25
  - 3.1.2 MetOcean data . . . 26
- 3.2 Installation vessel . . . 29
  - 3.2.1 Vessel . . . 29

3.2.2 Thialf cranes . . . 29
3.3 Installation strategy . . . 29
3.3.1 Pre-installation . . . 29
3.3.2 Single lift method . . . 30
3.3.3 Upper stabiliser frame . . . 31
3.3.4 Other components . . . 32
3.3.5 Limiting parameters . . . 33
3.4 Wind turbine . . . 33
3.5 OrcaFlex model . . . 33
3.5.1 Environment . . . 38
3.5.2 Load cases . . . 38

4 Base case scenario **40**
4.1 Wave-only . . . 40
4.1.1 Modal analysis . . . 40
4.1.2 Frequency domain analysis . . . 43
4.1.3 Time domain analysis . . . 45
4.1.4 Conclusion waves-only . . . 48
4.2 Wind-only . . . 49
4.2.1 Blade pitch analysis . . . 50
4.2.2 Time domain analysis . . . 51
4.2.3 Conclusion wind-only . . . 55
4.3 Wind and Waves . . . 55
4.3.1 Wind speed effect . . . 55
4.3.2 Varying the significant wave height and peak period . . . 57
4.3.3 Misalignment of wind and waves . . . 59
4.3.4 Limiting environmental conditions . . . 61
4.3.5 Conclusion wind and waves . . . 62
4.4 Base case results . . . 62

5 Concept Study **64**
5.1 USF functionalities . . . 64
5.1.1 Functionalities . . . 64
5.1.2 WTG rotation sensitivity . . . 65
5.2 Concepts . . . 66
5.2.1 Friction pads . . . 66
5.2.2 Slings . . . 69
5.2.3 Band brakes . . . 69
5.2.4 Tower modification . . . 71
5.2.5 Clamp based . . . 72
5.2.6 Concept evaluation . . . 73
5.3 Load Case . . . 73
5.3.1 Minimum tangential force . . . 73
5.3.2 Tower yield strength . . . 74
5.3.3 Buckling . . . 75
5.4 Concept design and analysis . . . 76
5.4.1 Materials . . . 76
5.4.2 Design 1: Friction pads . . . 78
5.4.3 Design 2: Band brake . . . 81
5.4.4 Design comparison . . . 83
5.4.5 Limitations . . . 86

6 Conclusion & Recommendations **87**
6.1 Conclusion . . . 87
6.2 Recommendations . . . 89
6.2.1 Analysis . . . 89
6.2.2 Single lift installation . . . 90

References **92**

A Additional Theory **94**
A.1 Buckling of thin-walled cylinders . . . 94

B System parameters **95**
B.1 WTG . . . 95
B.2 Thialf . . . 97
B.3 Connections . . . 98
B.4 Model . . . 99

C TurbSim **101**
C.1 Input . . . 101
C.2 Output . . . 102

D Base Case Results **104**
D.1 Load cases . . . 104
D.2 Wave-only analysis . . . 106
D.2.1 Frequency domain analysis . . . 106
D.2.2 Time domain analysis . . . 108
D.3 Wind-only analysis . . . 110
D.3.1 Blade pitch analysis . . . 110

E Concept study **113**
E.1 Concepts . . . 113
E.1.1 Concept 1: Blade installation equipment . . . 113
E.1.2 Concept 2: Lift-frames . . . 114
E.1.3 Concept 3: Motion compensated grippers . . . 115
E.2 Calculations . . . 116
E.2.1 USF horizontal loads . . . 116
E.2.2 Sling elongation . . . 116
E.3 Weighted Multi-Criteria Analysis . . . 118
E.3.1 Assigning of weights . . . 118

Nomenclature

Abbreviations

$CAPEX$	Capital Expenditure
CoG	Center of Gravity
CoM	Center of Mass
DoF	Degree of Freedom
FD	Frequency Domain
HLV	Heavy Lift Vessel
HMC	Heerema Marine Contractors
$JONSWAP$	Joint North Sea Wave Project
$LCOE$	Levelised Cost Of Energy
LLT	Lower Lifting Tool
MBL	Minimum Breaking Load
MSL	Mean Sea level
mT	Metric tonne
OWF	Offshore Wind Farm
OWT	Offshore Wind Turbine
PS	Port side
PSD	Power Spectral Density
RAO	Response Amplitude Operator
RNA	Rotor Nacelle Assembly
SB	Starboard
$Semi-sub$	Semi-submersible vessel
SWL	Safe Working Load
TD	Time Domain
USF	Upper Stabilising Frame
WL	Water Line
WOW	Weather Operating Window
WSD	Working Stress Design
WT	Wind Turbine
WTG	Wind Turbine Generator

List of Figures

1.1 Offshore wind capacity future prediction . . . 1
1.2 Thialf HLV . . . 3
1.3 RNA installation method . . . 4
1.4 Elisa-Elican Project . . . 5
1.5 Full WTG installation model . . . 7

2.1 Lift and drag on an airfoil . . . 12
2.2 Pierson-Moskowitz and JONSWAP spectra . . . 14
2.3 Water particle motion according to Airy wave theory . . . 15
2.4 Asperities seen on the surface of materials . . . 18
2.5 Stresses acting in thin-walled cylinders . . . 19
2.6 Single lobe buckling of a confined cylinder . . . 21

3.1 Arcadis Ost project location . . . 25
3.2 Mean wind speed bar chart . . . 26
3.3 Mean wind speed Weibull distribution . . . 27
3.4 Significant wave height bar chart . . . 27
3.5 Significant wave height Weibull distribution . . . 28
3.6 Peak period bar chart . . . 28
3.7 Full WTG installation labelled diagram . . . 30
3.8 USF diagrams . . . 32
3.9 Universal Model of the system . . . 34
3.10 Thialf coordinate system . . . 36
3.11 Wave and wind headings definition . . . 36
3.12 Crane slew angle definition . . . 37
3.13 Shackle diagram . . . 38

4.1 Full WTG LiftDyn model . . . 41
4.2 Hs-Tp combinations LiftDyn . . . 44
4.3 Operability curve wave-only case . . . 44
4.4 OrcaFlex model of the full system . . . 45
4.5 STD of the Thialf, crane tip and WTG bottom motions for various incoming wave directions. $H_s = 1$ m, $T_p = 6$ s. Note that the vertical scales are not the same on all plots. . . . 46
4.6 Pressure caused by waves on the pontoons of the semi-submersible. . . . 47
4.7 Wind-only model in OrcaFlex of the WTG and rigging. . . . 49
4.8 Blade pitch angle . . . 50
4.9 Nacelle - Connection z moment . . . 51
4.10 Tower connection maximum force plots for the rigging and WTG model. . . . 52
4.11 Tower connection maximum force plots for the full model. . . . 53
4.12 Wind-only ellipse plots of X-Y motion of the USF and LLT. . . . 54
4.13 Box plots of the tower connection forces and moments for wind and wave case. . . . 56
4.14 Tower tip limiting criteria check. . . . 57
4.15 Thialf time series showing the effect of varying the T_p and H_s. . . . 58
4.16 Ellipse plots of the USF, LLT and nacelle motion with varying H_s and T_p values. . . . 59
4.17 Ellipse plots of USF, LLT and nacelle for misaligned wind and waves . . . 60
4.18 Tower tip limiting conditions . . . 61

5.1 Maximum X and Y rotations of the USF . . . 64
5.2 WTG rotation sensitivity analysis . . . 65

5.3 GREP tool . . . 67
5.4 Saipem stability frame for Hywind project. . . . 68
5.5 Beatrice project support frame . . . 68
5.6 USF concept involving slings . . . 69
5.7 Band brake diagram . . . 70
5.8 Sensitivity analysis plot of the coefficient of friction and environmental loading safety factor . . . 74
5.9 Proposed USF designs . . . 76
5.10 Friction pad diagram . . . 77
5.11 Pad area sensitivity analysis . . . 79
5.12 Revised design of USF with friction pads . . . 80
5.13 Angle of wrap sensitivity analysis . . . 81

B.1 Tugger configuration . . . 99
B.2 OrcaFlex full model from different views . . . 100

C.1 TurbSim time series plots . . . 103

D.1 Nacelle - Connection force/moment plotted as a function of the blade pitch angle against the incoming wind direction. . . . 111
D.2 Tower connection mean force plots for rigging model. . . . 112
D.3 Tower connection mean force plots for the full model. . . . 112

E.1 Offlead and sidelead angle definition . . . 117
E.2 USF cross-section. . . . 118
E.3 USF rotations due to sling elongation. . . . 118

List of Tables

2.1 Heerema MC successful operational limits . . . 10
2.2 MetOcean parameters return periods . . . 10
2.3 Degrees of freedom . . . 14

3.1 Thialf main parameters . . . 29
3.2 USF main parameters . . . 31
3.3 Limiting parameters of the single lift installation . . . 33

4.1 Thialf natural periods from LiftDyn . . . 42
4.2 Critical modes of the system . . . 42
4.3 Maximum tower Z-moment magnitudes, wind-only. . . . 53
4.4 Maximum tower Z-moment, wind and waves. . . . 56
4.5 Maximum tower Z-moment magnitude . . . 61

5.1 Load case used for the USF designs . . . 73
5.2 Weighted criteria analysis. . . . 84
5.3 USF design comparison . . . 85

B.1 Blade geometric properties . . . 96
B.2 WTG component parameters . . . 97
B.3 DP data . . . 97
B.4 Starboard crane properties . . . 98
B.5 OrcaFlex model winches . . . 98
B.6 OrcaFlex model constraints . . . 99

D.1 Load cases base case model . . . 105
D.2 Summary statistics of Thialf vessel motions. . . . 108
D.3 Summary statistics of crane tip motions. . . . 109
D.4 Summary statistics of tower bottom motions. . . . 109

E.1 Ranking criteria and assigning weights for the weighted criteria analysis. . . . 119

1

Introduction

1.1. Offshore wind

Offshore wind energy capacity in Europe is increasing by several gigawatts annually, with 3.4 GW being installed in 2021 (WindEurope, 2022), and many more gigawatts planned to be installed in the next several years. WindEurope has created possible future scenarios that estimate the installed wind capacity in the next few years in Europe. According to the Realistic Expectations Scenario, which is based on current policies, offshore wind energy in Europe is predicted to increase on average by 5.6 GW annually until 2026. The predicted increase in offshore wind capacity per country can be seen in Figure 1.1. This rate of increase in wind capacity is currently not enough for the EU to reach its 40% renewable energy target, which is part of the 2030 climate and energy goals (WindEurope, 2022). This shows that there is still much room for improvements and developments in the wind industry, more specifically in the offshore industry, which will only account for 24% of the new installed capacity from 2022 until 2026. However, offshore wind shows much promise for the future due to higher full-load hours per year, longer lifetimes, and higher offshore wind speeds allowing for larger turbines, leading to higher electricity production per year. Onshore wind turbines are constrained by factors such as noise constraints and visual pollution, which limit the size of the turbines and rotor speeds (Dinh and McKeogh, 2018). Currently, the levelized cost of energy (LCOE) of offshore wind is higher than of onshore wind due to higher construction costs as a result of the offshore environment being harsher. Special installation vessels are also required, which makes the installation stage very costly (Guo et al., 2022). The LCOE in 2018 for onshore wind was estimated to be 0.06$/kWh and for offshore wind 0.13$/kWh (IRENA, 2019). However, in the years between 2011 and 2018, there has been a significant decline of 20% in the LCOE of offshore wind recorded. This resulted from factors such as increased rotor diameters and improved technology of installation methods and wind turbines (WT) (Jiang, 2021). Future trends predict that the LCOE will continue to drop for offshore wind, to rates of around 0.05 to 0.09$/kWh in 2030, making it competitive with other energy sources such as coal and gas (IRENA, 2019).

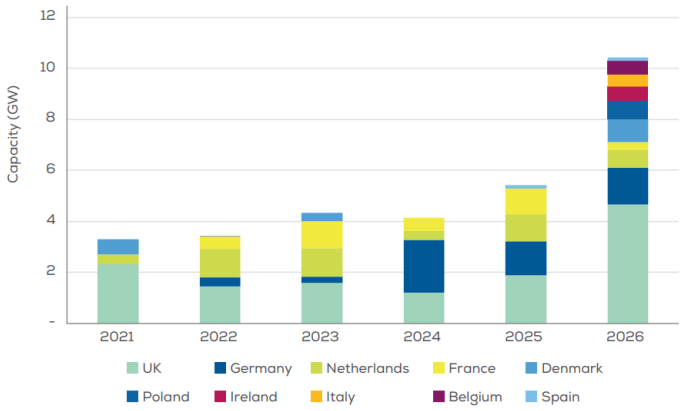

Figure 1.1: WindEurope's future offshore wind capacity prediction based on the Realistic Expectations Scenario (WindEurope, 2022).

1.2. Offshore wind turbine installation

The whole lifetime of an offshore wind farm (OWF) can be classified into several stages. One of these stages includes the installation and commissioning. Installation takes up as much as 25% of the overall costs of an offshore wind farm, compared to just 5% onshore (Guo et al., 2022). The reason why offshore wind farm installation takes up such a large portion of the project's capital expenditure (CAPEX), is because vessels and equipment are very specialised and hence expensive to hire (Guo et al., 2022). Seeing as the installation costs are much higher offshore compared to onshore, developments are needed to bring installation costs down. Offshore wind installation also has many complexities, which need to be considered for a successful project. Most offshore wind turbine (OWT) installation operations have very low workability due to limits being set for various parameters, such as sidelead/offlead angles and horizontal motions of the components being lifted. These limits are put in place to allow safe operation, and therefore, the MetOcean conditions, such as wind, waves, and current, need to be well determined beforehand so that the response of the system can be predicted. It is not only the forcing of the environmental loads but also the vessel's response to the environmental loading which needs to be considered. Wrongly predicting the loads of the vessel and wind turbine being installed could lead to a lot of money lost in the case of an accident happening. Therefore, during the planning and development stage, the loads that will be encountered during installation need to be correctly estimated with the available tools, and the limiting conditions determined from the limiting parameters. The limiting conditions refer to the environmental conditions which still allow for safe operation. Safe operation occurs if all the set limiting parameters are not exceeded. The following sections will serve as a brief introduction to offshore wind installation. Installation vessels and methods used will be described.

1.2.1. Offshore wind installation vessels

For offshore installation, there are several vessels available. The purpose of some of the vessels is to specifically install wind turbines, while other vessels such as barges and tugboats are used in aiding the installation operation by towing non-propelled vessels or transporting wind turbine components to the offshore site. The two most popular types of installation vessels for offshore wind turbines include the jack-up vessel and the semi-submersible (semi-sub) vessel. Many factors are considered when choosing the appropriate installation vessel during the planning stage. These factors include but are not limited to, market availability, availability of the vessel at the needed time (so it is not being used on other projects), cost of vessel hire, and size of the wind turbines being installed. Furthermore, the vessel and the crane on the installation vessel limit the size of the turbines, as the maximum possible wind turbine will not only depend on the lifting capacities of the cranes but also the deck space on the installation vessel or feeder barge. The jack-up and semi-submersible vessel will be further discussed in the following subsections.

Jack-up

Jack-up vessels have retractable pillars, which can be lowered into the sea floor and lift the whole vessel several metres into the air above the water. This makes installation easier, as the vessel is no longer floating and has additional stability to perform heavy lifting. Jack-ups can be equipped with propulsion so that they are able to move without the assistance of other boats, but they can also just be jack-up platforms without a propulsion system, in which case assistance for transportation is required. Jack-up vessels can have high chartering rates, between 70,000 to 145,000 € per day (Rippel et al., 2019). The soil conditions at the OWF site are very important for the deployment of jack-up vessels as the spudcans need a stable foundation. Additionally, the mobilisation process of the jack-up is very time-consuming which prolongs the installation time, as the legs need to be jacked down and up at every turbine location. Along with the installation process involving jack-ups being very time-consuming, it is also very weather sensitive as the lowering and retrieval of the jack-up legs need calm weather conditions (uit het Broek et al., 2019).

Semi-submersible

Semi-submersible vessels are beginning to emerge in the offshore wind industry, as the choice of installation vessel, with some successful projects being completed using them. An example of such a project is the Arcadis Ost wind farm, where Heerema MC installed the tower and rotor nacelle assembly (RNA). The pontoons of the semi-sub can be flooded, causing the vessel to submerge. They can have drafts of up to 40 m, meaning they are suitable for deep water operations (120-200 m) (Bai and Bai, 2010). In general, semi-subs have identical twin pontoons with between four to eight columns. Due to the pontoons and columns, the water plane area of the semi-subs is limited and therefore the features of the vessel affect the wave action and the effects it has on

the vessel. The vessels with twin cranes have them positioned on each side of the deck at the ship's bow (Wang et al., 2015). Semi-submersible crane vessels have high lifting capacities, so they can be utilised for the lifting of heavy wind turbine components of masses up to 20,000 tonnes. However, they do also come with high day rates(Ramachandran et al., 2021).Examples of semi-submersible vessels from Heerema MC include the Thialf, Sleipnir, and Balder. Sleipnir is the newest vessel of the three, having been constructed in 2019, and has a double crane, each having a lifting capacity of 10,000 tonnes. It has a deck dimensions of 102 metres in width and 220 metres in length. Along with installing wind turbines, it can also be used for the removal of jackets and topsides (Heerema Marine Contractors, 2022b). Balder was the world's first semi-submersible crane vessel, built in 1978. It has a lifting capacity of 6,300 tonnes and is equipped with a special dynamic positioning system used for positioning and propulsion (Heerema Marine Contractors, 2022b). The Thialf, pictured in Figure 1.2, is made with a double crane arrangement with a lifting capacity of 14,200 tonnes and can be deployed in shallow or deep waters. It is the second biggest semi-submersible crane vessel owned by Heerema MC and can be used for all kinds of installation operations (Heerema Marine Contractors, 2022b).

Figure 1.2: Heerema MC's semi-submersible crane vessel, the Thialf Heerema Marine Contractors, 2022b.

Wind turbine installation using a semi-submersible vessel means that the semi-sub is floating during installation. This brings in several benefits compared to installation vessels that are not floating during operation. For example, most semi-subs are equipped with dynamic positioning (DP) systems, and while on DP, the vessel can weather vane. The weather vaning capability allows for the vessel heading and position of each installation to be optimised and achieve maximum operability. Another benefit of a floating installation vessel is the avoidance of soil interaction. Since the vessel is floating there is no interaction with the seabed and therefore even in the case of bad soil conditions, there is no disturbance to the operation.

1.2.2. Offshore wind installation strategies

There is no correct way of installing a whole offshore wind farm or even an offshore wind turbine. In the wind industry, many strategies are being utilised for the installation of wind farms, and the choice of the method depends on many factors and variables such as the vessels being used, size of the wind turbines and wind farm, safety risks in lifting operations, and the weather operability, among many others. All these factors contribute to the overall installation costs and, from a profitability perspective, need to be kept as low as possible without compromising the safety and integrity of the project. Currently, the methods used for floating and bottom-fixed wind turbines differ slightly. The following sections will focus on installation methods used for bottom-fixed wind turbines and, specifically the wind turbine generator (WTG) installation (without the foundation).

In literature, there is no correct way of classifying wind turbine installation strategies. Often the strategies will be referred to by the number of components that are already assembled or the number of offshore lifts that are required. Pre-assembling components together onshore decrease the number of lifts needed offshore. In the industry, there is a disagreement about whether this is the preferred strategy or not, as fewer lifts decrease the need for a large weather window. However, the components become heavier, and therefore the lifts become more complex, which requires stricter requirements and guidelines. Ahn et al. (2017) classify the offshore wind turbine

installation strategies into three groups where the methods requiring multiple offshore lifts are classified as the component installation method and the other two methods are the partially integrated method and the integrated installation method. These three methods will be explained in more detail in the following sections.

Component installation

For the component installation method, the foundation, tower, and wind turbine are in most cases all installed separately. Before the installation of the WTG, first, the foundation needs to be installed. The foundation installation will depend on the type of foundation that has been decided on for the wind farm. The tower gets installed onto the foundation. The tower is manufactured onshore in sections due to limits in manufacturing and transportation of the sections. The tower sections can be transported to the OWF site from shore by barge or directly by installation vessel along with the other remaining components. With the help of a floating crane, the tower sections are installed onto the foundation one by one. High precision is needed for the tower installation as the tower sections need to be properly aligned with each other in order to be bolted together or connected in another way. After the tower installation, the RNA needs to be installed. For the components method, the RNA is not necessarily yet pre-assembled, and the blades and nacelle are transported to the offshore location as separate components, or one, two or three blades already mounted onto the nacelle. When two blades are already pre-installed on the nacelle, the method is often referred to as the bunny ear method, where the two blades represent the bunny ears.

It is also possible to install the whole RNA at once. This is either done by pre-assembling the nacelle with the three blades onshore and then transporting it, however, the transportation of the RNA fully assembled on the deck of a barge, can be technically challenging. Heerema MC has developed a new method, named the RNA method, which was used for the Arcadis Ost project in the Baltic Sea. For this method, all the WT components (tower, blades, and nacelle) were transported to the offshore location by a barge (Heerema Marine Contractors, 2019). There they were transferred from the barge onto a semi-sub vessel, which was responsible for the wind turbine installation. The tower was already pre-assembled onshore so it could be directly installed onto the foundation. Thereafter, the RNA was assembled on a dummy tower on the installation vessel. First, the nacelle, followed by one blade at a time. The whole RNA was then transferred onto the actual tower which was already installed. The RNA method is pictured in Figure 1.3, where the red and white tower represents the dummy tower.

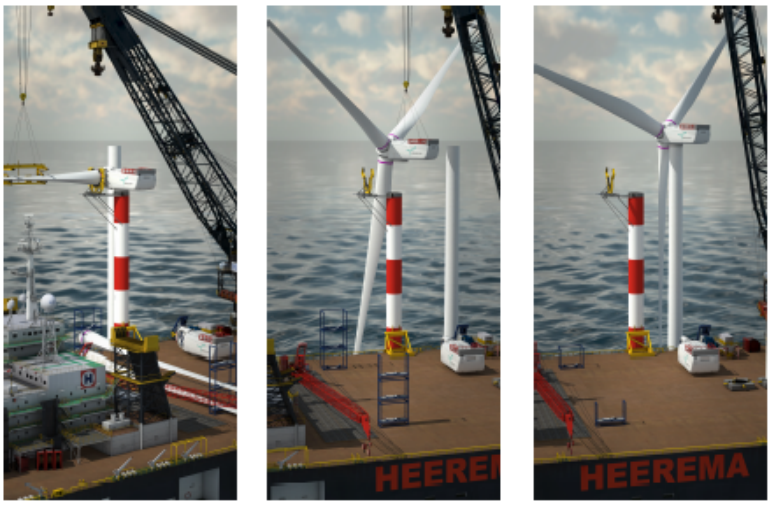

Figure 1.3: Heerema MC developed RNA installation method (Heerema Marine Contractors, 2019).

Installing each component separately has its advantages and drawbacks. An advantage is that deck space of barges and other vessels used for component transportation can be fully utilised, as many components are not pre-assembled. Additionally, since every component will be lifted separately, the use of large-capacity cranes is not necessary, decreasing the costs of vessel hire, as smaller vessels are more widely available. However, having to install each component separately requires more offshore lifts. Lifting a single blade also allows the blade to experience large vibrations if the wind conditions are too high. In addition, the foundations that are already in place might experience wave-induced motions due to their flexible modes, creating difficulties during the blade mating process. Seeing as most wind turbines have three blades, this challenge is encountered three times during

the installation process, which could give favour to the bunny-ear method or the three-bladed method (Jiang, 2021).

Partially integrated installation

The partially integrated method refers to the foundation being installed separately, while the installation of the tower and WTG with blades is integrated. The method can be referred to as the full WTG installation or single lift, as only one lift of the WTG components is needed. Preferably the foundation is also already installed with a transition piece for this method, however, this is not yet possible for all foundations. It is possible for gravity-based and suction bucket foundations. The WTG can be installed after the foundation has been installed. This installation can be done by assembling the whole WTG in a marshalling yard already, and then transporting it fully assembled to the offshore location. This method saves time offshore, as the WTG no longer needs to be assembled, however, the workability of the operation drastically decreases due to the transport requiring extremely calm seas. The alternative is to transfer the WTG components onto a barge and transport them to the offshore location. The components can then be assembled on the installation vessel and with one critical lift, be lifted off the vessel and installed onto the foundation. This method has many benefits, such as decreasing the time taken for installation offshore, increasing efficiency, and decreasing the costs of installation. However, currently, there are still drawbacks to this method, as special equipment and vessels are needed, which are not always available. Secondly, it is important to secure the WTG sufficiently as it is very susceptible to excessive motions due to environmental loads when all the blades are installed and it is hanging in the crane. This is a major problem with this method, and therefore solutions as to how the movement of the WTG during the lift can be restrained to not cause accidents or damage to the wind turbine need to be developed.

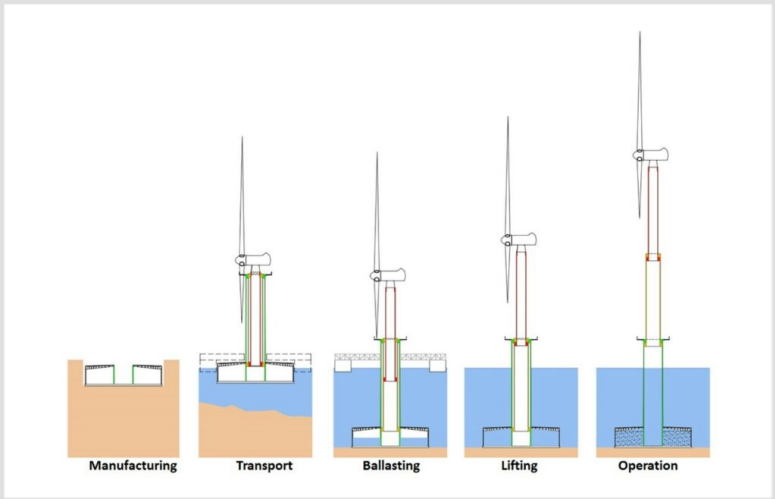

Figure 1.4: Installation steps of the Elisa-Elican project (Miceli, 2022).

Integrated installation

The integrated installation method allows for most of the wind turbine to be put together on land, decreasing the number of vessels having to be used and the amount of time needed to be spent offshore. Less time offshore decreases the costs of vessel hire. Onshore, the time taken for construction is more controllable as waves and such no longer create limiting weather conditions. However, again this method can only be used for foundations that can be installed with a transition piece. The integrated method has been used in commercial wind farms such as the Elisa/Elican gravity foundation project in Spain. The Elisa is a prototype but was the first bottom-fixed offshore wind turbine, which was installed without the use of heavy lift vessels (“Elisa – Elican Project”, 2017). This was possible due to the self-floating capabilities of the gravity-based foundation, which also has an integrated telescopic auto lift tower. These new developments allowed the wind turbine with the foundation to be fully assembled onshore. Figure 1.4 shows the installation steps. During the towing of the wind turbine structure, the gravity-based foundation allowed for the whole configuration to be self-floating, while the telescopic tower decreased the height of the centre of gravity of the WTG. At the location offshore, the foundation got ballasted and the telescopic tower was lifted to its final height. For this, cables and heavy lift jack-ups had to be used, so special vessels were still needed. The Elisa project used a 5MW wind turbine, which nowadays is no longer

considered state of the art. There are still improvements needed to facilitate larger turbines before this installation method becomes the standard in the industry. An additional issue with this method is that it can only be used for foundations which can be self-floating and be pre-installed with a transition piece. This method might not be the most useful for bottom-founded wind turbines, however, it is a method commonly used for floating foundations.

Installation strategy summary

Several problems have been identified in the previous sections regarding the installation methods for OWTs. One of them is that the methods currently being used, which include various component installations, require too many offshore lifts, prolonging the installation operation. A solution would be to start developing and using the partially or fully integrated methods described. The problem with the fully integrated method is that it cannot be applied to all foundations since they do not all have self-floating capabilities to make it possible. In that respect, the partially integrated method is the better solution to decreasing the number of offshore lifts. However, while it might solve the issue regarding the number of offshore lifts, the method comes with its own problems. The method has a lower workability/operability than the component installation method due to WTG assemblies' dynamic response to the environmental loading when fully assembled. The blades, which are pre-installed, are made in such a way as to capture as much wind as possible, leading to high aerodynamic forces. One of the consequences of such high environmental loads when the WTG assembly is being lifted is the large yaw moment that it will experience. The yaw moment is the moment that can cause the WTG to rotate around its vertical axis. A consequence of this rotation is the blades potentially striking the crane or vessel, along with other undesired events. This will happen if the WTG is not well restrained while hanging from the crane due to the environmental forces and moments. A possible solution to combat this problem is to make use of an additional component in the rigging that would prevent or limit rotation.

1.3. Problem statement

In the previous section problems and solutions to current methods used for offshore wind turbine installation have been identified. It has been suggested to make use of an additional component in the rigging to limit the motions of the wind turbine while hanging in the air during the partially integrated installation. Heerema MC has developed a concept, the Upper Stabiliser Frame (USF), which is aimed at doing just that. The USF is attached to the WTG tower at a point above the combined centre of gravity (CoG) of the WTG and its purpose is to limit yaw rotations of the WTG by counteracting the yaw moment caused by the environment through friction between the tower and USF, and stiffness in the wires of the rigging. However, the USF is currently only in the beginning of the development phase as it still has problems associated with it. One of the issues is that the effect of friction on decreasing the yaw rotation is limited and therefore, it is not certain how effective it is in accomplishing its purpose. To determine the viability of the partially integrated method with the USF, an investigation into the working of the USF is needed by examining its behaviour under various environmental loads. From this, the magnitude of the yaw moment acting on the WTG tower should also be obtained, as that will give an indication of the rotational restraint capacity the USF needs to possess to work effectively. The full WTG lift with the USF is seen in Figure 1.5. The yaw moment being considered is also labelled on the diagram with M_{zUSF}. Further explanation of the USF is given in subsection 3.3.3. Additionally, physical solutions for the connection at the USF and tower interface should be explored, as currently, the USF is only a concept and not a physical component yet. These solutions should yield the desired results of restraining the yaw moment and limiting the yaw rotation of the WTG without damaging the tower or posing additional restraints to the installation strategy.

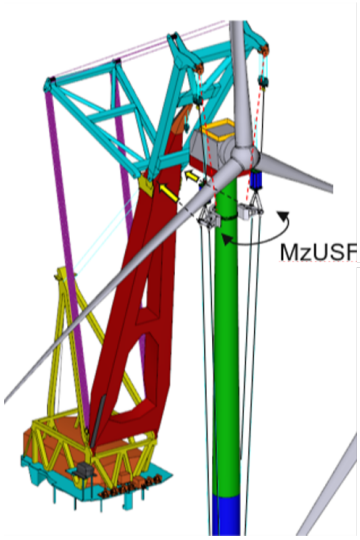

Figure 1.5: Model of the full WTG installation with the USF and the yaw moment labelled with M_{zUSF} (Heerema Marine Contractors, 2021a).

1.4. Research objective and questions

In this section, the main aim of the investigation is stated in the form of the research objective. From this objective, the research questions were created that formed the basis of the study.

1.4.1. Research objective

The problem investigated in this thesis was stated in section 1.3. To alleviate this problem, the following main research objective was formulated:

Determine the magnitude of the yaw moment that the Upper Stabiliser Frame is required to counteract, caused by the environmental loading, during a single lift offshore wind turbine installation on a fixed foundation, and investigate how the connection between the tower and Upper Stabiliser Frame can be made physically.

To help reach this objective, the following sub-objectives were required:

- Analyse available software for modelling a single lift offshore installation and decide on an appropriate one for the investigation.
- Model the base case scenario of the installation with the USF modelled as a rigid body, with constraints, only allowing motion in heave between the USF and tower. Perform simulations with the modelled system and obtain the maximum moment about the tower Z-axis for this initial configuration. Frequency and time domain analysis should be conducted.
- Critically analyse the base case scenario. The limitations of modelling the USF as rigidly connected to the tower should be determined, and the response of the system under the environmental loading analysed to see if it is as expected.
- Investigate the constraints of the connection between the tower and USF (tower yield strength, maximum allowable clamping force, minimum required frictional force).
- Investigate physical solutions for connecting the USF and tower that abide to the determined constraints by looking at concepts from other industries/projects.
- Choose the most promising working principles of the concepts and, with the appropriate and justified assumptions, create preliminary models for the USF for which basic calculations verifying the designs can be done.
- Critically analyse the designs to determine their reliability and ability to counteract the yaw moment. Also, assess the validity of the calculations done. This should assess how realistic the design of the connection between the USF and the tower is and how appropriate any assumptions taken are. Further, improvements to the designs should be stated.

1.4.2. Research questions

The research questions that needed to be answered to reach the thesis objectives:

- How can the full WTG lift by a crane of a floating vessel be modelled?
- How do the wind and wave loading affect the response of a WTG assembly during a single lift operation using a USF?
- What are possible solutions for connecting the tower to the USF while keeping the functionality of the USF to counteract the yaw moment under the given environmental loading?
- What are the limiting environmental conditions (significant wave height, peak period, wind speed) of the single lift method using the USF that keep the operational parameters within their limits?
- What is the yaw moment caused by the limiting environmental conditions during a single lift operation?

1.5. Thesis outline

In Chapter 1, a brief introduction to offshore wind turbine installation is given, along with the problem which will be investigated in this thesis. The research objective and the corresponding research questions are also stated. Chapter 2 gives an overview of the relevant theory behind the investigation. This includes the basics of aerodynamics and hydrodynamics. This chapter introduces LiftDyn and OrcaFlex as two possible software to model the system the thesis is concerned with. The theory behind their analyses is presented, and a comparison between them is made to determine which is the most appropriate for modelling the system later in the thesis. The scenario being considered in this thesis is presented in Chapter 3. This includes the location and the environmental conditions at the installation location. Further, all the components required for such an installation, and the way their modelling in OrcaFlex is done, are explained. Chapter 4 presents the base case modelling and simulations. Analyses where only the wind, only the waves, and a combination of wind and waves are presented. The analyses include frequency and time domain results, from which the yaw moment magnitude is obtained. The magnitude of the moment is used as a reference in Chapter 5, where solutions for the physical connection between the USF and tower are investigated. In this chapter, a concept study is presented, and the concepts are assessed. Finally, two designs for the USF are proposed and verified through basic calculations. The conclusion and recommendations for the thesis are given in Chapter 6.

2

Theoretical Background

Offshore wind turbines are purposely built in environments with high wind speeds to harness as much wind as possible. These high wind speeds often also lead to high significant wave heights, and hence harsh environments, which negatively impact the installation process, as many steps in the installation process require calm sea states to be performed.

In this section, the theory needed for solving the problem formulated in section 1.3 and for reaching the research objectives of section 1.4, is presented. This includes the theory of the aerodynamic and hydrodynamic loads experienced by the wind turbine and vessel during installation and the way this is modelled in the relevant and available software. Friction and behaviour of thin-walled cylinders are also introduced. Much of the theory regarding the sea environment can be found in the book by Faltinsen (1990) and serves here as the basis for the writing of the hydrodynamic theory. In section 2.6, the working principles of OrcaFlex and LiftDyn are described, as they were used for the necessary modelling in this investigation.

2.1. Operability

The operability of an operation is important as it determines the percentage of a given time frame that an operation can be executed. The higher the operability, the higher the chance that on any given day, the operation can be carried out as planned. The operability will depend on the operational and limiting parameters. For OWT installation, operation parameters include crane and ship properties. The limiting parameters include the crane capacity, off-lead/side-lead angle, and clearance between the load being carried by the crane and the hull of the ship. The limiting operating conditions need to be determined to have a safe installation of the OWT. The following sections on operability will go into more detail about the operating conditions of marine operations and the weather operating window (WOW) of such an operation. It is often also spoken about the workability of an operation. Workability has to do with the ability to perform certain operations under given conditions. Therefore, it is connected with its feasibility. This differs from operability as it has to do with the capability.

2.1.1. Operating conditions

Limiting operational parameters determine the environmental conditions under which marine operations can be carried out. For many operations with heavy-lifting cranes, the limits for operational parameters are not yet explicitly determined and can only be based on past experiences. The limiting environmental conditions are often given in terms of significant values of environmental parameters, such as peak period and significant wave height (Acero et al., 2017). The weather conditions will determine the response of the vessel. Based on that, it can be determined whether the given weather conditions allow for safe operation. The response will determine if the limiting parameters are exceeded or not. The limiting response is the response that is most critical for an operation and which first reaches safety limits that prevent safe operation (Schreier, 2022). The limiting responses in heavy lift operations often pertain to relative motions between the vessel and the body being lifted by the crane. The vessel response has to be determined before the operation happens. If the operating conditions lead to a vessel response that exceeds any of the limiting factors, the risk of something going wrong is greatly increased.

Operation	$\mathbf{H}_s$ [m]	$\mathbf{T}_p$ [s]	**Wind speed** [m/s]
Tower Installation	2	8	-
RNA assembly (blade installation)	1.5	8	12
RNA lift and set-down	1.5	8	12
Tower lift-off from barge to Thialf deck	1.5	8	12

Table 2.1: Limiting environmental conditions as determined by Heerema MC during simulations for various installation operations using the Thialf (Heerema Marine Contractors, 2018b).

Heerema MC has performed many simulations for different kinds of offshore installations and determined the limiting environmental conditions that lead to a successful outcome of the operation (limiting parameters not exceeded). Table 2.1 shows the limiting environmental conditions from simulations with the Thialf done by Heerema MC for other WTG installation operations. Limiting environmental conditions for a full WTG installation, as considered in this thesis, have not yet been completely determined, but some guiding limiting parameters have been determined based on design iterations. Those will be introduced in subsection 3.3.5, from which the limiting environmental conditions can be determined.

2.1.2. Weather Operating Window

A weather operating window is the time in which the weather conditions are appropriate for a given operation. This means the significant wave height, wind speed and wave period are all within allowable limits of safe operation.
DNVGL-ST-N001: Marine operations and marine warranty distinguishes marine operations as weather-restricted and weather-unrestricted operations. The operation period is given as in Equation 2.1 (DNV GL, 2018).

$$T_R = T_{POP} + T_C \tag{2.1}$$

In this equation, T_R is the operation period, T_{POP} is the planned operation period and T_C is the estimation of the maximum contingency time for the operation. Based on the equation, a weather-restricted operation is an operation for which T_R is less than 96 hours and T_{POP} less than 72 hours. These operations require close monitoring of the weather forecast before they begin. However, the weather forecast is not always accurate several days in advance, and therefore for operations that are weather-unrestricted, statistical extremes of MetOcean conditions need to be taken into account. Table 2.2 shows the necessary return periods of the MetOcean parameters depending on the duration of the operation.

Duration of operation	**Return period of MetOcean parameters**
Up to 3 days	Based on weather forecast
3 days to 1 week	1 year, consider specific season
1 week to 1 month	10 years, consider specific season
1 month to 1 year	100 years, consider specific season
More than 1 year	100 years, consider the whole year

Table 2.2: Return periods for MetOcean parameters depending on the duration of the marine operation (Chitteth Ramachandran et al., 2022).

2.2. Wind

The wind environment of a certain location can be obtained through the use of historical measurements of wind speed, direction, and spectrum. The wind speed and direction are used for determining the magnitude of the aerodynamic load distribution, which is important for the blades of the WTG. The wind loads on the blades, which are caused by wind pressures, are proportional to the wind velocity squared. The wind speed, U, is the average wind speed over a period of time. It can be given for different time periods, for example, 10 minutes, 1 hour or 3 hours. According to *DNVGL-RP-C205 - Environmental Conditions and Environmental Loads*, the recommended practice for representing the wind climate is by the 10-minute mean wind speed, U_{10}, at 10 m height and the standard deviation, σ_U, of the wind speed at 10 m height. 10 m height refers to the height above the mean sea level. Extreme wind conditions, such as extreme wind gust speeds can be given in terms of return periods of 1, 10, 50, or 100 years. Extreme conditions are important for certain design load cases. To obtain the response of the system modelled in this investigation, a wind field needed to be generated. The theory behind the wind field that was generated is given in the following sections.

2.2.1. Wind profile

The power law and logarithmic law are often used in the wind industry to define the wind profile. The wind profile is needed, as the wind speed is not uniform over height. For the wind profiles to be defined, a few characteristic parameters of the atmosphere are needed, as well as the wind speed at a certain defined height above the mean water level. From these parameters, the wind speed at any chosen height can be obtained (Nybø et al., 2020). *DNVGL-RP-C205* states that the normal wind speed profile can be given by the power law as shown in Equation 2.2, in cases of neutral atmospheric conditions (DNV GL, 2021). The wind profile also gives the wind shear.

$$U(z) = U_{ref} \left(\frac{z}{z_{ref}} \right)^{\alpha} \tag{2.2}$$

U_{ref} is the reference mean wind speed measured at the reference height, z_{ref}, and α is the power law exponent. The value of α can be determined from *DNVGL-RP-C205* and it depends on the terrain being considered. For this investigation, the terrain being considered is an open sea with waves. According to DNVGL-RP-C205, the value for α is 0.12.

2.2.2. Wind spectrum

The incoming wind is not constant through the duration of the operation but is instead fluctuating around a mean value. Due to this, the wind is considered irregular. A wind spectrum, based on several site-specific parameters, can be defined. This wind spectrum describes how the wind speed fluctuates around the mean wind speed value. There are several possible wind spectra that can be used, such as the Kaimal spectrum, von Karman spectrum, and Frøya spectrum. Which one to use depends on the location being considered. All three mentioned spectra assume wind turbulence that is homogeneous and stationary over time and space and also that it is isotropic. Further, they all follow a Gaussian (normal) distribution. The Kaimal spectrum makes use of the assumption that the vertical wind profile follows a logarithmic law, while the von Karman spectrum supposes that the integral scale of turbulence remains constant in time. This can be described by a frozen-in-time representation of turbulence. The Frøya spectrum is based on Kolmogorov's theory (Burton et al., 2011). In the theory scaling relationships between the spatial scales and energy of turbulence are assumed. *DNVGL-RP-C205* states that the Frøya wind profile model is recommended for offshore locations unless measured data suggests otherwise. The spectrum is a special case of the logarithmic wind profile. A limitation to it is that extrapolation of the expression to heights beyond the range for which it has been calibrated should be avoided. This would mean heights over 100 m. Due to this another model is considered for this investigation. For the Baltic Sea, the Kaimal spectrum is often used. The spectrum can be used to describe turbulent wind and is meant for neutral atmospheric conditions in the surface layer, which will be assumed in this investigation (Nybø et al., 2020). It is given by:

$$S_u(f) = \frac{6.868\sigma_U^2 \left(\frac{L_u}{U_{10}} \right)}{(1 + 10.32\frac{fL_u}{U_{10}})^{5/3}} \tag{2.3}$$

where σ_U is the wind speed standard deviation, f is the wind frequency (in Hz), U_{10} is the 10-minute mean wind speed, and L_u is the integral length scale of the component and it depends on the height above the water plane (DNV GL, 2021). To calculate L_u reference is made to *IEC61400-1* (IEC, 2005) or *Eurocode 1* (European Standards, 1991).

2.2.3. Aerodynamic Theory

Aerodynamic theory is necessary for this investigation, as it helps with the justification of the dynamic behaviour of the WTG during the installation. As will be explained later, the wind was only applied to the WTG, which is hanging in the air. This means that the aerodynamic loads were only experienced by the WTG and the wind did not directly act on the vessel.

Lift and drag

Wind turbine blades are made in such a way as to harness as much energy from the wind as possible. This means that the aerodynamic loading on the blades during installation when the blades are already mounted to the nacelle, can be significant. When looking at the aerodynamic loading using the blade element momentum (BEM) theory, the blade is usually split into airfoils, as pictured in Figure 2.1. This is essentially the profile of a blade. The angle that the incoming wind makes with the airfoil is called the angle of attack, denoted with α. The incoming

wind will cause a pressure difference between the suction and pressure sides of the airfoil, resulting in lift and drag forces being created. Lift occurs in the direction perpendicular to the incoming wind and drag occurs in the direction parallel to the wind. An increased angle of attack will lead to increased lift but also increased drag. The drag and lift coefficients (C_l and C_d, respectively) both hence depend on the angle of attack. During operation, an optimal angle of attack needs to be found to minimize drag and maximize the lift. However, during installation, the blade is not rotating as it would during operation, and therefore the distribution of aerodynamic forces on the blade differs during lifting and rotation. The rotating blade essentially experiences another incoming wind component due to the blade moving while rotating. This is not a real wind, but due to the motion of the blade it leads to an effective inflow velocity and in principle could affect the angle of attack. When rotating, the rotational speed increases from the root to the tip, so to maintain the optimal angle of attack along the whole blade length, the blade is twisted.

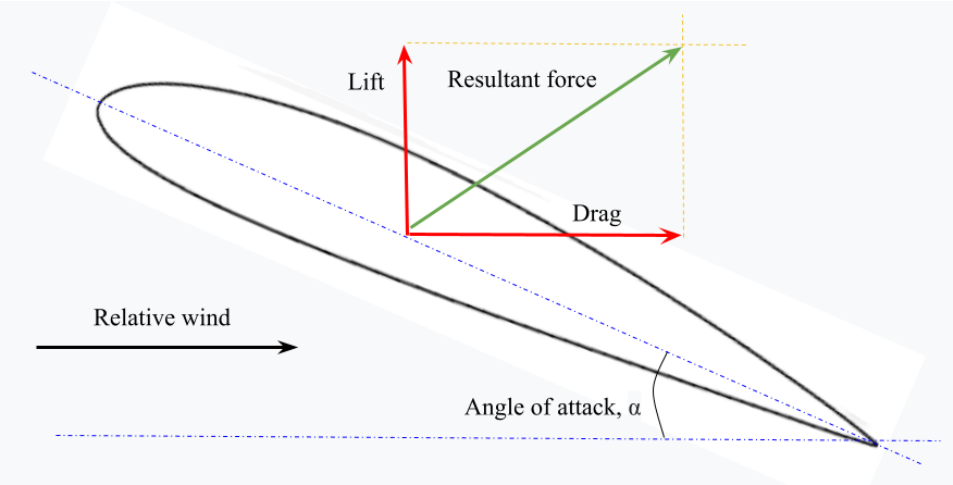

Figure 2.1: Diagram of an airfoil, with the lift and drag forces labelled.

For the installation, the angle of attack will determine the lift and drag coefficients, which will determine the lift and drag load. The lift and drag loads are given in Equation 2.4 and Equation 2.5, respectively.

$$l_i = C_{l_i} \frac{1}{2} \rho_{air} V_0^2 c_i \tag{2.4}$$

$$d_i = C_{d_i} \frac{1}{2} \rho_{air} V_0^2 c_i \tag{2.5}$$

In these equations, the subscript i represents the segment of the blade, c is the chord length, ρ_{air} is the air density and V_0 is the incoming wind velocity.

Blade pitch

The pitch of the blades is also an important parameter as it manages the loads caused by the wind. The pitch angle can be adjusted during operation so that the turbine can regulate the rotational speed of the rotor and the torque. Through this, the turbine can operate safely without wind turbine components getting damaged due to excessive loads. During installation, the pitch angle is also important, as again by adjusting the angle, the loads acting on it can be minimised so that no components are damaged or excessive motions excited. This is an important parameter to investigate for the installation of the full WTG, as the optimal pitch angle can greatly reduce the WTG motions while hanging in the air.

2.3. Waves

Waves are an important environmental load on offshore structures. They interact with structures and cause wave-induced motions on them. Waves can be categorised into different types depending on how they originated. For example, wind waves are caused by wind in the area, and swell waves are caused by weather events far from the location to which the waves eventually propagate. For this investigation swell waves were not regarded. In the Baltic Sea, swell waves are locally generated, as the only connection to the ocean is through the narrow Danish

strait. The swell generated in the Baltic Sea is limited by the size of the Baltic Sea area and hence is not dominant. Therefore for this investigation, only wind waves were accounted for. The following sections will describe how sea states are modelled through wave spectra and some additional hydrodynamic theory will be given, which is based on the textbook by Faltinsen (1990).

2.3.1. Wave characteristics

Waves and sea states can be characterised by several different characteristics. Some of these, like the significant wave height and peak period, have already been mentioned. Other relevant parameters include the wavelength λ, which is defined as the distance between two successive crests, and the wave height H, which is the vertical distance from trough to crest. The wave amplitude, ζ, is half of the wave height. These parameters are used for regular wave theory. For irregular waves, the wavelength and height are not constant. The local wavelength in this case can then be determined by the distance between two consecutive zero up-crossings. Water depth along with the aforementioned parameters, is a relevant parameter to determine which theory is applicable to a given situation. Certain combinations of water depth, wave height, and wave period can lead to shallow, intermediate, or deep water scenarios. Often the wave steepness parameter and the wave shallowness parameter will be used to determine which theory is valid for the given water depth, wave period, and wave height.

2.3.2. Wave spectrum

A wave spectrum shows the distribution of energy of the wave components. It is the power spectral density function of the vertical sea surface displacement (DNV GL, 2021). There are two well-known wave spectra being used to model waves in offshore problems. The spectra are obtained from the statistical parameters of a specific site. These parameters include the significant wave height and the zero crossing period, both measured as a function of the wind speed (Veldkamp and Van Der Tempel, 2005).

The first one is the Pierson-Moskowitz spectrum, which was created based on measurements from the Atlantic Ocean. The environmental conditions, such as the wind speed and significant wave height, are assumed constant for long periods (fully-developed sea) and the spectrum is for deep waters. Equation 2.6 shows the spectrum equation, where $f_p = 2\pi/T_p$ is the spectral peak frequency.

$$S_{PM}(\omega) = \frac{5}{16} H_s^2 T_p \left(\frac{f}{f_p}\right)^{-5} \exp\left(-\frac{5}{4}\left(\frac{f_p}{f}\right)^4\right) \tag{2.6}$$

The second wave spectrum is the Joint North Sea Wave Project (JONSWAP), which is based on an extensive study done in the North Sea and is used for sea states with limited fetch waves and deep waters. This spectrum is a modification to the Pierson Moskowitz spectrum. Equation 2.7 shows the equation of the spectrum. In the JONSWAP spectrum, the peak enhancement factor, γ, is set to 3.3 for situations in the North Sea while using a peak enhancement factor of 1 would result in the Pierson-Moskowitz spectrum. The spectral shape of the JONSWAP is slightly different as it has a higher and sharper peak. This comes from the fact that JONSWAP is for young sea states, meaning the sea state is not fully developed. The JONSWAP spectrum is:

$$S_J(\omega) = (1 - 0.287 \ln\gamma) \frac{5}{16} H_s^2 T_p \left(\frac{f}{f_p}\right)^{-5} \exp\left(-\frac{5}{4}\left(\frac{f_p}{f}\right)^4\right) \gamma^{\Gamma} \tag{2.7}$$

where γ is the peak enhancement factor and Γ is

$$\Gamma = \exp\left(-0.5\left(\frac{\frac{f}{f_p} - 1}{\sigma}\right)^2\right) \tag{2.8}$$

where σ is a spectral width parameter. It depends on whether f is larger than f_p or not. Figure 2.2 shows an example of both spectra.

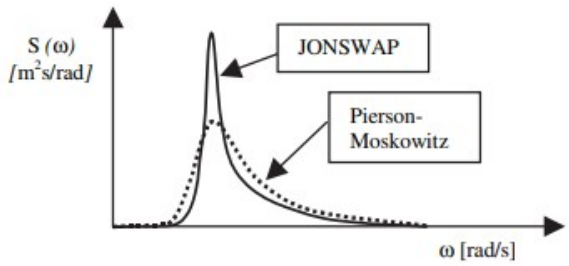

Figure 2.2: Examples of the JONSWAP and Pierson-Moskowitz spectra (Veldkamp and Van Der Tempel, 2005).

There is also a possibility to make use of a two-peak spectrum, which better represents wind, and swell waves. However, as mentioned earlier, swell will not be accounted for in this investigation. As a possible further extension for this investigation, the effect of swell on the operation can be investigated. This is further discussed in the recommendations (section 6.2).

2.3.3. Motions

When a floating rigid body is being acted upon by environmental loads, such as wind and waves, and is not constrained, it can move in 6 degrees of freedom (DoF), three translational and three rotational. The three translational motions are referred to as surge, sway, and heave and represent translational movement in X-, Y-, and Z-directions, respectively, when considering a right-handed coordinate system fixed with respect to the mean position of the body. The three rotational degrees of freedom are roll, pitch, and yaw and correspond to rotation about the X-, Y- and Z-axis of the body, respectively. Often the motions are referred to with subscripts in equations. The subscripts are numbered from 1 to 6. Table 2.3 shows the degree of freedom and the corresponding subscript used in equations.

The Greek letter η is used to represent the displacement of a body, with η_1 representing the surge displacement for example. The equation that represents the motion of any body can be seen in Equation 2.9. In the equation, $\times$ denotes the vector product and **i**, **j** and **k** are unit vectors along the X-, Y- and Z-axis, respectively.

$$\begin{aligned} \mathbf{s} &= \eta_1\mathbf{i} + \eta_2\mathbf{j} + \eta_3\mathbf{k} + \omega \times \mathbf{r} \\ &= (\eta_1 + z\eta_5 - y\eta_6)\mathbf{i} + (\eta_2 - z\eta_4 + x\eta_6)\mathbf{j} + (\eta_3 + y\eta_4 - x\eta_5)\mathbf{k} \end{aligned} \tag{2.9}$$

Table 2.3: Degrees of freedom.

#	DOF
1	Surge
2	Sway
3	Heave
4	Roll
5	Pitch
6	Yaw

2.3.4. Potential flow theory

Potential flow theory can be utilised to perform inexpensive analysis with regard to computation and can produce acceptable results. However, some aspects of fluid flow are neglected in potential flow theory, which could result in inaccurate results.

The basic assumptions behind potential flow theory include that the fluid is incompressible and inviscid and that the fluid motion is irrotational. For these assumptions, a velocity potential ϕ is introduced. It has no physical meaning. However, it is convenient for mathematical analysis. To solve the problem of the velocity potential, the solution to the Laplace equation (Equation 2.10) is required, along with relevant boundary conditions. The boundary conditions include the kinematic and the dynamic free-surface conditions. For further information regarding

this, reference is made to Faltinsen (1990).

$$\frac{\partial^2\phi}{\partial x^2} + \frac{\partial^2\phi}{\partial y^2} + \frac{\partial^2\phi}{\partial z^2} = 0 \tag{2.10}$$

2.3.5. Linear wave theory

Linear or Airy wave theory can be derived by assuming a horizontal sea bottom and a free surface of infinite extent. The theory is used for propagating waves and can be applied in situations with finite and infinite water depth. Linear refers to the wave-induced motions and load amplitudes being linearly proportional to the incident wave amplitude, ζ_a.

The relationship between the wavelength and water depth is important to distinguish between shallow, intermediate, or deep waters. Figure 2.3 illustrates this relationship for the deep water and intermediate water case. In shallow and intermediate waters, the water depth is small compared to the wavelength, and the sea floor will have an impact on the wave characteristics. In deep water, the sea bed does not have an influence on the wave. Wave kinematics no longer have an effect on submerged structures, which are at a depth larger than half the wavelength of the incoming waves. This is represented by the relation $\frac{d}{\lambda} > 0.5$, where d is the water depth at the location at the bottom of the structure, and λ is the wavelength.

The particle kinematics include horizontal and vertical velocity and acceleration. They are obtained from the surface elevation equation. In deep water, the water particles follow a circular path, while in intermediate and shallow water, the trajectory becomes more oval (elliptical). The horizontal and vertical velocities are obtained from the velocity potential in waves and the dispersion relation. The velocities and accelerations differ for shallow, intermediate, and deep waters. The horizontal and vertical velocities in infinite (deep) water depth are:

$$u = \omega\zeta_a e^{kz}\sin(\omega t - kx) \tag{2.11}$$

$$w = \omega\zeta_a e^{kz}\cos(\omega t - kx) \tag{2.12}$$

The horizontal and vertical acceleration in infinite water depth are:

$$a_1 = \omega^2\zeta_a e^{kz}\cos(\omega t - kx) \tag{2.13}$$

$$a_3 = -\omega^2\zeta_a e^{kz}\sin(\omega t - kx) \tag{2.14}$$

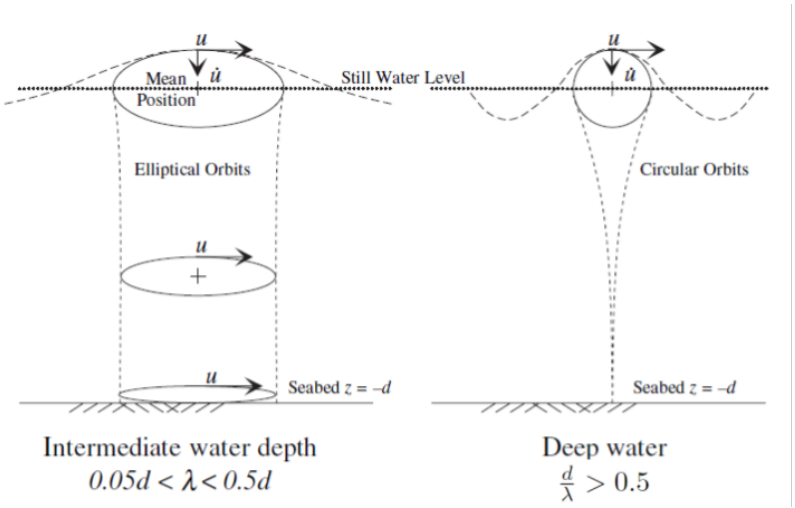

Figure 2.3: Water particle motion in intermediate and deep water according to Airy linear wave theory. (Veldkamp and Van Der Tempel, 2005).

2.3.6. Response in linear waves

Waves can be considered as regular or irregular waves. In nature, regular waves are very uncommon, and waves generated by wind or storms are most often irregular. Irregular waves are more challenging to work with, nevertheless, due to linear theory and through the use of the superposition principle, they can be decomposed into several regular harmonic waves. So, the response can be obtained by adding together regular waves with different amplitudes, directions, and wavelengths. This is seen as sufficient from a hydrodynamical point of view.

When steady state conditions are assumed, it refers to no transient effects due to initial conditions and that the linear dynamic motions and loads on the given structure are harmonically oscillating with a frequency corresponding to the frequency of the wave loads that excited the structure. The problem can be split into a diffraction and radiation part.

- The diffraction problem concerns the situation in which the body is fixed and is interacting with incident regular waves. It is concerned with finding the wave excitation loads consisting of the diffraction and Froude-Krylov loads. The loads consist of forces and moments.
- The radiation problem concerns a situation in which there are no incident waves, but the body is forced to oscillate in its six DoFs. The goal is to find the hydrodynamic loads in the form of the added mass, damping, and restoring terms.

The forces from the diffraction and radiation problems can be added together due to linearity. Together they give the total hydrodynamic forces and moments. The forces and moments together are referred to as generalized forces.

Added mass, damping, and restoring terms

In the radiation problem, there are no incident waves, however, outgoing waves are still generated due to the forced motion of the body. This body motion causes oscillating fluid pressure on the surface of the body. The resulting forces and moments are obtained by integrating the fluid pressure forces over the surface of the body (Faltinsen, 1990). The added mass and wave-radiation damping loads resulting from harmonic motion mode η_j are given are Equation 2.15. The subscript j refers to the degree of freedom from 1-6, as introduced earlier.

$$F_k = -A_{kj}\frac{\mathrm{d}^2\eta_j}{\mathrm{d}t^2} - B_{kj}\frac{\mathrm{d}\eta_j}{\mathrm{d}t} \tag{2.15}$$

A is the added mass coefficient and B the damping coefficient. The subscript k, again, refers to the degree of freedom from 1-6.
Restoring forces come from hydrostatic and mass considerations (Faltinsen, 1990). The restoring forces come from the restoring coefficient C, as seen in Equation 2.16.

$$F_k = -C_{kj}\eta_j \tag{2.16}$$

Froude-Krylov and diffraction loads

Two effects on the fluid pressure when a structure is fixed and interacting with incident waves will occur. The first is the induction of linear dynamic pressure by undisturbed waves. The pressure field of these undisturbed waves causes a force known as Froude-Krylov. The second effect comes from the structure changing the pressure field. The generalised force that arises from this is the diffraction force.

2.3.7. Deep-water floating system: Semi-submersible

A semi-submersible vessel performing an offshore installation operation can be considered to be a deep-water floating system when operating in deep-water conditions. Potential flow forces are inertia-dominated, while wave diffraction and viscous forces are of lesser importance when considering cross-section dimensions of the semi-sub relative to the wave characteristic dimensions (wavelength and wave height). Large wave loads on the structure occur in the wave frequency range. The motions from these loads are called wave frequency (WF) motions and are mainly linearly excited. To avoid any resonant effects, the semi-sub is designed to have natural periods outside the WF range. Surge, sway, and yaw natural periods of the semi-sub are usually greater than 100 seconds. Heave, roll, and pitch natural periods are often greater than 20 seconds.

Apart from WF motions, slow drift or low frequency (LF) and mean drift motions can also occur. Non-linear effects cause slow drift and mean drift motions. These motions can be induced by waves, non-steady currents and also wind. Slow drift motions come to be from resonance oscillations and are connected to second-order effects. Apart from nonlinear effects causing resonance of the semi-sub, resonance can also be caused by swell or other long waves with periods in the range of the heave natural period of the semi-sub.

Due to the change in the semi-subs buoyancy forces, heave resonance can be caused. Semi-subs usually have small water plane areas, which lead to small vertical motions compared to other floating installation vessels. This is because only a small amount of the wave energy will be transferred, which will cause small first-order heave motions. The semi-sub will remain nearly completely stable in waves (Journée and Massie, 2001). This is directly related to the small water plane area of the vessel and its large relative mass. They are designed to avoid heave resonance and also so that the maximum heave motion in severe seas is less than half the maximum wave amplitude. Since their natural period is well out of the incoming wind-generated wave period, they are usually not sensitive to WF motions, however, they can have dominant LF responses in roll and pitch.

Dynamic positioning of semi-subs can be done through the use of thrusters. For a vessel, the DP is used to eliminate unwanted surge, sway, and yaw motions by counteracting the mean wave, current and wind loads. The DP cannot react to High-frequency wave and WF motions are filtered out of the thruster forces, as a DP system cannot react to them. So, DP systems are concerned with counteracting slowly-varying motions of the vessel.

2.4. Friction

Friction defines the force that resists motion between two surfaces in contact with each other. It is a fundamental concept used in physics and originates from interatomic, intermolecular, and intergranular interactions between the two contact surfaces.

Coefficient of friction

An important quantity related to the complex phenomenon of friction is the coefficient of friction, μ. It is a dimensionless quantity used to define the frictional force, F_f, between two surfaces and their normal force, F_N, acting perpendicular to the contact surface. It can be expressed through the following equation:

$$\mu = \frac{F_f}{F_N} \tag{2.17}$$

If the coefficient of friction between the two surfaces involved and the normal force are known, then the equation can be rearranged to find the frictional force. Friction opposes motion between two surfaces, and therefore the motion will be opposed while $F_t \leq \mu F_N = F_f$, where F_t is the tangential or the applied force. If the applied force is greater than μF_N, slip will occur. In general, the coefficient of friction will depend on various factors, such as the roughness and material properties of the surfaces, but also the pressure applied. For the two surfaces in contact to not get damaged, the shear strength of the weakest of the two surfaces involved must be sufficiently high to allow the applied tangential force. To determine this Equation 2.18 can be used, where the maximum tangential force $F_{t,max}$ is determined based on the real contact area, A_{real} and the limiting shear strength tau_{min}.

$$F_{t,max} = A_{real}\tau_{min} \tag{2.18}$$

The real contact area will be better explained in the next section.

Asperities

Usually, rougher surfaces will have higher coefficients of friction than surfaces that are smooth. This is due to rougher surfaces having more asperities, which can interlock with the other surface. Asperities are bumps or peaks on a surface of a material (irregularities). When two surfaces are in contact, the asperities of one surface interlock with the asperities of the other surface and create a complex network of contact points. When the interlocking of asperities resists motion, friction arises. Figure 2.4 shows a visual representation of asperities on a microscopic level. Asperities lead to rougher surfaces having more points of contact between them, increasing the interatomic and intermolecular interactions. Due to asperities, the actual contact area (A_{real}) between surfaces is lower than the apparent surface area since contact between the surfaces is only made at points where asperities interlock. The actual contact area can increase with increased contact stress and becomes close to the apparent contact area when the contact stress nears the yield stress limit of the material with the lowest stiffness. When such stress is

applied, the asperities have more or less been flattened, and full contact between the two surfaces is possible. This is also the point where the maximum frictional force is reached. When considering the hardness of the material, softer and more ductile materials will have a higher coefficient of friction than hard and brittle materials. This is due to the soft and ductile material being able to change shape and conform to the surface of the other material, increasing the area of the surfaces in contact with each other (Blau, 2001).

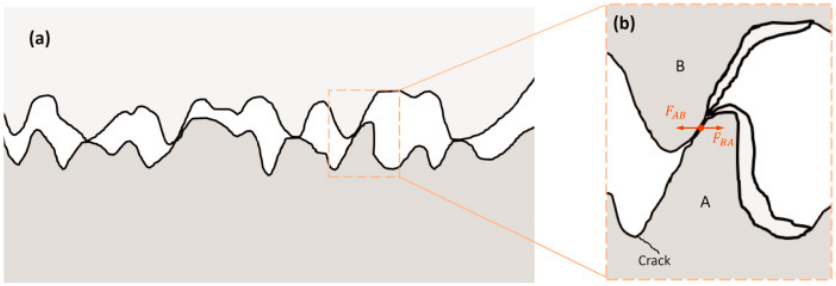

Figure 2.4: Asperities seen on the surface of materials. (a) shows multiple asperities of two surfaces and how they can interlock, (b) shows a single asperity from both surfaces interlocking (Malekan et al., 2021).

Static and dynamic friction

Friction can be divided into static and dynamic friction. In the initial situation concerned with static friction, the two surfaces are not yet moving relative to one another. The static frictional force is the force that prevents motion between the surfaces and depends on the normal force and the coefficient of static friction. The asperities work as described above and in order for relative motion between the two surfaces to be initiated, the static frictional force needs to be overcome. In s dynamic friction situation, the asperities continuously break and reform while the two surfaces move relative to each other. Dynamic friction is also known as kinetic friction and refers to the frictional force that arises when two surfaces are moving relative to one another (after slip has occurred). The force will depend again on the normal force and, in this case, the coefficient of dynamic friction. The coefficient of dynamic friction is usually lower than the coefficient of static friction between the same two surfaces due to asperities breaking constantly, and so the dynamic frictional force is lower than the static frictional force (Awrejcewicz and Olejnik, 2005). This means less force is required to keep an object in motion while sliding over a surface than it is required to get the object moving in the first place.

2.5. Thin-walled cylinders

Thin-walled cylinders are used in a variety of engineering applications, ranging from pipelines, jacket structures, and wind turbine towers. It is vital that for such applications, the structural integrity remains intact by avoiding reaching the limits of relevant failure modes. Thin-walled cylinders are cylinders with thickness-to-diameter ratios over 100 (Vasilikis and Karamanos, 2009). The stresses acting in the cylinders and buckling of thin-walled cylinders will be briefly introduced.

2.5.1. Stresses

In thin-walled cylinders, three types of stresses are often experienced. These include the circumferential (hoop) stresses (σ_θ), axial/longitudinal stresses (σ_L), and radial stresses (θ_r) (Iturgaiz Elso, 2012). The direction in which the stresses act are depicted in Figure 2.5.

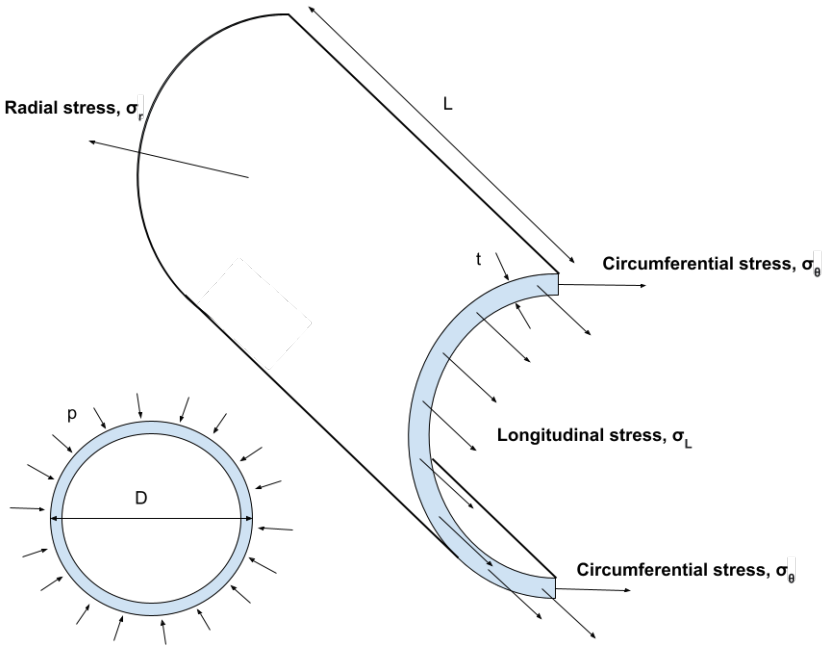

Figure 2.5: Stresses that arise in thin-walled cylinders. L is the length of the cyclinder, t is the thickness of the cylinder and d is the diameter of the cyclinder

The hoop stress in a thin-walled cylinder arises due to differences in pressure inside and outside the cylinder. This difference can arise due to a liquid inside the cylinder (hydrostatic pressure) or the application of an external pressure on the outside of the cylinder. It is an important stress in maintaining the shape of the structure. The force trying to split the cylinder arising from the external or internal uniform pressure is shown in Equation 2.19. This equation is valid as long as the thin-walled approximation holds.

$$F = 2\int_0^{\frac{\pi}{2}} prL\cos(\theta)d\theta = 2prL \tag{2.19}$$

where p is the pressure, r is the radius of the cylinder, L is the length of the cylinder, and θ is the angle over which the pressure is applied. $F = 2prL$ is the force in the case the pressure is applied over the full circumference of the cylinder. The force acts on an area represented by Equation 2.20.

$$A = 2tL \tag{2.20}$$

From the force and the area, the circumferential stress can be obtained ($\sigma = \frac{F}{A}$).

$$\sigma_\theta = \frac{F}{A} = \frac{2prL}{2tL} = \frac{pr}{t} \tag{2.21}$$

Axial stresses in the cylinder act in the longitudinal direction and essentially arise from forces trying to split the cylinder along its length. The force caused by the pressure is shown in Equation 2.22.

$$F = \int_0^r 2p\pi r dr = p\pi\frac{r^2}{2} = p\frac{\pi D^2}{4} \tag{2.22}$$

where again p is the pressure, r is the radius of the cylinder, and D is the diameter of the cylinder. The area on which the force is applied is equal to the cylinder cross-section approximated by Equation 2.23.

$$A = \pi Dt \tag{2.23}$$

This leads to the axial stress in a thin-walled cylinder to be as shown in Equation 2.24.

$$\sigma_L = \frac{F}{A} = \frac{p\frac{\pi D^2}{4}}{\pi Dt} = \frac{pr}{2t} \tag{2.24}$$

Radial stresses in thin-walled cylinders are stresses working normal to the cylinder and are often neglected due to them being very small compared to the circumferential and axial stresses.

2.5.2. Buckling

Buckling in thin-walled cylinders occurs due to compressive forces acting on them. The compressive forces could lead to excessive hoop compression or axial compression. Examples of thin-walled cylinders facing problems with buckling include buried steel pipelines and steel liners. The reason for hoop stresses arising in the wall of the cylinders/pipes is often due to thermal effects or hydrostatic pressure. For a thin-walled cylinder, some of the main parameters for buckling include the diameter-to-wall thickness ratio, Young's modulus, and the material yield stress in the circumferential direction. For a thin-walled cylinder, buckling will likely be the failure mode, whose limits are exceeded first. Due to this, the critical buckling pressure is of great importance for thin-walled cylinders, as surpassing the pressure will result in structural failure.

Theory of elastic stability

The elastic equilibrium of thin-walled cylinders that buckle is not stable. To determine beforehand if the elastic equilibrium of a given thin-walled cylinder is stable, the standard methods used in the theory of elastic stability, which include the method of adjacent equilibrium and energy method, should be applied (Flügge, 1960). A shell carrying a certain load, known as the basic load, will encounter basic stresses and basic displacements as a result of the load. By adding an additional deformation, such as a lateral deflection, the elastic equilibrium is disturbed. Deformations of the shell are related to the stresses and the strains, and come to rise due to additional forces acting on the shell. If no such force acts on the shell, then the disturbance does not exist. The energy method seeks to find the energy necessary to produce the deformation under no additional loading applied. The energy concerned with this consists of two parts. The first is the work which has to be done against the external forces, and the second is the increase in strain energy. The work done is essentially the gain in potential energy of the basic load. The adjacent equilibrium method does not look at the energy but instead seeks the condition under which a zero loading will cause the deviation. It was mentioned that forces acting on the shell will cause deformations, however, if no such force acts on the shell, then the disturbance does not exist. For such a situation, the elastic equilibrium is stable. An increased basic load will lead to less force required to produce the same disturbance. When the basic load is further increased to a critical value, the disturbance will occur without any additional forces acting on the shell. In this case, the elastic equilibrium is neutral with respect to the given disturbance. The load required to reach the neutral equilibrium is known as the critical load, or the buckling load. For a neutral equilibrium, it is possible that the disturbance, which can be a system of additional stresses and displacements, will occur spontaneously. This is the buckling of the shell. In general, when the load is small enough, the elastic equilibrium is always stable. However, when the load exceeds the critical load, the equilibrium becomes unstable. This leads to any kind of additional disturbances making the shell leave its equilibrium position (Flügge, 1960).

Buckling of unconfined cylinders

A cylindrical shell can be subject to a uniform pressure acting on its walls (q_1, external pressure), an axial compression applied at the ends (q_2) or a shear loading applied at the ends causing a torque (q_3). These are basic loads, and they produce stress resultants (basic stress system). For the case of buckling of a thin-walled cylinder and buckling of a circular ring under external pressure, the same formula for the critical load can be applied. This is, if the edges of the cylinder are free, or its length is long enough to neglect any stiffening effects of the constraints at the edges (Timoshenko and Gere, 1989). The value of the critical load can be obtained from three differential equations for the disturbed equilibrium. For the complete derivation and background theory, one should refer to Timoshenko and Gere (1989), and Flugge (1960). From Timoshenko and Gere (1989), the critical pressure for long circular tubes under uniform external pressure is:

$$p_{cr} = \frac{E}{1-\nu^2}(\frac{t}{D})^3 \tag{2.25}$$

where p_{cr} is the buckling pressure, E is Young's modulus, ν Poisson's ratio, t is the wall thickness of the confined cylinder, and D is the diameter of the cylinder. Equation 2.25 can be used as long as the proportional limit of the material is not exceeded by the corresponding compressive stress (Timoshenko and Gere, 1989). The critical compressive stress is shown in Equation 2.26.

$$\sigma_{cr} = \frac{E}{1-\nu^2}(\frac{t}{D})^2 \tag{2.26}$$

Buckling of confined cylinders

Many different cases of thin-walled cylinder buckling have been investigated, most of which concern a loading in the axial direction and unconfined cylinders, as explained before. The buckling of a wind turbine tower due to

a clamping force somewhere along its length is a special case and does not have an exact solution for the critical buckling pressure. In this case, the loading is applied in the radial direction. The wind turbine tower in this case is also in a confined space due to the frame enclosing it. This scenario could potentially lead to single-lobe buckling, as pictured in Figure 2.6. Due to the confined space, Equation 2.25 is not fully applicable. Glock (1977), introduced a solution for a confined elastic cylinder, where it is assumed there is no friction between the inner and outer cylinder and that there are no variations in stress and deformation in the axial direction. The equation for the critical buckling pressure as derived by Glock is presented in Equation 2.27 and comes from the energy formulation (Glock, 1977). For further derivation of the formula, reference is made to Iturgaiz Elso (2012). In Equation 2.27 it is assumed that the flexural modulus of elasticity is approximately the same as the tensile modulus.

$$p_{GL} = \frac{E}{1-\nu^2}(\frac{t}{D})^{2.2} \tag{2.27}$$

where p_{GL} is the buckling pressure, E is the Young's modulus, ν Poisson's ratio, t is the wall thickness of the confined cylinder and D the diameter of the cylinder. Limitations of this equation being applied for the wind turbine tower scenario include that it is derived for elastic materials and buckling caused by hydrostatic pressure (Iturgaiz Elso, 2012). The tower is made from steel, which shows elastic-plastic behaviour and there is no fluid flowing through the tower.

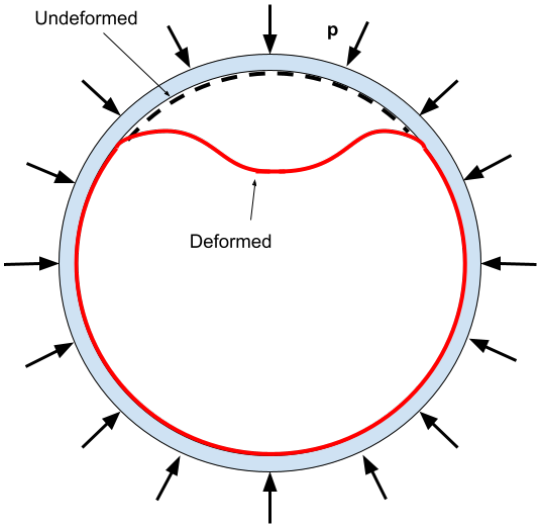

Figure 2.6: Single lobe buckling of a confined cylinder. The red line is the deformed cylinder due to the external pressure, p, acting on it. The dotted black line represents the original shape of the cylinder.

Vasikilis and Karamanos (2010) investigated the structural response of elastic and steel cylinders confined in an elastic medium using a two-dimensional model with nonlinear finite elements. This was done to develop design guidelines for confined steel cylinders. The results for elastic cylinders show agreement with Glock's formula, nevertheless, results for steel cylinders show slightly different results due to buckling happening in the inelastic range. For this, a general methodology has been adopted based on a "shell slenderness" parameter, λ (Vasilikis and Karamanos, 2010). The full methodology is presented in Appendix A. The results for the buckling pressure from the methodology and from the numerical finite element analysis concur with each other.

2.6. Software

Seakeeping problems and various marine operations can be modelled with the help of various software. The software can be used to perform different types of analyses such as frequency or time domain. In this investigation, LiftDyn will be used for the frequency domain (FD) analysis and OrcaFlex for the time domain (TD) analysis. How both of the software perform the analysis is described in the following sections.

2.6.1. LiftDyn

LiftDyn is an in-house software used at Heerema MC, in which linear hydrodynamic models can be quickly built and analysed in the frequency domain. The software is very useful for determining workability and possible risks

of offshore operations, as the response of the vessel, crane, and lifted object can be obtained for given sea conditions. The software also allows for the forces in the hoisting arrangement or the possibility of impact between the lifted object and the barge to be determined, both of which are possible limiting factors to the operation. Information regarding LiftDyn comes from the LiftDyn Theory Manual created at Heerema MC (Heerema Marine Contractors, 2018a).

The program solves systems made up of 6 DoF rigid bodies connected to each other or the earth. The connections are made by springs, dampers, or hinges. Once the model is built, the structural mode shapes of the modes of the system can be animated, through which the corresponding natural periods are also obtained. The animation of the mode shapes illustrates the hydrodynamic behaviour of the system and shows the dominant motions. By solving the corresponding system of matrices, the Response Amplitude Operators (RAOs) can also be calculated and then post-processed to a motion, velocity, or acceleration RAO for any point relative to another point. From the RAOs produced, the corresponding significant response can be obtained. The RAOs are based on a given sea state, defined by the user through a wave spectrum, such as the Pierson Moskowitz, JONSWAP, or a specific user-defined spectrum. If the interest of the analysis is the operability of an operation, limiting parameters can also be added in order to obtain operability curves. The operability curves show the allowable maximum wave height as a function of the spectral period. The results obtained in LiftDyn can be exported and used in other applications for further analyses, such as a weather downtime assessment (Heerema Marine Contractors, 2018a).

The equation of motion solved in LiftDyn is shown in Equation 2.28. The equation is a single matrix and for n bodies in a system, it consists of $6n$ equations.

$$(\mathbf{M} + \mathbf{A}(\omega)) \cdot \ddot{X}(\omega, dir) + \mathbf{B}(\omega) \cdot \dot{X}(\omega, dir) + \mathbf{C} \cdot X(\omega, dir) = F(\omega, dir) \tag{2.28}$$

M is the mass matrix, **A** is the added mass matrix, **B** is the damping matrix and **C** is the stiffness matrix. They are all defined with respect to the body's centre of gravity (CoG). The damping matrix includes only the hydrodynamic damping The generalised forces applied on the rigid bodies are contained in the force matrix F. X represents the unknown motion vector with the motions in 6 DoF. The force and motion vectors are both assumed to be harmonic functions of the wave frequency, ω. dir refers to the wave direction. A vector of the main wave directions for which the RAOs are computed exists. To obtain other directions, the hydrodynamic properties are interpolated. A hydrodynamic database is used to derive the added mass, damping, and hydrostatic properties.

Equation 2.28 is a second-order linear differential equation. Due to this, it can be solved in the frequency domain and written as a simple matrix-vector equation, as shown in Equation 2.29. The complex motion vector X_c can be found by solving the equation for every wave frequency and direction. X contains the amplitude and phase difference of each mode.

$$[\mathbf{C} + i\omega\mathbf{B} - \omega^2(\mathbf{M} + \mathbf{A}(\omega))] \cdot X_c(\omega, dir) = F_c(\omega, dir) \tag{2.29}$$

Setting the force F_c in Equation 2.29 to 0 yields the eigenvalue problem, which is used to determine the natural periods/frequencies of the system. Overall, LiftDyn is used to quickly analyse linear, stationary, and dynamic problems. It has a visual interface, which helps in the minimisation of user errors.

2.6.2. OrcaFlex

OrcaFlex builds a mathematical computer model of the system, in this case, a vessel with a crane and a tower, and WTG assembly. The statics and dynamics of the system can be calculated. The following information comes from Orcina, which has created documentation for OrcaFlex (Orcina, 2022).

In the static analysis, the positions and orientations of the bodies in the model are determined. In these positions, the forces and moments are all in equilibrium. These results give the starting point of the dynamic simulation for the problem of the wind turbine installation. OrcaFlex models are invariable nonlinear, therefore, an iterative approach is needed, which uses the multi-dimensional form of Newton's method.

The dynamic analysis can be split into frequency and time domain analysis. The frequency domain analysis uses the results of the static analysis and linearizes the problem. The analysis can solve for wave frequency or low-frequency solution frequencies. Linear transfer functions are generated, which map the stochastic environmental or loading process to the response process of the system. At every examined frequency the response of

the system can be obtained from the linear transfer functions. This is an iterative process until convergence of the solution is reached. The reason for the iterative process is the linearisation of the quadratic viscous drag load. The results obtained as the output include statistics and spectral density graphs. Spectral density graphs are one-sided power spectral density (PSD) plots of the chosen results.

In the time-domain analysis, the mass, damping, stiffness, and loading are calculated for each time interval. For this, the instantaneous time-varying geometry is considered. The integration with respect to time can be done implicitly or explicitly. The results obtained from the time-domain analysis include time histories of response variables. OrcaFlex solves the following equation of motion in the time domain:

$$M(p,a) + C(p,v) + K(p) = F(p,v,t) \tag{2.30}$$

where $M(p,a)$ is the system inertia load, $C(p,v)$ is the system damping load, $K(p)$ is the system stiffness load and $F(p,v,t)$ is the external load. These loads are all functions of either position, p, velocity, v, acceleration, a or simulation time, t. In this equation of motion, either the implicit or explicit time integration schemes can be implemented. The explicit scheme is essentially the semi-implicit Euler with a constant time step. The static analysis determines the initial positions and orientations of all bodies/objects involved in the simulation, from which the forces and moments acting on all bodies can be calculated. These forces include the weight, buoyancy, hydrodynamic and aerodynamic drag, hydrodynamic added mass effects, and contact forces, among others. These forces and moments make it possible for each object's local equation of motion to be determined. This local equation of motion is then solved for the acceleration vector at the start of each time step. This is followed by performing an integration using a semi-implicit Euler integration. For implicit integration, the EOM is solved at the end of the time step. At the end of the time step, the position, velocity, and acceleration are initially unknown. To solve them, an iterative solution method is required. This results in substantially more time required for the computation than for the explicit scheme. On the contrary, the explicit scheme is stable for larger time steps compared to the implicit scheme, which often results in the implicit scheme being faster, especially when longer simulation times are used.

The user can define the wind and wave spectrum for the OrcaFlex simulations. Within OrcaFlex, it is not possible to apply a spatially varying turbulent wind field, as is required to obtain realistic offshore conditions. Currently, OrcaFlex allows defining a constant wind field by specifying speed and direction, which do not change over time. Further, it is also possible to make use of the NPD, API and ESDU spectrum. These spectra allow a constant wind direction, and with a reference mean speed and elevation, OrcaFlex is able to parameterise the spectrum to determine the statistical variation about the mean speed. It has been shown that for offshore installations of wind turbines, making use of a full uniform wind field does not give accurate or realistic results regarding the motions of lifted objects. Since OrcaFlex itself cannot produce a spatially varying wind field, TurbSim is utilised. TurbSim is capable of calculating 3D spatially varying full wind fields that can be imported into OrcaFlex. The wind field created by TurbSim is based on the Kaimal model, which is recommended in *IEC61400-1*. The Kaimal model is used as it is similar to the Mann model. The results match well when comparing the results of TurbSim and externally generated IEC turbulence with a Mann model. Some assumptions of the Kaimal spectrum, which is used for the Kaimal model, have already been stated in subsection 2.2.2. The Kaimal model uses a one-dimensional Fast Fourier Transform (FFT), with which it is able to generate time histories from spectra. This is applied independently to each turbulence component. The Mann model does not use a particular turbulence spectrum and assumes a power-law relationship between height and wind speed. The Mann model differs from the Kaimal model as it is based on a three-dimensional spectrum tensor representation of turbulence. For this, a 3D FFT is necessary to generate all three components of turbulence at the same time (Burton et al., 2011). Both models have some limitations due to the assumptions and simplifications they make. Both models neglect small-scale spatial variations due to assuming horizontal homogeneity. This is not always true in real life, where wind characteristics can vary on smaller scales as well. Further, the Mann model assumes that the statistical properties of the wind field stay constant over time, which is often not the case as a result of seasonal or diurnal variations. It has been observed that the TurbSim spectrum contains more energy at higher frequencies. In some instances, this leads to too much excitation of higher frequency components, however, comparing a 2D turbulence model to the 3D model with spatial variation created by TurbSim, shows the 2D model does not yield satisfactory results and provides too many errors in the response energy levels of frequencies and output parameters (Bussemakers, 2020).

For the wave spectrum, OrcaFlex allows defining of a few well-known wave spectra into the model, including the JONSWAP spectrum, which has already been introduced.

The vessel motion within the program is defined from load RAOs, which represent the forces and moments acting on the vessel. The RAOs also define a phase, used to describe the motion of the vessel being acted upon incoming waves. With the use of the vessel's mass, inertia, and possibly any other external loads from the EOM, the motion of the vessel can be derived. The Heerema MC owned vessels are already modelled, therefore, the specific load RAOs can be imported. They are imported from WAMIT, a diffraction analysis software, in the same was as for LiftDyn. Within WAMIT, the forces and moments in the frequency domain can be determined. This means that the imported load RAOs in OrcaFlex, are frequency dependent.

Overall, OrcaFlex offers the possibility to perform frequency and time domain analysis of complex offshore systems. Coupling aerodynamic and hydrodynamic loads on the structure is possible to obtain a coupled response.

2.6.3. Software comparison

LiftDyn and OrcaFlex are both viable options to use for the modelling of the investigation. The key difference between the two is that LiftDyn can only perform frequency-domain simulations, while OrcaFlex can also do time domain. Additionally, LiftDyn can produce RAOs based on only wave loading, while OrcaFlex can incorporate the full environmental loading (wind, waves, current) for the static and dynamic analyses. Both of the software solve similarly constructed equations of motion and offer many post-processing options. However, OrcaFlex will be the main software used during the thesis investigation. This is due to the fact that it makes time-domain analyses possible. However, LiftDyn will also be used to perform basic frequency domain analyses of the whole system and modal analyses. The LiftDyn interface makes some frequency domain analysis very easy to perform and, therefore, will be used to obtain the operability curves in the wave-only cases (section 4.1). For the time domain analysis and cases where the wind is also considered, OrcaFlex is the best and only option and will therefore be used. Section 3.5 describes the model used for the base case and the assumptions made. Additional information on the modelling can also be found in Appendix B.

3

System and scenario

In this chapter, the scenario analysed in the thesis is described. This includes the installation procedure, the vessel and wind turbine used, as well as additional components required for the full WTG installation to be physically possible. How the scenario was modelled in OrcaFlex will then be described, and any simplifications and assumptions made regarding the model will be stated.

3.1. Scenario

The scenario which will be analysed is similar to the Arcadis Ost project, for which Heerema MC has been commissioned to install the wind turbines. For the purpose and aim of this investigation, the scenario for the thesis deviates from the Arcadis Ost project; for example, Heerema MC is using the RNA installation method to install the wind turbines, and in this investigation, the single lift method will be looked at.

3.1.1. Location

The location of the Arcadis Ost Project is in the Baltic Sea, 10 NM Northeast of the German island Rügen. The wind farm covers an area of 29 km^2, and its location is shown in Figure 3.1 (marked with a black cross). The water depth in the area is between 40 and 46 m, which is usually too deep for monopiles, however, for this project, XXL-monopiles were used ("About Arcadis Ost 1", 2022). The seabed consists of chalk, glacial clay, and soft soil, making challenging soil conditions, however, the installation operation is floating, and therefore soil conditions are not of great importance. Monopile deflection is relevant for the overall installation procedure, but it was not considered for this investigation, as only the part of the installation when the WTG assembly is free hanging in the air was investigated.

Figure 3.1: Map showing the approximate location of the Arcadis Ost project in the Baltic Sea marked with a black cross (*Google Maps*).

3.1.2. MetOcean data

For some of the installation operations to be possible, the MetOcean data for the specific location is required. Based on the wind and wave spectra described in the previous chapter, the required MetOcean parameters include the mean wind speed, significant wave height, and peak period. In the following sections, some basic analysis of MetOcean data is done for the location in the Baltic Sea. This was done in order to see what the usual conditions are like for different times of the year at the location so that when further analyses were done, relevant MetOcean parameters could be used for the various load cases that were investigated.

Mean wind speed

The average wind speed is based on measurements at 10 m above sea level. The mean wind speed per month was obtained by averaging the recorded wind speed of every month between the years 1979 and 2019. The wind speed was recorded once per hour for every hour of the day and is based on a one minute recording. This aligns with *DNVGSL-ST-N001 - Marine operation and marine warranty*. Figure 3.2 shows the mean wind speed per month between 1979 and 2019. It can be seen that the wind speed during the summer months is significantly lower than during the winter months, meaning operability in the summer is much higher as the chance of waiting on weather decreases. However, the Arcadis Ost project took place during the months of November, December, January, and February, therefore, the winter months were also looked at. The average wind speed during the four mentioned months is 9.08 m/s. The months of June, July, and August have an average wind speed of 6.54 m/s, which is significantly lower than in the winter months. But 9.08 m/s is lower than the limiting wind speed mentioned in Table 2.1 for the various operations. However, the wind speed mentioned in the table refers to the maximum allowable wind speed, while 9.08 m/s is the average wind speed, with recorded wind velocities up to 30 m/s being recorded.

In Figure 3.3, a Weibull distribution has been fitted over a histogram of the mean wind speed for the winter months. This plot more clearly shows that there is still a decently high probability of the wind speed exceeding 12 m/s.

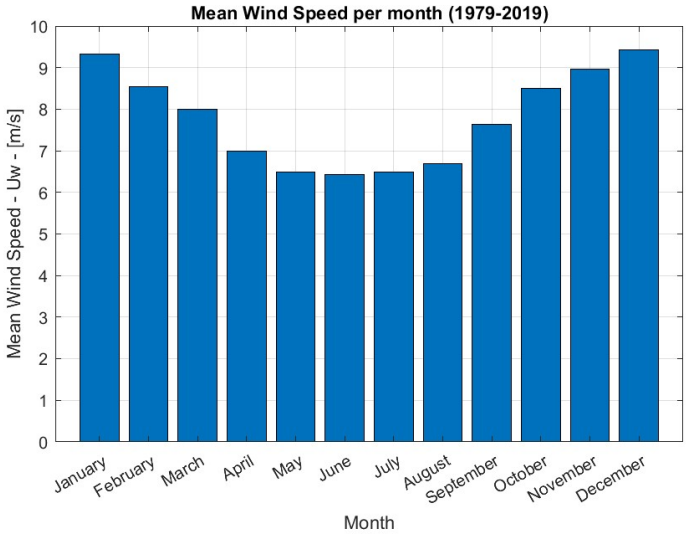

Figure 3.2: Mean wind speed at 10 m height per month at the Arcadis Ost location based on measurements between 1979 and 2019.

Significant wave height

The significant wave height per month based on data from 40 years is shown in Figure 3.4. It can be seen that just like for the average wind speed, the significant wave height is lower in the summer months than in the winter months. From the data, the significant wave height with a 40-year return period is 1.10 m.

The significant wave height data can be grouped and transformed into a histogram. A Weibull distribution can be fitted to the data, as seen in Figure 3.5, which can be used to determine the probability of it exceeding or staying below a certain value. For example, the probability that the significant wave height will be below 1.5 m during

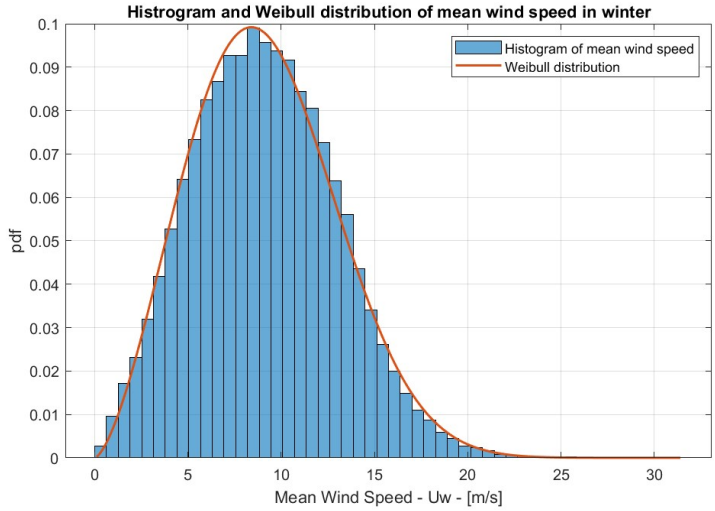

Figure 3.3: Histogram of the mean wind speeds with a Weibull distribution fitted over the data for the winter months at the Arcadis Ost site.

the installation months is 0.751. The value of 1.5 m is considered the limiting significant wave height for RNA installation from Table 2.1, which could potentially also be the limiting significant wave height for the full WTG lift.

The significant wave height in the Baltic is much lower than the significant wave height in the North Sea. In the North Sea the significant wave height can be over 2 m for 60% of the time (Faltinsen, 1990). This is why the installation of the Arcadis Ost project in the Baltic was possible in the winter months. If the project location was in the North Sea, this would not be a possibility.

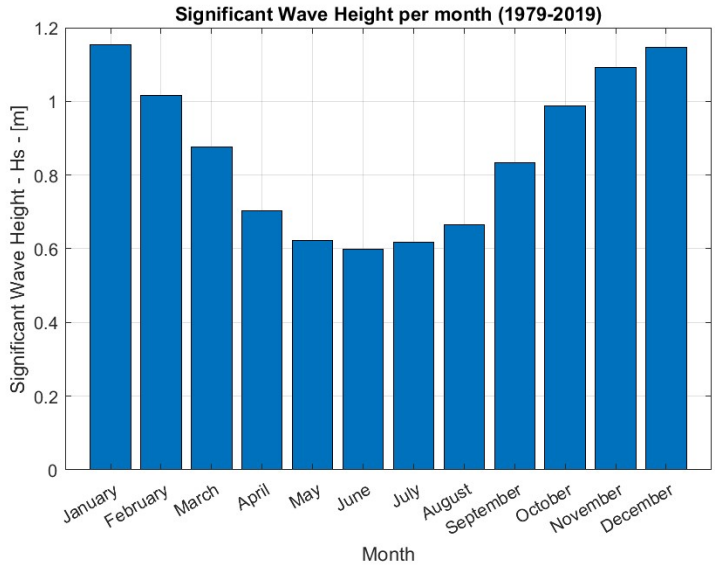

Figure 3.4: Bar chart showing the significant wave height per month at the Arcadis Ost location based on measurements between 1979 and 2019.

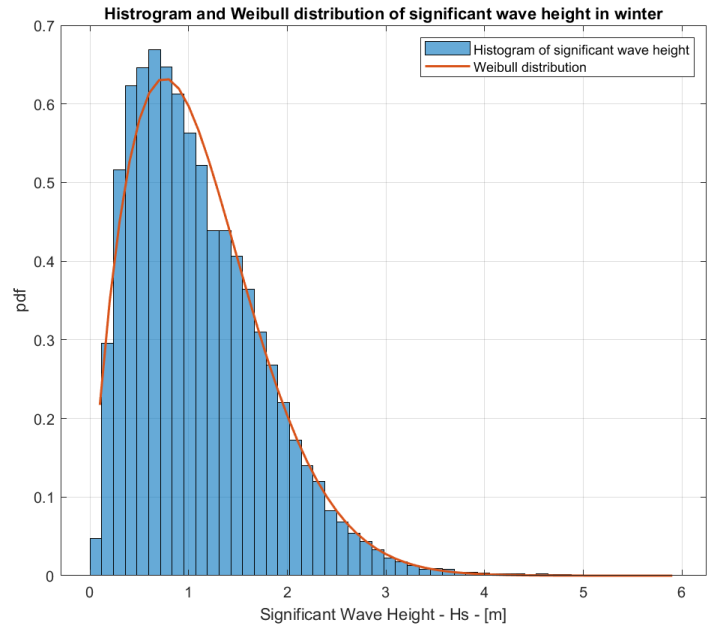

Figure 3.5: Histogram of the significant wave height with a Weibull distribution fitted over the data for the winter months at the Arcadis Ost site.

Wave peak period

The peak period throughout the year at the location in the Baltic Sea ranges between approximately 3.8 and 4.8 seconds. This is illustrated in Figure 3.6, with the winter months having longer wave periods than the summer months. The months of November, December, January, and February have an average peak period of 4.76 s. This value is lower than the natural periods of the vessel (see Chapter 4 for the modal analysis of the Thialf and the system as a whole). This means that the wave frequency range and the vessel's natural periods do not coincide, and can hence, during steady-state conditions, only be excited by nonlinear effects.

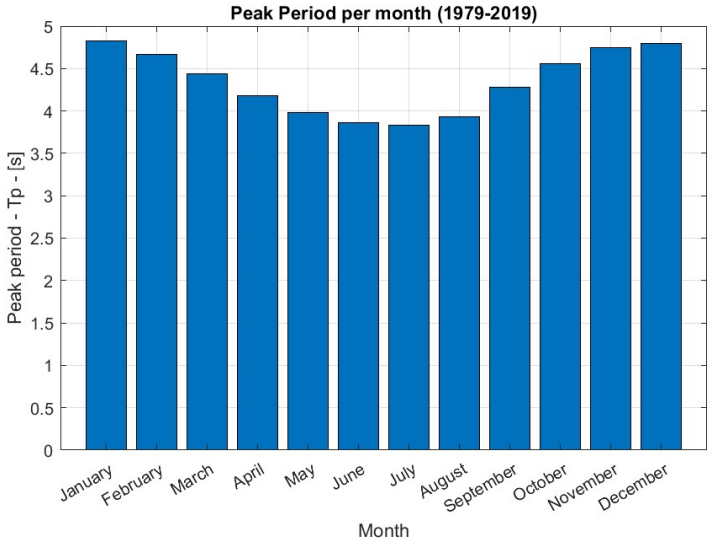

Figure 3.6: Bar chart showing the peak period per month at the Arcadis Ost location based on measurements done between 1979 and 2019.

3.2. Installation vessel

In this section, the semi-submersible vessel, Thialf, and its cranes are described in more detail. The Thialf has already been briefly introduced in subsection 1.2.1, but more specific information is given in this section, along with the crane specifications.

3.2.1. Vessel

The Heerema MC SSCV Thialf is considered in the investigation as the installation vessel. The semi-sub can be seen in Figure 1.2. The vessel is made of two pontoons, each with four columns. It has a dual crane arrangement, capable of lifting 14,200 metric tonnes combined. More information regarding the cranes is given in the following section. The Thialf uses a class III dynamic positioning system and is equipped with six retractable azimuthing thrusters, which are used for propulsion and position-keeping. It can have a draught between 11.8 - 31.6 meters. During transit, the draught is set to around 12 meters, while during lifting operations, the vessel is ballasted to have a draught of around 26 meters. This is done so that the pontoons are submerged, and the effects of wave and swell are reduced. The main parameters of the Thialf are summarized in Table 3.1. Note that the mass of the Thialf excludes the water ballast, booms, and blocks of the crane.

Table 3.1: Main parameters of the Thialf (Heerema Marine Contractors, 2021b)

Parameter	Magnitude
Length overall [m]	201.6
Breadth [m]	88.4
Main Deck Height [m]	49.5
Operational Draught [m]	11.8-31.6
Displacement [m^3]	1.814×10^5
Mass [mT]	79533

3.2.2. Thialf cranes

The Thialf has two cranes mounted on the portside and starboard side of the vessel's stern. Current Thialf crane capacity and lifting height do not make the single lift WTG installation possible for the chosen wind turbines. For the installation strategy to be possible, another Heerema MC concept needs to be utilised, namely the delta jib. The delta jib is a crane extension allowing for lifting new generation wind turbines, which have outgrown the capabilities of currently installed cranes. The delta jib can be seen in Figure 1.5. It is the light blue part of the crane. It allows for the lifting of heavier and higher constructions by reeving the main hoist wires to new positions. With the delta jib, reaching a lift height corresponding to a hub height of the waterline (WL) + 165 m is possible.

3.3. Installation strategy

In this section, the single lift method is explained. The scope of this investigation does not cover the whole duration of the described method, but only the part in which the WTG is free hanging from the crane in the air. This is because the load-in phase and assembly of WTG components on deck have already been studied in detail during other projects Heerema MC has done. For clarity, however, the whole description of the installation process is given. The Upper Stabiliser Frame, along with other rigging components needed during such a lift operation, is described in more detail.

3.3.1. Pre-installation

A barge collects the WT components at a pre-assembly yard, Rønne Port, which is located on the Danish island of Bornholm. The offshore location is 40 nm southwest of Rønne Port. The components of three WTGs (three tower sections, three nacelles, and three sets of three blades) are loaded onto a barge and transferred to the offshore location in the Baltic Sea. At the OWF location, the Thialf waits for the arrival of the barge (Thialf stays in field throughout the duration of the project), and the components, using the cranes on the Thialf, are transferred onto the deck of the Thialf.

3.3.2. Single lift method

The single lift method is essentially the load transfer of the WTG between the vessel crane and the offshore foundation. A labelled diagram of all the components relevant to this installation strategy can be seen in Figure 3.7. The process of the installation that takes place after the components are transferred onto the Thialf is briefly described in the following steps:

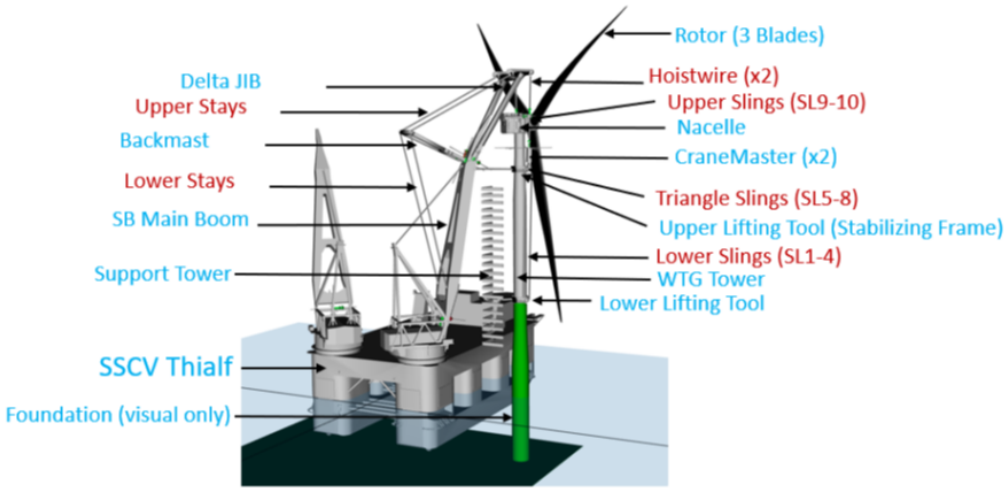

Figure 3.7: Labelled diagram of the full WTG installation scenario.

- The WTG tower sections are assembled with the help of the support tower. The nacelle is then installed on top of the tower, followed by the installation of the blades. The Guided Root End Positioning (GREP) tool and Blade Installation Tool (BIT) are used to help. More on the GREP and BIT is discussed in section 5.2.
- Rigging can be attached once the WTG has been fully assembled. The rigging includes the delta jib blocks, heave compensators (referred to as CraneMasters, used for set-down of WTG on foundation), upper rigging, USF, lower rigging, and Lower Lifting Tool (LLT).
- After the WTG has been securely fastened, it is lifted from the support tower to the installation elevation, and the crane is slewed to hang right above the foundation. The slew angle is kept so to keep the crane tip close to the deck of the vessel.
- The tower's orientation is adjusted with the help of tugger lines. The bolt holes of the tower and foundation need to align.
- The WTG is lowered onto the foundation so the tower bottom guiding system overlaps with the foundation and creates a horizontal restraint.
- The latching/ pull-in system between the tower bottom and foundation is engaged, followed by the tower bottom being pulled down to the foundation. This is achieved by slowly lowering the crane block until the moment when contact is made between the tower bottom flange and the foundation.
- The latching system cylinders are pressurized with a maximum and minimum pressure. This is to avoid overloading the flange during the transfer of the WTG load to the foundation.
- The load transfer occurs by lowering the crane block further. The transfer of the weight is done in steps of 25% until the foundation takes the complete WTG weight.
- The WTG is temporarily secured on the foundation before it is bolted down permanently.
- The crane is then moved out and boomed down.
- Rigging can be released. The first step is to remove the USF by releasing slings and pulling the USF in the direction of the crane using the tuggers connected to the USF.
- The remaining rigging equipment, which will be explained in the following sections, is released together through hydraulics. Tuggers are also connected to the tool and are utilised to control the swinging motions that might arise.
- Rigging is transferred back to deck.

Some benefits of the single lift method have already been mentioned in Chapter 1, such as the reasons why a floating installation vessel is a better choice than an installation vessel that relies on fixating itself on the seabed during installation. A benefit of this specific method, where the WTG gets assembled with the help of a support tower on the vessel, is the fact that relative motions of different components get removed. For example, during a component installation where the tower is already installed onto the foundation, the tower experiences an offset due to the environmental loading. This offset, and relative motion between the tower and the components that need to be installed onto it (nacelle and blades) makes the installation more difficult. However, the relative motions are removed if the tower is assembled in the support tower, which is fixed on the vessel. This simultaneously also reduces the installation time of the whole wind turbine.

3.3.3. Upper stabiliser frame

The main parameters of the USF are shown in Table 3.2. During a full WTG lift, the WTG assembly will experience an anti-symmetric loading from the environmental loads. This will result in, among other things, a rotational force around the Z-axis (vertical). Heerema MC developed the Upper Stabiliser Frame (USF) to restrain this rotational motion. With respect to the WTG assembly, the USF has a translational restraint in the X- and Y-directions, while it is free to move in the Z-direction. It is also free to rotate along the X- and Y-axes, but rotation along the Z-axis is restrained. The reason for free translation of the USF being possible in the Z-direction relative to the WTG is that the USF needs to be able to compensate for the sling's elongation during the tensioning of the rigging. The idea of how the rotational Z restraint should be achieved is currently through friction. Welding of the USF is not allowed. Rotation between the USF and tower is unacceptable, as it could lead to the reduced clearance between the blades of the WTG and the rigging. Another outcome of relative rotation would be that since the concept works with friction, if the tower is turned one way due to applied force, it might not rotate back due to the friction which is present. This friction cannot be overcome without additional force being applied. The loading on the tuggers used to connect the USF to the crane will also experience an uneven loading, and a counter moment of hoists will arise when the USF is rotated.

The USF is part of the rigging used for a full WTG lift, and the rest of the rigging can be classified with reference to the position of the USF. The rigging below the USF is the lower rigging, and the rigging above the USF is the upper rigging. Another functionality of the USF is to transfer the lift points to a point that is above the combined WTG CoG and also to transfer the horizontal lifting loads to the tower. Horizontal lift loads arise due to the sidelead and offlead angle made with the crane. Figure 3.8 shows several views of the USF with specific dimensions. From the diagrams, it can be seen that there are four upper and four lower lift points to which slings are connected. The lower slings are connected to the LLT, and the slings above are part of the triangle slings connecting to a shackle, as seen in Figure 3.7.

Table 3.2: Main parameters of the USF (Rentoulis, 2022)

Parameter	**Magnitude**
Weight [mT]	110
CoG [m]	[0,0,0]
Radii of gyration [m]	[3.54, 3.54, 5]
No. of lift points	4 upper, 4 lower
Dimensions (L$\times$B$\times$H) [m]	$18 \times 10 \times 3.5$
Transverse distance lift points [m]	4.0
Longitudinal distance lift points [m]	18.0

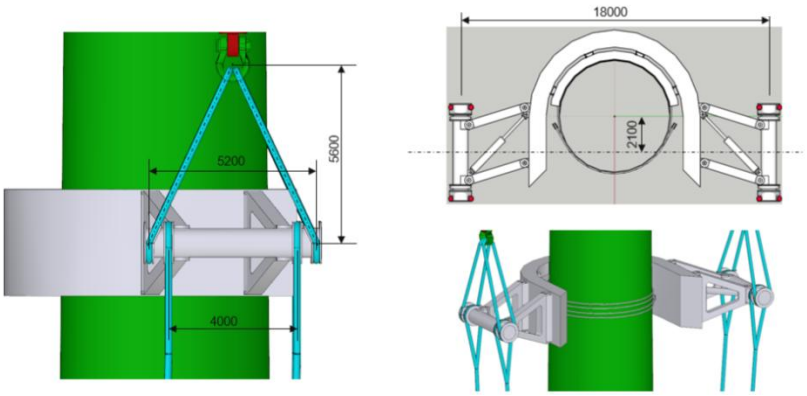

Figure 3.8: Detailed drawings of the USF with specific dimensions.

3.3.4. Other components

In order to safely secure the WTG while it is being pre-assembled on deck of the Thialf, and also while it is being lifted onto the foundation, components other than just the USF are required for safe fastening. Some of these components are explained in the following sections. The equipment that will be used is not allowed to cause damage to the WTG, for example, coating damage, and also its weight should be minimised, as it contributes to the overall capacity requirement of the crane.

Support tower

The support tower is located on the Thialf and is used during the assembly of the WTG to give support to the tower and the rigging arrangement. It helps the working of the GREP, which is used for blade installation. The reaction forces at the bottom of the WTG tower are decreased due to the clamp, which is located near the top of the tower. The support tower also contains bumpers for the set down of the tower and winches to help aid the installation of the middle section of the WTG tower. It is located on the starboard side of the vessel, from which the SB crane can easily lift the WTG assembly.

Lower Lifting Tool

The Lower Lifting Tool (LLT) was created and is used with the purpose to transfer the vertical WTG lifting loads into the tower bottom flange during the lifting. It is supposed to reduce the impact load during set down while providing stability. It should help with obtaining the correct orientation so that the bottom flange of the tower and the flange on the foundation connect. It has 4 lift points, which need to be evenly loaded during the lift. The 4 lift points allow for a connection between the LLT and USF to be made. The LLT is pre-installed onto the tower bottom section on the Thialf and can be removed once the foundation is securely installed on the foundation. It is removed by opening the hinge in the center. The estimated weight of the LLT is 200 mT and it has a diameter of 9 m. Power to the LLT is provided via an umbilical, connected to the Thialf. The centre of gravity of the LLT is 1 m above the centre base of the tower (Rentoulis, 2022).

Damping tuggers

Damping tuggers connect the boom of the starboard crane with the USF. They are required as they decrease the motions of the WTG relative to the crane boom. Two tuggers are connected from the centre of the USF to two points on the crane boom.

Damping tuggers dampen the oscillations of the WTG hanging from the crane, which are caused by the movement of the vessel and crane tip. Without damping tuggers, the oscillations could exceed operational safety limits and lead to uncontrolled motions and large loads on the WTG components.

Passive heave compensation system

A passive heave compensation system, labelled as CraneMaster in Figure 3.7, is important during set down to prevent a hard impact between the bottom of the tower and the foundation. With the whole WTG being installed onto the foundation, when the load transfer stage is taking place, any crane tip-induced motion will result in

highly dynamic forces. The rigging at this point is still under tension and, therefore will be greatly affected by the dynamic forces. This is outside the scope of the investigation and, therefore, will also not be modelled.

Slings

Slings used for offshore lifting operations are made of high-strength materials. They can withstand extreme conditions that can be encountered offshore. The slings connect various rigging components to each other, and each has a specified axial stiffness. All the slings are connected to the lifting equipment in a way that the load is distributed evenly and so that any snagging, in the case of the slings becoming slack, is prevented.

Crane block

There are two crane blocks used. Each crane block is connected to a hoist wire. The main purpose of the crane blocks is to redirect the force direction and increase the lifting force, which enables the crane to lift the heavy loads. The blocks connect to the sheaves on the crane boom above. The blocks are reeved into 16 parts per block from the main drums.

3.3.5. Limiting parameters

The importance of limiting parameters or limiting criteria has already been mentioned in section 2.1. The limiting parameters should not be exceeded during operation as otherwise, safe operation cannot be guaranteed. The full WTG installation involves a difficult offshore lift, which is very susceptible to motions being excited by the environmental loading. For this installation strategy, many different limiting parameters can be identified, which, if limits are exceeded, would lead to unsafe operation. Some criteria pertain to limits set by manufacturers of the various components, for example, the nacelle acceleration limits. These limits must be obeyed so that the components within the nacelle do not get damaged. However, due to the scope of this investigation, such limits will be disregarded and assumed not to be exceeded.

The relevant limiting criteria for this investigation include various rotations and translations of the WTG when being lifted and limits related to the cranes. Heerema MC has already determined the limiting criteria for the full WTG installation lift to be used for the frequency domain analysis in LiftDyn, however, these limits could be subject to change in the future while various design iterations are tested. A table with an overview of the limiting criteria can be seen in Table 3.3. These limits will be used for the analyses in OrcaFlex as well.

Table 3.3: Limiting parameters used in LiftDyn to generate operability curves for the single lift operation. The limits are given as maximum allowable values/magnitudes (Rentoulis, 2022).

Parameter	Value	Description
Roll [deg]	0.5	Vessel roll
Pitch [deg]	0.5	Vessel pitch
Sidelead [deg]	2	Crane sidelead at each hoist
Offlead [deg]	2	Crane offlead at each hoist
XY tip[m]	1.5	Horizontal motion of the WTG bottom
Z tip [m]	0.5	Vertical motion of the WTG bottom
Clearance nacelle [m]	2	Relative horizontal motion between crane sheaves and the nacelle

3.4. Wind turbine

For the Arcadis Ost project, the Vestas V174-9.5 MW turbines have been used. For this investigation, it has been decided to consider a larger turbine, namely a 17 MW wind turbine. 17 MW wind turbines are currently not yet being used, however, based on the growth of wind turbine size in the past years, 17 MW wind turbines will become available in the near future. The 17 MW wind turbine being considered has blades 122 m in length and a rotor diameter of 250 m. The tower has a height of 134 m, with 34 m of the tower already pre-installed. The material of the tower is steel S355. The WTG has a dry weight of 2000 mT and a hub height of 165 m.

3.5. OrcaFlex model

In the previous section, the various components of the system that were looked at in this investigation were introduced. Some of the mentioned components were not modelled as it was assumed they would not greatly affect

the outcome of the investigation. The main simulations of this investigation were run using OrcaFlex, therefore, the OrcaFlex model is introduced in more detail. The corresponding LiftDyn model is introduced in section 4.1. In this section, the way the components were modelled in OrcaFlex and any assumptions that have been made regarding the modelling are discussed and justified.

The OrcaFlex model is created by running a Python script in which a Universal Model of the system is created, and the systems statics are solved in AGES, which is an in-house Heerema MC software. The Universal Model environment refers to a Python package aimed at creating a framework between existing general modelling applications within Heerema MC. The visual representation of the system in the Universal Model interface can be seen in Figure 3.9. Once the statics are solved, the results can be exported to OrcaFlex.

The system is made up of many bodies with 6 DoF. The final system is a multi-body system with multiple degrees of freedom. For some of the bodies, some degrees of freedom have been constrained, while others are left free. The different bodies are either rigidly connected to each other or have constraints placed on them to limit rotations or translations. Specific constraints are presented in Appendix B in Table B.6. Each body in the system has its own local body reference frame, with its origin fixed at the body's centre of mass (CoM). These specific reference frames will be used when discussing the forces and moments of a particular body. The vessel reference frame, which will be introduced in this section, also serves as the environmental reference frame that determines the wind and wave directions.

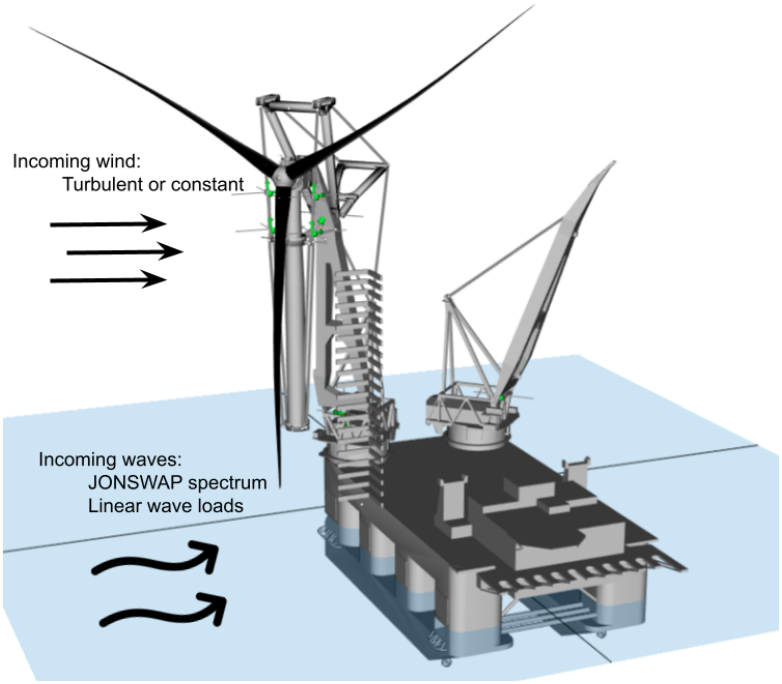

Figure 3.9: Visual representation of the Universal Model of the system, which is used to calculate the system statics.

Wind turbine

In the OrcaFlex model, the wind turbine modelled is an upscaled version of the 15 MW NREL wind turbine. The 15 MW NREL wind turbine is a reference wind turbine used in the industry for basic modelling and research purposes (Gaertner et al., 2020). The 15 MW wind turbine has a rotor diameter of 240 m and acts as an open-source model with detailed WTG properties available to the public. The NREL wind turbine has already been scaled up to a rotor diameter of 250 m to represent a 17 MW wind turbine by Heerema MC. From this, the aerodynamic properties could be derived. The blade is divided into 50 segments, with each segment having its own geometric properties. These geometric properties can be found in Table B.1 in Appendix B. The specific WTG parameters of the model can also be seen in Appendix B in Table B.2. It must be noted that the height of

the tower being lifted is shorter than the blades, and that is because a part of the tower is already pre-installed on the foundation.

Thialf

The model of the Thialf used in this investigation was based on hydrodynamic data of the Thialf, which has been derived from the HMC Thialf standard hydrodynamic database for shallow water (39 m depth). The operational draught is 22 m in all the simulations. Additional data regarding the way the Thialf is modelled, such as the damping and stiffness coefficients are considered classified information by Heerema MC, and therefore not shared.

The vessel function in OrcaFlex is used to model the Thialf. Hydrodynamic properties are applied to the hull of the vessel. The included effects in the calculation of loads on the Thialf include wave loads (1st order), added mass and damping, and additionally applied damping in the form of linear damping to account for the viscous part of the damping. The first-order wave loads are calculated from the load RAO data imported from WAMIT. It has been decided to omit any second-order effects for simplification and also because it was assumed their effects on the vessel would be limited due to the nature of the waves that were considered. More information regarding the waves simulated is given in subsection 3.5.1, where it is seen that non-steep waves were used. In non-steep wave environments, the nonlinear part of the wave-vessel interaction is usually less significant than in steep waves. Due to this, it was expected that second-order effects would be small compared to linear effects and could be omitted without greatly influencing the accuracy of the results. The primary motion of the Thialf is treated as wave frequency. To get a proper visual representation of the Thialf, a shaded drawing is imported. The shaded drawing is a visual file created in the Universal Model to give the Thialf the right shape. The mass of the Thialf is 79533 mT, in which the inertia data of the ballast water, booms, and blocks are excluded. The CoG of the vessel with respect to its local coordinate system, which will be defined in the following sections, is $[78.01, -0.05, 30.81]$ m.

Thialf's DP system is also modelled in OrcaFlex through various links that represent the real DP system data. The specific data is shown in Table B.3 and further details on how the modelling of the DP system is done are also discussed in Appendix B. Any kind of system damping has been disregarded and only linear stiffness is included.

Vessel coordinate system

The vessel coordinate system can be seen in Figure 3.10. The positive X-direction is towards the bow and it has its origin at the stern. The positive Y-direction is towards PS and the origin is at the centre line. The positive Z-direction is upwards and the origin of it is the keel. The surge, sway and heave directions for the vessel are fixed (Orcina, 2022). From this coordinate system, a reference frame for the wave and wind directions can also be defined. Following seas have an angle of 0 degrees and go from aft to forward. Beam seas have an angle of 90 or 270 degrees with the vessel. Head seas refer to an angle of 180 degrees (negative X-direction) and go from forward to aft. The definition of these directions is visually represented in Figure 3.11.

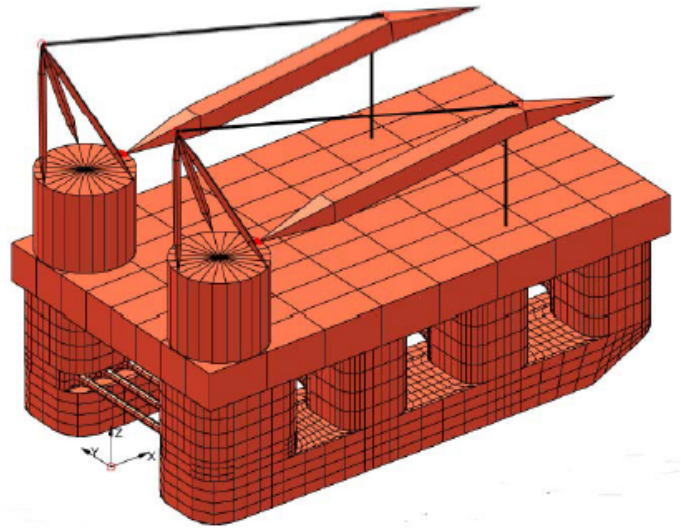

Figure 3.10: Thialf coordinate system (Heerema Marine Contractors, 2021b).

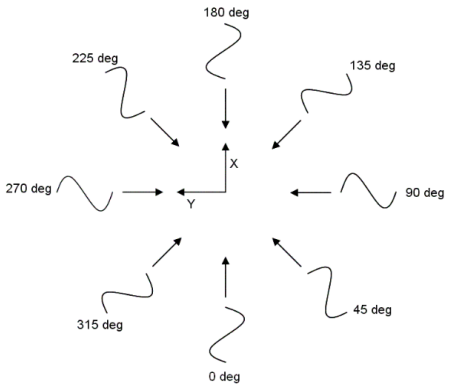

Figure 3.11: Wave and wind heading definition with respect to the vessel global coordinate system (Heerema Marine Contractors, 2018a).

Cranes

For the installation, the starboard crane will be used. A slew angle of 315 degrees is assumed, and with the delta jib extension, the crane radius is 65 m. The definition of the slew angle is illustrated in Figure 3.12. The boom angle is 79.5°, and the position of the Thialf is so that the crane tip is exactly above the CoG of the WTG (2.1 m from the monopile centre line).

In OrcaFlex the cranes are modelled as 6D buoys, with again shaded drawings imported from Universal Model for visual representation. The original cranes consist of one crane boom. The delta jib is modelled as an additional two 6D buoys rigidly attached to the original crane boom of the starboard crane. One of the additional buoys is referred to as the jib and the other one as the back mast. For stability, stays are also modelled as winches connecting the various crane components and the crane house. More information regarding the starboard crane inputs can be found in Table B.4.

USF

In the base case scenario, the USF is modelled as a rigid body with a specified mass and constraints between the tower and USF, which allow only for heave motion between the two. This means horizontal translations and all rotations are constrained. Table B.6 gives an overview of the specific constraints for the degrees of freedom of the USF in the OrcaFlex model. It is modelled as a 6D buoy and is connected to the tower at a point 70 m from the bottom of the tower. It has a mass of 110 mT and has 4 lift points, which connect down with the LLT through slings (two on each side), and connect up to a shackle.

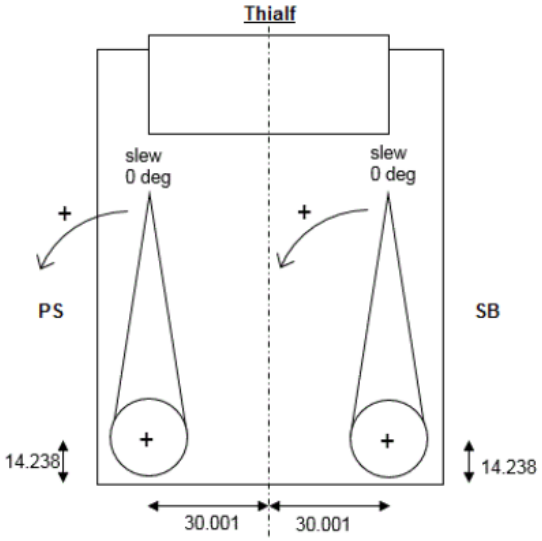

Figure 3.12: Diagram of the Thialf from the top, with the slew angles of the cranes defined (Heerema Marine Contractors, 2018a).

LLT

The LLT will also be modelled as a 6D buoy in OrcaFlex, representing a rigid body with a certain mass. The LLT will not have specific translational or rotational constraints like the USF, however, it will be rigidly connected to the tower, meaning its motions will be governed by the motions of the tower. The mass of the LLT is 200 mT.

Winches

Winches are used in OrcaFlex to represent slings, hoist wires, and tuggers. They are each modelled with a certain stiffness and initial length, in which the model is in static equilibrium. For more detail regarding the properties of the winches used in the model, Table B.5 can be looked at.

The damping tuggers are modelled in OrcaFlex and connect the origin of the USF to two points on the SB crane boom. They are assumed to work perfectly and not add stiffness to the system. They have a linearized damping value of 15 mTs/m per tugger. In OrcaFlex the damping coefficient has units of seconds. This way the damping force that is applied to the WTG attached to the tuggers is proportional to the velocity of the winch drum. This allows for the damping effect to be similar to the behaviour of the damping tuggers in real life.

Shackle and crane blocks

The shackles and blocks will be modelled as 6D buoys. The shackle 6D buoy will be a point with negligible mass, while the blocks will be cubes with a mass of 70 mT each. Four slings, two on each side of the USF will connect at the point (0,0,0) of the local coordinate frame of the shackles, as seen in Figure 3.13. Then, from the same point, a sling will connect the shackles with the crane blocks. Due to the connection being made in such a way, constraints of the shackle are required. The constraints essentially limit the rotational motion of the shackle, and allow only translation in the X-, Y- and Z-directions. Figure 3.13 shows a schematic representation of a shackle connected to 3 slings, like in the model and its local coordinate system. The rotational degrees of freedom labelled in the diagram are not possible in the model. It should also be noted that the shackle in the diagram is not representative of the actual shackle used for this operation but serves purely a visual purpose.

The blocks also have the same rotational constraint as the shackles, meaning that again only translations in the X-, Y- and Z-directions are possible.

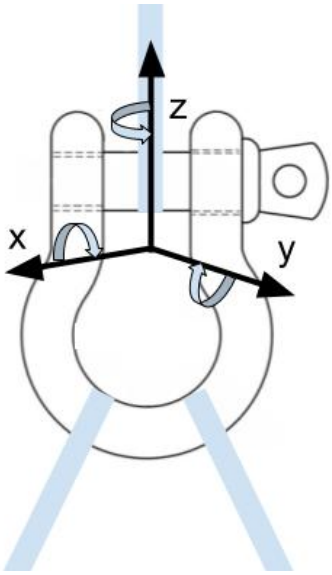

Figure 3.13: Schematic diagram of the shackle and sling configuration. The local coordinate system of the shackle is shown, of which all the rotational degrees of freedom are constrained in the OrcaFlex model. In the model, all the slings connect to the shackle at the same point, but they do not connect to each other.

3.5.1. Environment

The environment in OrcaFlex refers to the environmental conditions. For the simulations in this investigation, only the wind and waves will be considered from the possible environmental loads. The JONSWAP spectrum, as already mentioned in Chapter 2, will be used for wave modelling. While JONSWAP is not based on conditions in the Baltic Sea, it has been decided to use it anyways, as it generates sufficiently acceptable waves for the purpose of the thesis and it can easily be defined in both LiftDyn and OrcaFlex. The value of the significant wave height and peak period will depend on the load case being investigated. From the brief MetOcean analysis done earlier in this chapter, it has been found that the significant wave height is likely to be around 1 m at the location in the Baltic Sea, and therefore this value will be investigated. From Table 2.1, it can be seen that 2 m was the limiting significant wave height for tower installation. This value will be the largest value of the significant wave height investigated in this thesis. Further, a low value of the significant wave height, 0.5 m, is also considered to represent calmer seas. As for the peak period, a low value of 4 seconds is considered, but longer wave periods are considered as well, as the semi-submersible is more susceptible to wave excitation from waves with longer periods. The response of the Thialf and other components under such excitation is of interest for the analysis. Since a simplified analysis of the system is done, only one seed number is considered for all simulations (assumed stationary process).

For the mean wind speed at 10 m height (U_{10} as introduced in subsection 2.2.2), three different speeds are considered; 5, 10, and 12 m/s. 5 m/s should represent a low wind speed, 10 m/s an average wind speed and 12 m/s, the limiting operational wind speed. The mean wind speed at 10 m will be further denoted as U in this thesis. It has been mentioned that TurbSim will be used to generate a spatially varying turbulent wind field, however for some analyses, also a constant and uniform wind field will be used, for example in subsection 4.2.1, where the optimal blade pitch angle for installation is investigated. The turbulent wind consists of a stationary (mean) part and a wind gust. The wind gust is the part that causes a spectrum.

3.5.2. Load cases

For this investigation, several load cases were considered. The design load cases were defined for time domain simulations. The load cases have been chosen specifically for the numerical study that is done in this thesis and do not come from design codes. In the load cases several environmental parameters, but also model parameters, are varied. These include the incoming wind and wave directions, the wind velocity, the type of wind field, the significant wave height, the peak period, and also the blade pitch angle. An overview of the load cases can be found in Table D.1.

It was chosen to consider all the different wind and wave directions as illustrated in Figure 3.11, in order to obtain results for different kinds of seas (following, beam, quartering, head) and incoming winds. Furthermore, different mean wind speeds were considered to see the effect of the wind magnitude on the operation. The chosen speeds and the values for the peak period and significant wave height have been briefly justified in the previous section. The different combinations per load case depended on the analysis which was being conducted with the load case.

For all time domain simulations, it has been decided that a duration of 3600 seconds was required to yield satisfactory results. Furthermore, an additional 300 seconds were simulated before, which were disregarded during the post-processing to avoid taking transient effects into account. It was assumed that transient effects disappeared after the initial 300 seconds and that the system became stationary thereafter. A time step of 0.1 seconds and the implicit time domain method in OrcaFlex were used.

4

Base case scenario

In this Chapter, the base case scenario was modelled, and frequency and time domain simulations were run using LiftDyn and OrcaFlex. Different cases, wind-only, wave-only, and wind and waves, were considered to see how specific environmental loads influence the behaviour of the system. The results of the simulations are presented and discussed. Base case scenario refers to the system being modelled as described in section 3.5, where the USF and tower are rigidly connected and no relative rotation between the two is possible.

4.1. Wave-only

A wave-only scenario is investigated to get a better understanding of the impact the wave loading has on the overall system behaviour. The model used for the wave-only case is the whole model as described in Chapter 3. Both OrcaFlex and LiftDyn were used. The main time domain simulations were done in OrcaFlex, while some basic frequency domain analyses were completed in LiftDyn. The model used in LiftDyn can be seen in Figure 4.1. The LiftDyn model is generated in a similar way to the OrcaFlex model, where a Python script is run to create a Universal Model and then exported to LiftDyn. The statics of the system are also solved through AGES (Heerema MC in-house software). The frequency domain post-processing is then done in LiftDyn or through additional MatLab or Python scripts reading the outputs from LiftDyn. A difference with respect to the OrcaFlex model is that the rotor is modelled as a rigid body without aerodynamic properties. This is because the wind is not being considered for this analysis. The blades are modelled with the same properties (e.g. mass, CoG, radii of gyration, etc.) as the actual blades, however without the addition of aerodynamic coefficients. In the Python script, the hydrodynamic parameters of the vessel are added. These parameters have been derived by WAMIT. Additionally, the DP system has been modelled by specifying an additional damping matrix with correct damping values based on the real Thialf DP system. In both OrcaFlex and LiftDyn, second-order wave effects are not considered. The script also defines various variables, such as the water depth and Thialf draught, with which the Thialf can be correctly ballasted, based on real ballast data collected from Heerema operations with the Thialf. A water depth of 40 m and a draft of 22 m was used for the Thialf. The global coordinate system can be seen in Figure 3.10. This coordinate system was used to define the wave direction. Since the slew angle was stated to be 315 degrees, it means that the WTG is facing in the direction of 135 degrees. This means that when head sea waves were being simulated, the WTG faced 45 degrees away from the incoming waves. The standard approach of LiftDyn with regards to the damping in the model has been used, meaning the minimum damping is set to 1.5% of the critical damping. This is required to avoid undamped modes which could result in unrealistic responses. 1.5% of the critical damping is applied to any element on the diagonal of the system damping matrix which is less than that (Heerema Marine Contractors, 2018a). With LiftDyn a modal analysis and a frequency domain analysis can be performed.

4.1.1. Modal analysis

A modal analysis allows for a better understanding of the system's dynamic behaviour. The methods which LiftDyn and OrcaFlex use to solve for the periods of the modes of the system have already been explained in section 2.6. The added mass matrix of the Thialf is frequency-dependent, which means that the added mass at the natural frequency must be used in the eigenvalue calculations. The problem is that before solving the eigenvalue problem of the system for its natural periods, the natural period is not known, therefore, the correct value of the

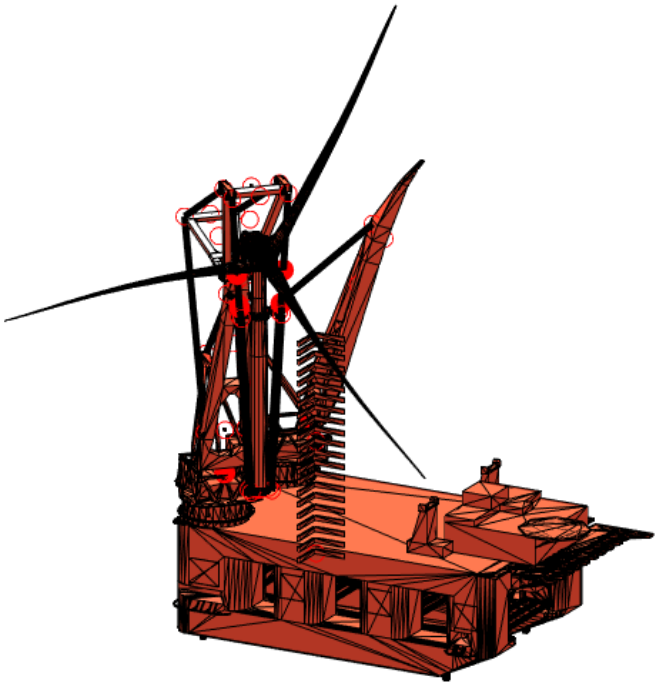

Figure 4.1: LiftDyn model, based on input from the Universal model, of the full WTG lift. This model was used for the wave-only simulations in the frequency domain.

added mass is also not known. LiftDyn uses an iterative approach to find the natural periods. Initially, LiftDyn uses the median of the frequency range for which the added mass is available. The hydrodynamic database from which the Thialf added mass is taken from has available added mass and damping values for frequencies between 0.025 rad/s and 2 rad/s. This results in the median frequency being 1 rad/s. For each obtained mode, the analysis is repeated using the added mass at the corresponding natural frequency. This step is repeated until the natural frequency becomes constant to two decimal places. OrcaFlex does not take into account the frequency-dependent added mass of the Thialf, but instead, the infinite added mass, which leads to slightly different natural periods of the Thialf and the system when determining them in OrcaFlex than when the same is done in LiftDyn. It has been chosen to use LiftDyn to perform the modal analyses.

The natural periods of a structure or a system are a relevant phenomenon to be studied, as the periods govern, to an extent, the behaviour of the system in waves. Critical modes should be shifted outside the wave frequency range if conditions permit (Journée and Massie, 2001).

Thialf modal analysis

When a modal analysis is done for just the Thialf (without the WTG assembly and cranes), the natural periods of the six degrees of freedom of the Thialf are obtained. In LiftDyn, the eigenvalue of the system is solved by setting F_c in Equation 2.29 to 0. Since an iterative approach is used in LiftDyn, as explained earlier, a value of 1 rad/s is used as ω for the added mass in the first iteration. The resulting natural periods from the analysis are presented in Table 4.1.

The Thialf has a draft of 22 m during the installation operation, and therefore a large portion of the vessel is under the free surface, making it less susceptible to wave-induced motions. Waves that pass under the vessel can cause the pitch, roll, and heave motions of the vessel due to the waves interacting with different parts of the vessel hull. It can be seen that the yaw, surge, and sway natural periods are all over 150 seconds, and hence far away from the frequency range of the incoming waves. Roll, pitch, and heave have much lower natural periods, around 20 seconds, and are therefore more susceptible to being excited under the incoming waves, especially if waves with longer periods or swell waves are being encountered. In such situations, the natural periods of the vessel, become excited or amplified by the incoming wave forces. While the incoming waves could only cause

linear effects on the system, it should be investigated in the future how second-order effects, such as difference frequency effects could excite the long vertical modes (heave, pitch and roll), or the even longer horizontal modes (surge, sway and yaw). As mentioned before already, it was decided not to incorporate second-order effects in the analyses in this thesis for simplification and also because non-steep waves were considered.

The natural periods of the Thialf are important, as their excitation could lead to unsafe operation under specific sea states due to resonance occurring. Therefore, careful consideration has to be taken into determining under what kind of waves the excitation of the various motions is still acceptable for executing the installation of the offshore wind turbines so that the crew and equipment on board the Thialf remain safe and protected from the various effects of the environmental forces. In the case that a wind field is also considered, the wind must also be closely monitored, as given the natural periods of the Thialf, they can potentially also be excited by wind gusts depending on the related frequency content.

Table 4.1: Natural periods, T_n of the Thialf calculated in LiftDyn.

Mode	T_n [s]
1 Yaw	199.62
2 Surge	162.92
3 Sway	159.79
4 Roll	24.07
5 Pitch	19.84
6 Heave	16.93

Whole system modal analysis

A modal analysis of the whole system as pictured in Figure 4.1 has also been conducted. The system has natural periods as low as 0.02 seconds. The table of the critical modes and the corresponding periods is presented in Table 4.2.

Table 4.2: Critical modes and their corresponding periods, T_n, for the whole system.

Mode	T_n [s]
7 WTG yaw	15.53
8 Side ward pendulum	12.54
9 Forward pendulum	12.01
10 Thialf heave	11.39
11 Side ward pendulum	4.81

Critical modes include modes with natural periods within the wave frequency range for the wave-only analysis, however, for the combined wind and wave loading, the modes within the wind frequency range are also of relevance. This corresponds to natural periods between 2-15 seconds for waves and between several seconds to minutes for wind. Such modes have a higher chance of being excited than modes with periods outside that range. This means for a wave-only scenario, the yaw, surge, and sway of the vessel are unlikely to be excited. Considering the system, the most relevant motions that should be limited include pendulum motions of the WTG, and also the yawing of the WTG (rotation around its Z-axis). The critical modes have been identified and their effect discussed.

From the modal analysis, it was found that the WTG in the rigging arrangement can result in pendulum and double pendulum motions if excited at the right frequency. This is due to the slings running from the crane to the crane jib blocks and continuing to the LLT. It has also been observed that double pendulum motions are also possible due to the shackles. However, such pendulum motions are only excited at periods of less than 0.1 seconds, which is not relevant for the environmental loading. It must also be noted that there is a difference in the natural periods of the forward-backwards pendulum and the sideward pendulum. Usually, for pendulums, this is not the case, but due to the WTG hanging from two hoist wires, there is no symmetry. A sideward pendulum is defined as swinging in the Y-direction of the WTG (parallel to the rotor plane), while a forward pendulum is

in the X-direction of the WTG (perpendicular to the rotor plane). The sideward pendulum of the USF and LLT is the most critical for excessive WTG tower bottom tip motions. The sideward pendulum is in phase, meaning both hoist wires swing in the same direction simultaneously, and has a natural period of 4.81 seconds. With this natural period, it can easily be excited under the incoming wind and waves. Another sideward pendulum is excited at a period of 12.54 seconds and is critical for the USF motions. The magnitude of excitation of this pendulum motion is lower than the one with a period of 4.81 seconds. It must be remembered that excited motion at resonance depends on not only the excitation load but also the damping. A forward-backwards pendulum is also excited in the wind and wave frequency range. It has a natural period of 12.01 seconds and can also cause excessive USF motions. Other critical mode shapes include the WTG yaw (natural period 15.35 seconds) and the heave motion of the Thialf, which also excites the up and down motion of the WTG.

Having identified critical modes of the system and their natural periods, it can be seen that additional attention must be paid to the pendulum motions. Many of the limiting parameters, as presented in Table 3.3, relate to the WTG motions which are induced by the pendulum motions. The identified pendulum mode shapes all fall within the incoming wind and wave frequency range, suggesting a high likelihood of resonance occurring for those modes. This is highly unwanted and solutions to reducing these motions or changing the natural periods of the modes need to be considered. The natural periods can be changed by changing the lengths of the slings and hoist wires involved. This is a possibility since the natural period of a single pendulum, given in Equation 4.1, suggests that a longer pendulum length would lead to longer natural periods.

$$T_n = 2\pi\sqrt{\frac{L}{g}} \tag{4.1}$$

In the equation, L represents the pendulum length and g the acceleration due to gravity. The pendulum length can be increased/decreased by changing the crane tip height for some of the modes. However, increasing the natural period might not necessarily remove the possibility of resonance, especially if real environmental conditions are considered, where swell is also part of the incoming waves. Swell waves tend to have longer periods, and hence increasing the periods of the modes might not solve the issue directly. It has been decided for the purpose of this investigation to stick with the original configuration of the system, however, for future investigations more attention should be paid to the modal analysis and how to avoid resonance of the system. An alternative would be to also consider the feasibility of a damping mechanism, which affects the response at resonance. The aim of the damping mechanism would be to limit the excitation of the system as much as possible.

4.1.2. Frequency domain analysis

In LiftDyn, a frequency domain analysis can be done, from which the results can be used to obtain operability curves based on limiting parameters. Heerema MC has already conducted a basic FD analysis for the full WTG lift in LiftDyn and for verification, the same analysis is repeated to confirm the results that have already been obtained. The specifics of the analysis are further explained in Appendix D.

For the FD analysis, several sea states are considered which consist of various H_s and T_p combinations. However, it has been decided to stick to a limiting H_s value of 2 m for the full WTG lift operation. As explained in Appendix D, *DNVGL-RP-C205* is used to determine the specific H_s and T_p limits, which can be seen in Figure 4.2.

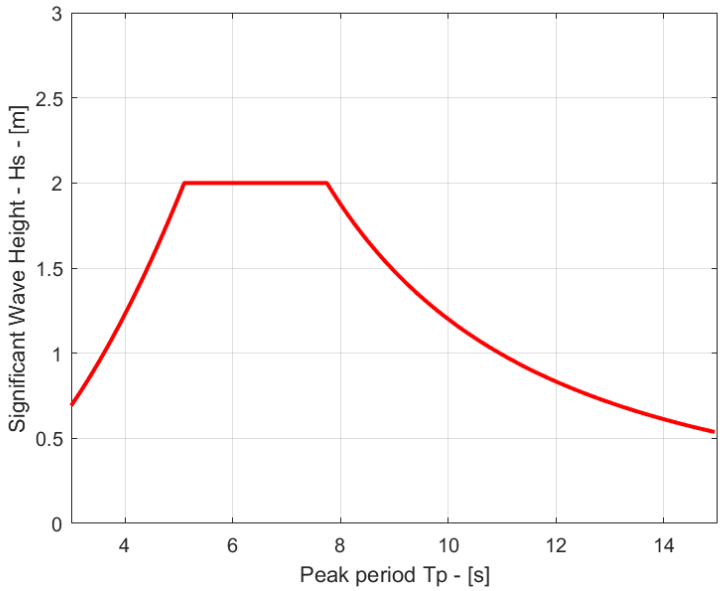

Figure 4.2: $H_s - T_p$ combinations used for the frequency domain analysis in LiftDyn of the full model.

Operability curves

As already stated, the operability of the installation strategy can be obtained based on a frequency domain analysis in LiftDyn. For this, the limiting parameters and their limiting values need to be determined before operability curves can be created. The limiting parameters have already been presented in Table 3.3, and so, the operability curves generated in LiftDyn have been based on them.

The operability curves are created for wave directions between 0 to 360 degrees, with bins of 45 degrees. The operability curve for 180 degrees is shown in Figure 4.3. The other operability curves can be found in Appendix D.

All the operability plots for the different incoming wave directions show similar results. Operability is quite high up to a peak period of around 10 seconds. At this point, the allowable significant wave height reduces to around 1 m for most directions. This shows the system is sensitive to swell and longer wave periods in general. At high peak periods, the nacelle clearance is the governing limiting parameter for all wind directions. At lower peak periods, the vertical motion of the WTG tip (Z tip) becomes governing for some directions.

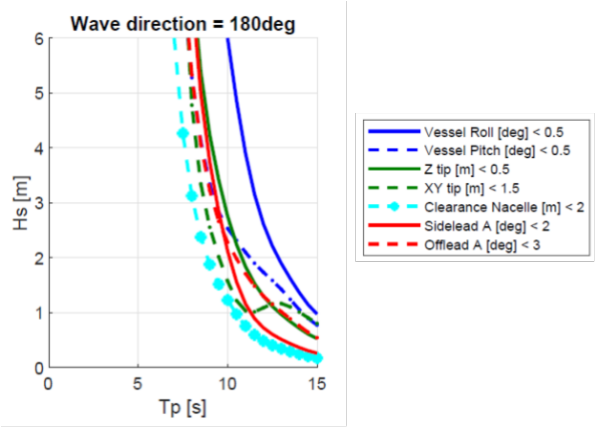

Figure 4.3: Operability curve for the wave-only case, with an incoming wave direction of 180 degrees.

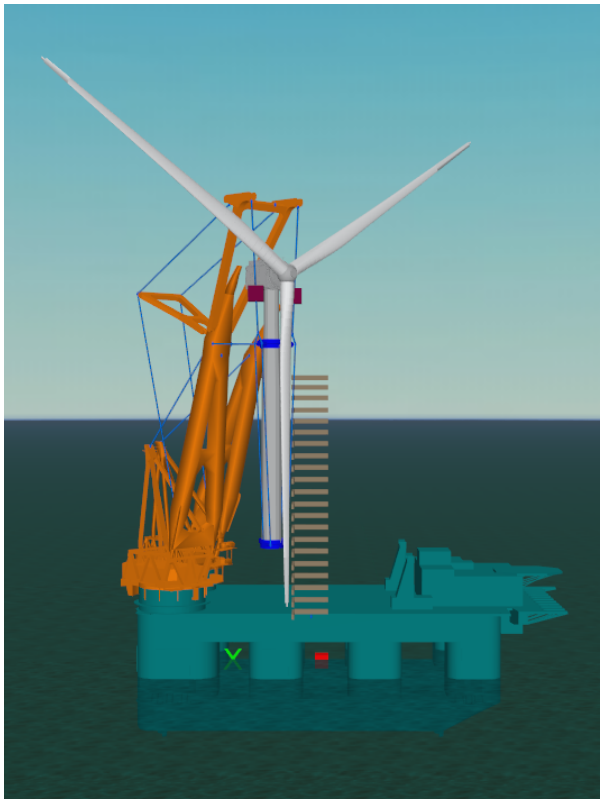

Figure 4.4: Model of the whole system in OrcaFlex.

4.1.3. Time domain analysis

An OrcaFlex time domain analysis was done, where several load cases with different incoming wave directions were tested. The wave direction was varied from 0 to 315 degrees in bins of 45 degrees and the response of the full model was looked at. For all wave directions, a H_s of 1 m and T_p of 6 seconds were used. This analysis was conducted in order to find the most appropriate incoming wave direction for the installation. The most appropriate wave direction is deemed the wave direction that yields the least motions of the Thialf and other components in the system, such as the crane tip and bottom of the tower. The worst wave direction was also considered, as it was important for the wind and wave analysis in section 4.3. The OrcaFlex model used for the analysis can be seen in Figure 4.4. More views of the model can be seen in Figure B.2. As already mentioned in section 3.5, only first-order wave effects and added mass and damping loads were included in the calculations.

Thialf motions

The incoming wave direction plays an important role in the resulting motions of the Thialf. To see the specific effect of the simulated wind directions, statistics of the motions of the Thialf were obtained for all the load cases. The maximum, minimum, mean values and standard deviation were obtained, and from this, it was possible to determine which wave direction leads to the least movement of the Thialf. A table with an overview of statistical parameters for the Thialf is presented in subsection D.2.2. The statistical parameters are based on a 3900 second simulation, of which the first 300 seconds were disregarded to avoid transient effects. Figure 4.5 shows the STD of translational and rotational motion of the Thialf in sub-figures a) and b), respectively.

Thialf surge was most excited in head sea waves. This is reasonable, as the waves are going from fore to aft, causing motion in that direction. Thialf sway was least excited in head sea and following seas. This is, again a reasonable result, as the waves in these situations are coming from behind or in front, meaning the sideward sway motion of the Thialf is unlikely to be excited under such conditions.

The incoming waves from all directions resulted in a similar standard deviation for Thialf heave, which in all cases was less than 0.01 m. This is a very small value as the waves simulated did not have a period near the natural heave period of the semi-sub. The period of the waves was 6 seconds. From the modal analysis done earlier,

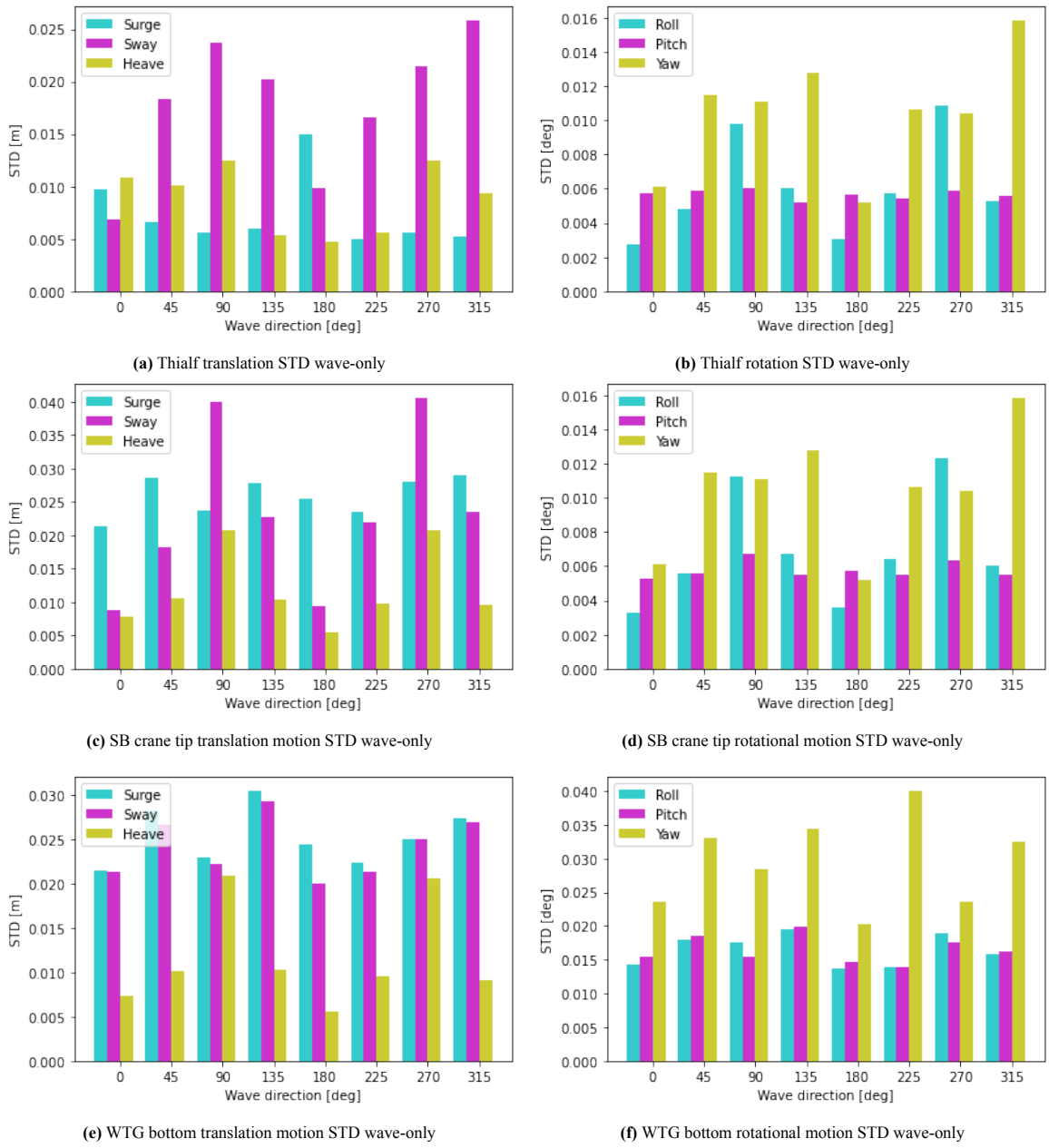

(a) Thialf translation STD wave-only

(b) Thialf rotation STD wave-only

(c) SB crane tip translation motion STD wave-only

(d) SB crane tip rotational motion STD wave-only

(e) WTG bottom translation motion STD wave-only

(f) WTG bottom rotational motion STD wave-only

Figure 4.5: STD of the Thialf, crane tip and WTG bottom motions for various incoming wave directions. $H_s = 1$ m, $T_p = 6$ s. Note that the vertical scales are not the same on all plots.

it can be seen that 6 seconds is far from the heave natural period of the Thialf. In subsection 2.3.7, it has already been explained that semi-subs are specifically designed to have natural periods outside the wave frequency range, and hence the very limited excitation in heave of the Thialf, is expected. Additionally, the nearly negligible heave motion can be explained by Airy wave theory. The water depth was set to 40 m for the investigation, and by using a simple relationship between peak period and wavelength ($\lambda = 1.56T^2$), a characteristic wavelength of 56.16 m is obtained for $T = 6$ s (Krogstad and Arntsen, 2000). This relationship can be used for linear deep-water conditions, which is applicable to the situation. Using the Airy deep water criteria of $\frac{d}{\lambda} > 0.5$, and the values of the water depth and wavelength from the load cases, it can be concluded that deep water conditions apply to this situation ($\frac{d}{\lambda} = \frac{40}{56.16} = 0.71 > 0.5$). The operational draft of the Thialf for this investigation was set to 22 m. Half of the wavelength is approximately 28 m, so that means that according to Airy wave theory, the waves should be affecting the Thialf over the whole draft. However, near the bottom of the pontoons, the linear wave effects should become very small. This can be checked with the equations for the particle kinematics for the

velocity and acceleration in the Z-direction. The equations are given in Equation 2.12 and Equation 2.14, respectively. Both equations are exponential and therefore insinuate that the incident wave effects will result in very small linear excitation at the depth of the bottom of the pontoons. Only considering the exponential parts of the kinematic equations e^{kz}, where $k = \frac{2\pi}{\lambda}$, and z the depth at the bottom of the pontoon, leads to $e^{kz} = 0.085$. This indeed confirms that the linear excitation due to the incident waves will be very small at the depth of the pontoons.

The vertical dimensions of the pontoons are very small in comparison with the remaining part of the Thialf. Due to this, the difference in depth at the top and bottom of the pontoon is small. The pressure caused by the waves on the top and bottom sides of the pontoon is 180 degrees out of phase with one another. The pressures are illustrated by the red and green arrows in Figure 4.6. The difference in pressure gives the vertical force on the pontoons, and due to them being 180 degrees out of phase, they tend to cancel out. Since the difference in depth is not large, neither is the difference in the pressure on the top and bottom and so the ability to cancel each other out leads to very small excitation in heave, seen by the minimum, maximum and standard deviation in Figure 4.5.

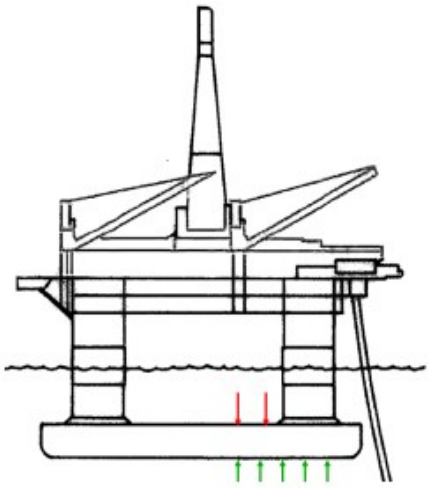

Figure 4.6: Pressure experienced on the top and bottom of the semi-submersibles pontoons, represented by red and green arrows. The pressures are 180° out of phase

The excitation of the Thialf in roll was also very limited, however, a small difference in the standard deviation of the load cases with beam sea and quartering sea conditions compared to head sea and following sea conditions was observed. For the pitch, the direction of the incoming waves did not make a significant difference, as the pitch motion was limited for all directions. The yaw standard deviation was particularly high for beam sea and quartering seas. For these directions, the Thialf encounters the waves under an angle, causing it to align itself with the waves and hence rotate around its vertical axis.

From this analysis, it can be said that the preferred orientation of the Thialf is so that head sea or following seas are encountered. However, concluding that incoming waves from 0 or 180 degree directions are the best for the whole full WTG lift operation, based on the Thialf motions alone is insufficient. The crane tip and WTG motions due to excitation of the Thialf as a result of the incoming waves also need to be analysed to see the preferred direction of the incoming waves of the whole system.

Crane tip motions

The SB crane tip motions will be analysed through a statistical analysis, just like the Thialf motions were. The SB crane tip will be referred to as crane tip from now on. An important detail to keep in mind is that the crane is slewed to 315 degrees, meaning that if the waves are coming from 0 degrees, this would actually be 135 degrees in the local crane reference system. However, the results for the crane tip are given in the Thialf reference system, so a direct comparison between results can be made. The specific statistical parameters for the crane tip are given in Table D.3.

In Figure 4.5 sub-figures c) and d), the STD for the different incoming wave directions for the different motions of the crane tip can be seen. From sub-figure c), it can be seen that the surge STD is more or less the same for all the wave directions, meaning the incoming wave direction does not influence the motion of the crane tip in surge greatly. There are however clear differences in the sway STD. If the STD of the crane tip in sway is compared to the STD of the Thialf for sway, it can be seen that sway is a lot more excited for the crane tip than the Thialf for some directions, more specifically in beam sea conditions (90 and 270 degree incoming waves). Heave is also a lot more excited for the crane tip than the Thialf on average for all wave directions. Incoming wave directions of 90 and 270 degrees, again cause the most excitation for the crane tip for heave. It should be noted that for all wave directions, heave motion results in the lowest STD of the crane tip motion. A conclusion for the translational motions of the crane tip is that beam seas result in the largest excitation of the translational motions of the crane tip, and head seas the least. This corresponds to the results from the Thialf.

Looking at sub-figure d), it can be seen that roll is also most excited in beam seas. For pitch, there are no huge differences in the STD between incoming wave directions. The yaw STD is the largest in quartering seas, more specifically the incoming wave directions of 135 degrees and 315 degrees.

Tower bottom motions

Another statistical analysis is done for the tower bottom of the WTG. The tower bottom motions relate to some of the operational limits as shown in Table 3.3, such as the Z tip motion and XY tip motion. Figure 4.5 shows the STD of the translational and rotational motions of the WTG bottom in sub-figures e) and f). The statistical parameters on which the figures are based are presented in Table D.4. The results are given in the Thialf reference system. The two figures show slightly different results than the results from the crane tip. One of the largest differences is that the surge and sway STD are very similar for all wave directions. But just like for the crane tip, heave has the lowest STD. This is again linked to the low excitation of the Thialf in heave. Due to this reason, the Z tip limiting value is not exceeded for any incoming wave direction under the given wave conditions. Motions of the tip in the horizontal plane also do not exceed the limit of 1.5 m.

The sway and surge STD for the tower bottom motions for all incoming wave directions are similar in magnitude. This is different to the Thialf motions, where sway and surge differed greatly per direction. The sway motion magnitude of the tower bottom is similar to the sway motion of the Thialf, but the surge motion magnitude is much greater for the tower bottom than the Thialf. Just like for the crane tip, the yaw STD for head and following seas is lower than the other incoming wave directions since the Thialf in those situations rotates less as well.

Overall, it can be concluded that waves do induce WTG motions while it is hanging in the crane. The significance of these motions will be determined by performing a coupled wind and wave analysis in section 4.3.

4.1.4. Conclusion waves-only

The intent of the wave-only analysis was to see the influence the Thialf interacting with incoming waves has on the dynamic behaviour of the crane tip and the WTG hanging from the crane. The results of the analysis performed showed that the wave direction influences the response of the crane tip and WTG.

The most favourable motions of the WTG occur when the waves are coming from a global direction of 180 degrees, which means head sea conditions for the vessel. Under this wave direction, the Thialf motions are least excited and lead to the least excitation of the WTG assembly. Additionally, the least favourable motions of the analysed components occur in quartering and beam seas. For these directions, Thialf encounters the waves under an angle. In such situations, the Thialf has a tendency to align itself with the waves. The directions in which the Thialf motions are largest are in most cases also the directions in which the crane tip and WTG bottom motions are largest, as they do not necessarily directly depend on the wave direction but on the motion of the Thialf. The WTG hanging in the crane will move in the same direction as the Thialf, however, the magnitude of the motions will depend on the peak period and significant wave height of the waves.

Comparing the results obtained from the statistical analysis with the limiting parameters in Table 3.3, it can be seen that the vessel roll and pitch are well within the safe operational limits, as for all directions they remain under 0.1 degrees, while the limiting value for both is 0.5 degrees. This also corresponds to the results presented in the operability curves, where it can clearly be seen that for the vessel roll and pitch limit to be exceeded, a very

high significant wave height would be needed for a peak period of 6 seconds or the peak period would have to be longer for a significant wave height of 1 m. The Z tip motion being smaller than 0.5 m is also still well within the safety limits. This is especially due to the size of the Thialf and hence the overall low excitation in heave.

4.2. Wind-only

The wind-only case was simulated using OrcaFlex, and time-domain analyses were done. For the analysis, different models were used. The full model is pictured in Figure 4.4 (explained in detail in section 3.5). Unlike for the wave-only analysis, where aerodynamics did not play a role, aerodynamic properties needed to be added to the relevant components for wind-only analysis. It has already been mentioned that the WTG is modelled as a rotor component in OrcaFlex, and therefore has blades with specific aerodynamic properties. The blades are made up of 50 airfoils, each with specific aerodynamic properties, which can be seen in Table B.1. Through a MatLab code, the model could be altered and drag properties were added to the tower and nacelle as well. The wind loading was not applied to the USF or the LLT. As a second model, a system which includes just the rigging configuration and WTG was looked at. This model is a simplification of the system but should yield similar results to the full model since the wind loading is only applied to the WTG. The model of just the rigging and WTG can be seen in Figure 4.7. The rigging is hanging from two points at the location of the crane tip, as in the full model. It has to be kept in mind that both models do not take any shielding effects that may occur into account. Shielding may happen due to the presence of the vessel or any other components blocking the wind. Depending on the direction of the wind, they can have significant effects on the overall system behaviour. More on this will be mentioned in the recommendation section. To make the comparison between the results of analyses with the two models easier, it has been decided to make the definition of the wind direction relative to the rotor orientation the same in both models. This means that for both models a wind direction of 135 degrees refers to the wind coming in the perpendicular direction to the rotor plane from the front.

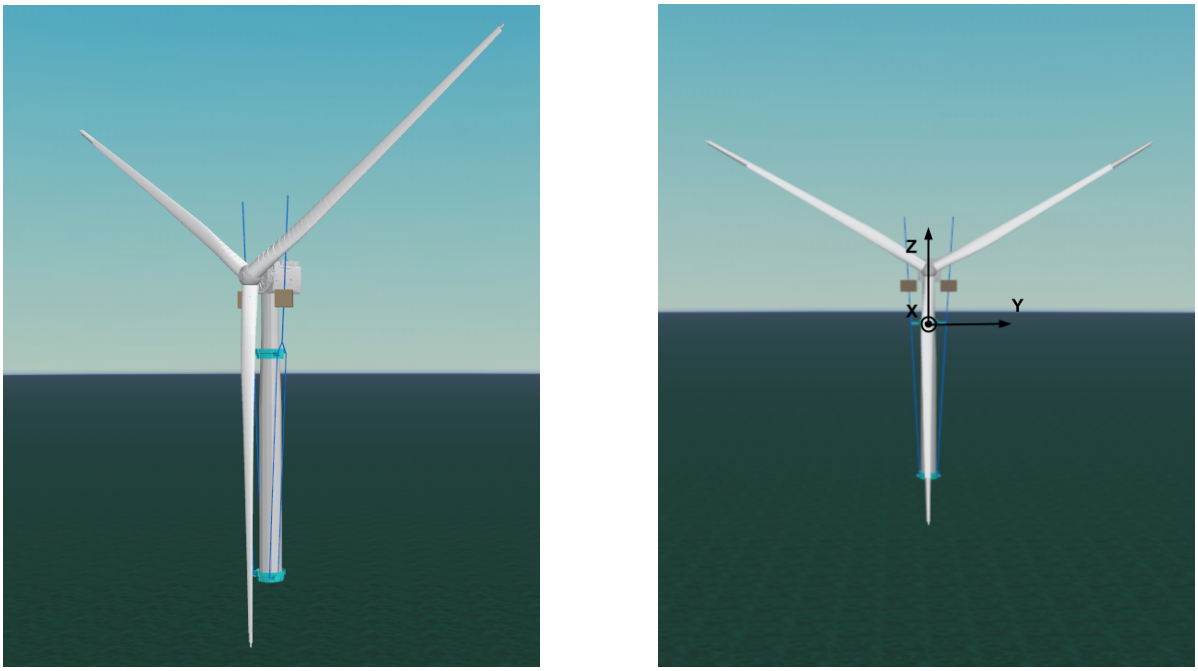

(a) Model of WTG and rigging from 180 degree wind direction.

(b) Local reference system of the WTG-tower connection shown.

Figure 4.7: Model in OrcaFlex used to perform simulations for the wind-only case. The model consists of the rigging and the WTG.

The wind load on the rotor is achieved by using the airfoil-specific properties, as already mentioned. Adding a wind load to the nacelle and tower is done through a different approach. For the nacelle, a wind drag coefficient of 1 is used in the X- and Y-directions of the local nacelle reference frame (Rentoulis, 2022). The area to which the drag coefficient is applied is 12×11 m^2 in the X-direction and 12×24 m^2 in the Y-direction, which are the sizes of the sides of the nacelle. The tower also has a drag coefficient applied to areas exposed to the wind. This area is based on the diameter of the top and bottom of the tower (6.8 m and 8 m, respectively).

The rigging is suspended from two hoist wires. The height of the bottom of the tower with respect to the mean sea level (MSL) is set, as the WTG needs to be hanging at a given height above the foundation in order to be installed. The height of the crane tip is on the other hand not a set variable, as the height can be changed. Due to this, depending on the height of the crane tip, the length of the hoist wires can change, which leads to changes in the behaviour of the system, as discussed in the modal analysis presented in section 4.1. The lengths of the hoist wires and slings in the system are important, as they influence the pendulum periods of the system, therefore are important for the overall system behaviour. In this investigation, the crane radius is set (65 m), and therefore so are the crane tip height and hence the length of the hoist wires (34.2 m).

Another parameter for the wind-only case, which could influence the dynamic behaviour of the system, is the blade pitch angle. The WTG is able to change the pitch angle to optimise power production, however, during installation, the pitch can also be changed to limit the loads. Changing the pitch means that the orientation of the blades with respect to the incoming wind changes, which results in the lift and drag coefficients changing. These changes result in the lift and drag that is generated to change, which affects the overall system dynamics.

For the wind-only case, the blade pitch angle, the incoming wind direction, as well as the magnitude of the wind speed are investigated. The tower yaw moment is also determined for the various models and is later compared to the combined wind and wave loading tower yaw moment.

4.2.1. Blade pitch analysis

The blade pitch angle was investigated for different wind directions. The importance of the blade pitch angle has already been discussed in subsection 2.2.3, where the lift and drag coefficients were introduced. Figure 4.8 shows the definitions of the pitch angles with respect to the blades and the coordinate system used for this analysis. Note that wind directions in this analysis are aligned with the local coordinate system of the wind turbine, unlike the wind directions for the models in Figure 4.7 and Figure 4.4.

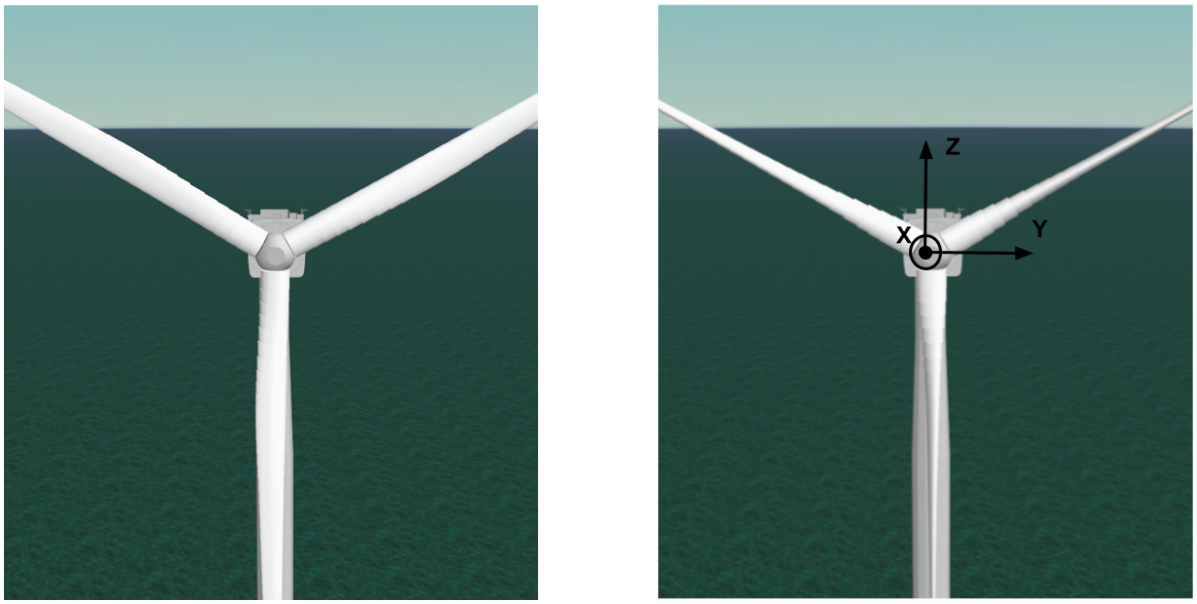

(a) 0-degree blade pitch angle.

(b) 90-degree blade pitch angle.

Figure 4.8: Definition of the blade pitch angle. When the pitch is 90 degrees, the leading edge of the blade is at the front and the trailing edge is at the back.

To see the static forces and moments generated due to different pitch angles, a test was done, in which the WTG tower was fixed to a point and a wind loading was applied. The wind direction was varied, as well as the pitch angle, while the wind speed was set to a constant uniform speed of 10 m/s. The pitch angles between 0 and 90 degrees in bins of 15 degrees were tested. The connection force of the nacelle was plotted against the wind direc-

tion for the various pitch angles. The results for the Z-moment of the nacelle can be seen in Figure 4.9. Based on the coordinate system in Figure 4.8b, the Z-moment represents the moment around the vertical. Plots for all the other forces and moments are given in subsection D.3.1 in Figure D.1.

A 0-degree pitch angle will not generate any lift and hence is not desired for energy production, however, this is not of relevance during installation and is instead desired, as the environmental loading is lower in such a situation according to the results in the plot. In this situation, the motions the blades would induce on the rest of the system should be lower. Also, the possibility of damaging the blades or WTG during installation is decreased.

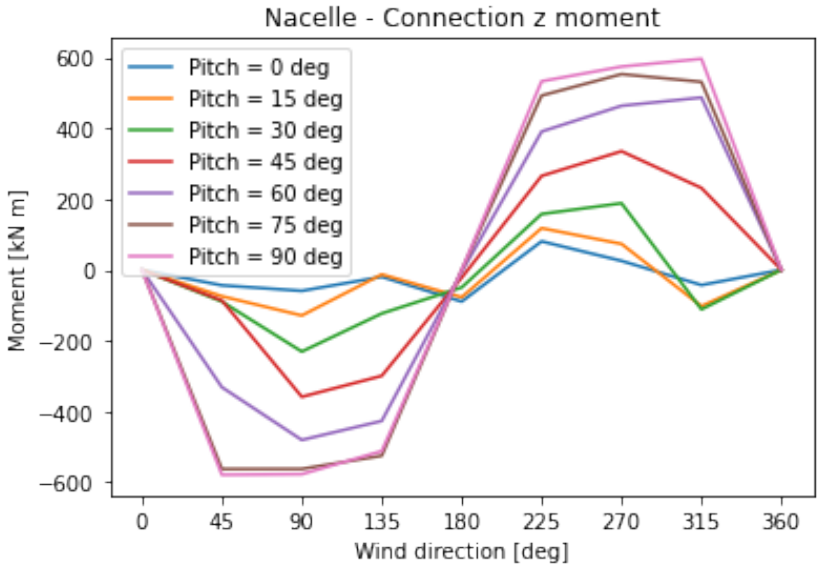

Figure 4.9: Nacelle - Connection Z-moment plotted as a function of the blade pitch angle against the incoming wind direction.

The yaw moment is important during installation, as a large yaw moment will allow for the heading of the WTG to change and cause difficulties in the installation procedure. Therefore, a low yaw moment is desired. When the blade pitch is 0 degrees, the yaw moment remains small and does not vary much for different incoming wind directions. For other blade pitch angles, depending on the wind direction, the yaw moment can be quite large, such as when the blade is pitched to 90 degrees and wind comes from any direction not perpendicular to the rotor plane.

For further investigations in this thesis, only a 0-degree pitch angle is considered. The wind direction is investigated in more detail, as it is important to see the wind-induced motions of the vessel through the WTG and crane tip. These motions are also of relevance in the coupled wind and wave analysis.

4.2.2. Time domain analysis

In this section, the rigging configuration (Figure 4.7) and the full model (Figure 4.4) were looked at in a wind-only scenario to see if and how the wind induces vessel motions through WTG motions. The yaw moment of the tower was also examined, as the magnitude of this moment is representative of the yaw moment the USF has to restrain. The yaw moment is taken around the centre line of the tower, as that is the origin of the tower's reference frame. The most and least suitable wind directions for the operation were also looked at. Statistical analysis of the time domain analysis was done to get relevant results.

WTG and rigging

The model shown in Figure 4.7 was used to obtain the maximum forces and moments that the tower encounters with a turbulent wind loading, with a mean wind speed at 10 m height of 5, 10 and 12 m/s. As already mentioned, the reference frame used for this model is so that the orientation of the wind turbine rotor plane is the same as in the full system model (Figure 4.4) with respect to the wind. This is so that an easier comparison can be made between this analysis and the analysis of the full system.

The results of forces and moments for various incoming wind directions are shown in Figure 4.10. The maximum magnitude of all the forces and moments is plotted per direction. The main focus of this thesis is the yaw motion or Z-moment of the tower, and hence the focus of this analysis is on the last plot in the figure, which shows the maximum magnitude tower Z-moment for various incoming wind directions. It should be noted that the results for 90 and 270 degrees are missing, as in these situations the incoming wind was parallel to the rotor plane and the BEM failed to converge in those cases. The BEM solver is required to calculate the forces that act on each individual blade segment and also to determine the optimal angle of attack. In OrcaFlex, when BEM fails to converge, there could be several reasons for this issue, such as wrong input parameters or blade damage. However, these are not the reasons in this case, instead, it was due to the load acting on the blades changing sign (from positive to negative) when the wind is coming from that particular direction. OrcFlex struggles with this when using a 2D-quasi model, as it goes outside the assumptions within OrcaFlex.

The bottom right plot of Figure 4.10 shows that the maximum magnitude of the Z-moment for all the examined wind speeds occurred when the incoming wind direction was 135 degrees, so when the wind was coming perpendicular to the rotor plane. The larger the wind speed, the greater the magnitude of the moment encountered as well. This also holds for the other forces and moments, as seen in the plots. Specific values of the maximum Z-moment magnitude are presented in Table 4.3.

From the plots presented in Figure 4.10, it can be seen that all wind speeds follow a similar pattern for the different wind directions. This is shown by the shape of the lines which connect the various data points make. The plots of the mean moment have been attached to the appendix in Figure D.2. In those plots, it can more clearly be seen how certain wind directions cause positive moments while other wind directions result in a mean negative moment.

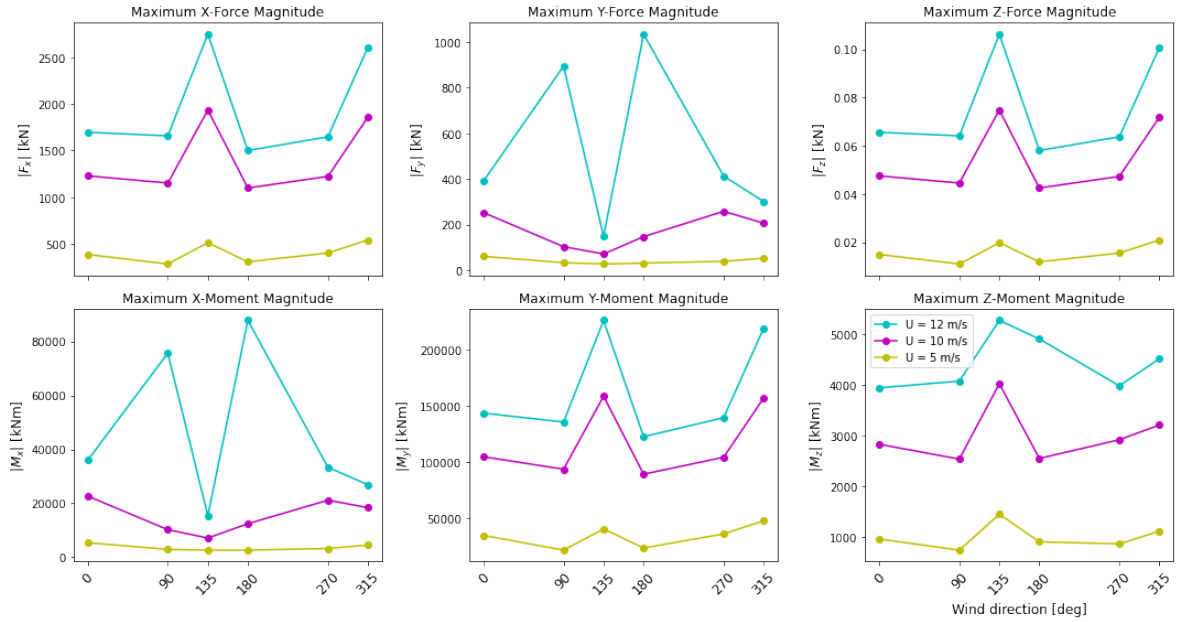

Figure 4.10: Maximum force and moment magnitude plots of the tower connection for different incoming wind directions of the rigging and WTG model. Mean wind speeds of 5, 10 and 12 m/s were used as the TurbSim input values. The points plotted are represented by circles in the plots.

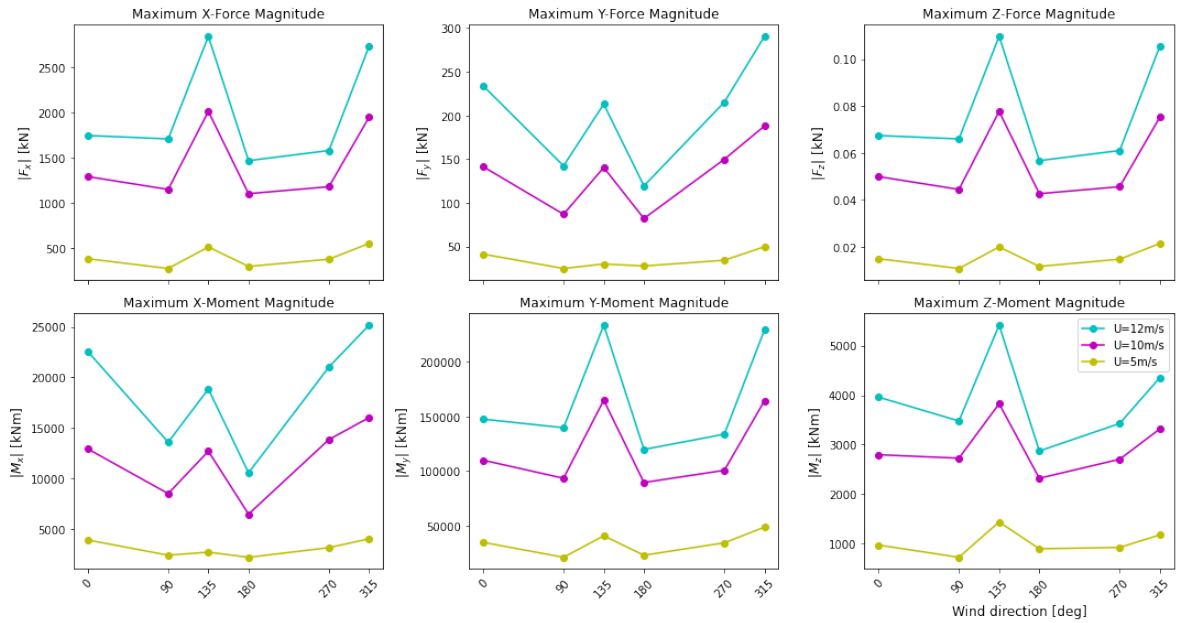

Figure 4.11: Maximum force and moment magnitude plots of the tower connection for different incoming wind directions of the full model. Mean wind speeds of 5, 10 and 12 m/s were used as the TurbSim input values. The points plotted are represented by circles in the plots.

Full system

The model in Figure 4.4 was used for the analysis discussed in this section, which included calm waters and a turbulent wind field. The maximum magnitude for the forces and moments were again plotted for the model for different wind directions and wind speeds and are presented in Figure 4.11. The plot for the maximum Z-moment shows very similar results to the model of just the WTG and rigging. Again the maximum Z-moment magnitude was recorded when the wind was perpendicular to the rotor plane (135 degrees). Further, again for all the plots the different wind speeds follow the same pattern in general for different wind directions. An overview of the maximum Z-moments of the tower for the relevant cases is presented in Table 4.3.

Table 4.3: Maximum Z-moment magnitudes of the tower for the wind-only cases.

	|Z- moment| [kNm]		
Wind speed [m/s]	Rigging+WTG (135 deg)	Full model (135 deg)	Full model (180 deg)
5	1457.53	1437.50	894.63
10	4022.11	3826.57	2319.92
12	5266.86	5415.17	2870.88

Along with finding the maximum moment, the motions of the USF and LLT in the horizontal (X-Y) plane were also looked at. The time series data were first plotted as X-Y plots and then converted into ellipses for a better representation of the maximum paths taken by the different components. These results are presented in Figure 4.12 for wind directions of 90, 135 and 180 degrees of the vessel reference system. These wind directions are representative of the best and worst wind conditions when considering the Z-moment magnitude. The wind directions are labelled on the plots for the LLT. For the USF and LLT, it can be seen that slightly different paths are followed. While both components are slightly rotated with respect to the main X-axis (due to the crane slew angle), the paths of the LLT are nearly concentric with increasing wind speed. The path of the USF as the wind magnitude increases seems to shift the path away from its initial position towards the positive Y- and negative X-direction. This could be due to the damping tuggers being attached to the USF working in the given direction.

The USF and LLT both have the largest path when the wind direction is 135 degrees for all wind speeds, and also with increasing wind magnitude, the amplitude of motion of the USF and LLT also increases. This is represented by the results of 12 m/s wind speed having the largest ellipses in all the plots. Further, it can be seen that the wind direction has an effect on the path of the components, as, for example when the wind is coming

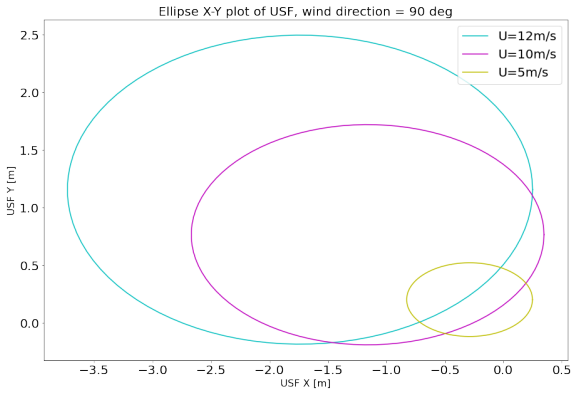

(a) USF, 90 degrees incoming wind.

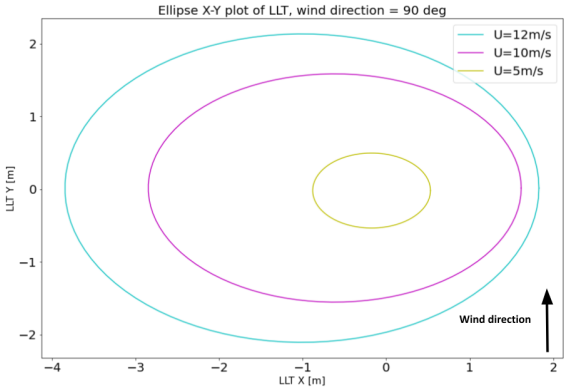

(b) LLT, 90 degrees incoming wind.

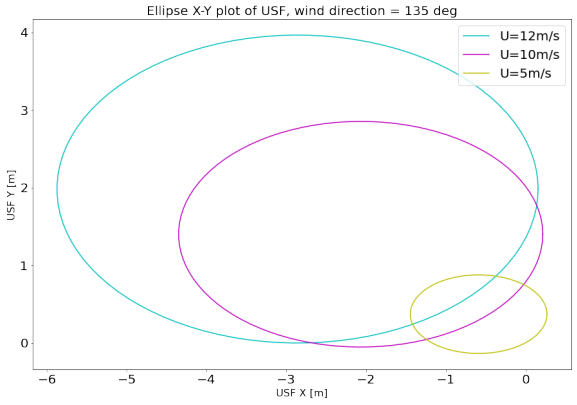

(c) USF, 135 degrees incoming wind.

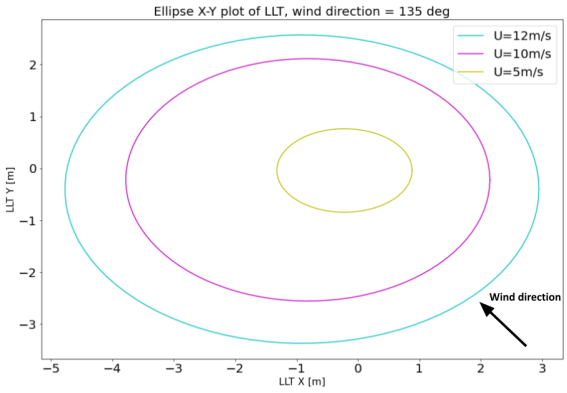

(d) LLT, 135 degrees incoming wind.

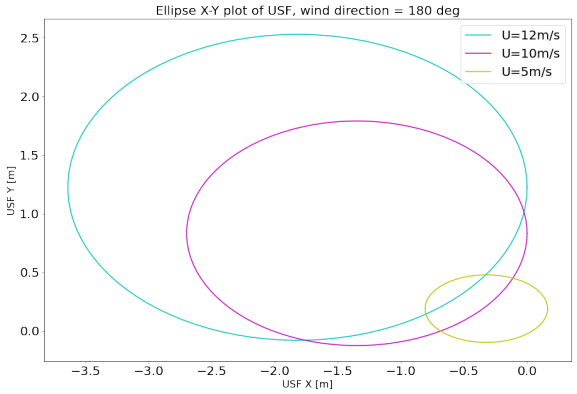

(e) USF, 180 degrees incoming wind.

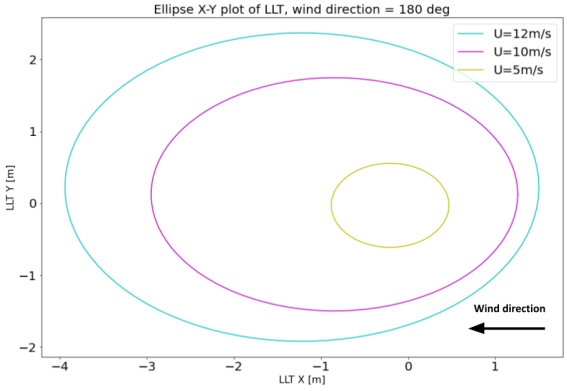

(f) LLT, 180 degrees incoming wind.

Figure 4.12: Ellipse plots of X-Y motion of the USF and LLT for a wind-only case. The incoming wind direction is labelled on the plots on the right side.

from the negative X-direction (180 degrees), the LLT and USF motions are also pushed more in that direction. An important aspect to note is the amplitude of the motions. Limiting criteria of the single lift method have been stated in Table 3.3, and one of them corresponds to the XY motion of the tower bottom and another to the XY motion of the nacelle. The limit of the tower tip bottom is represented by the LLT motion, as the LLT is connected at the tower bottom. From the LLT plots in Figure 4.12, it can be seen that in general, the amplitudes in the X- and Y-direction of the LLT exceed the advised limit of 1.5 m for wind speeds of 10 and 12 m/s. This is a problem as exceeding pre-defined operational limits could lead to dangerous situations. Therefore, in the next section where the combined wind and wave loading was investigated, the tower tip bottom operational limit was kept in mind to find the limiting weather condition which would still allow safe operation.

4.2.3. Conclusion wind-only

The intent of the wind-only analysis was to see the behaviour of the WTG under various wind loads and wind directions. From the blade pitch test, it has been decided to continue all further analyses with just the 0 degree pitch angle, as promising results for the different forces/moments have been obtained.

The wind-only analysis also yielded the tower yaw moment, which is one of the objectives of the investigation. The yaw moment was obtained from the case with only the WTG and rigging and also from the full model. The magnitudes of the moments were comparable to each other and increased for increasing wind speed magnitudes and certain directions (incoming wind perpendicular to the rotor plane). The required rotational restraint capacity of the USF can from these results be taken as approximately 5.5×10^3 kNm when the mean wind speed at 10 m is 12 m/s and the incoming wind direction is 135 degrees. However, these specific environmental conditions lead to the exceedance of some operational limits, therefore, 5.5×10^3 kNm is not the correct moment that the USF needs to counteract.

4.3. Wind and Waves

In the previous sections, wind-only and wave-only analyses have been conducted of the whole model or of part of the model. The behaviour of the system under these environmental loads has been analysed and has been combined to obtain a coupled environmental loading of wind and waves on the whole system for time-domain analyses in OrcaFlex. The model of the system used is seen in Figure 4.4.

From the previous analyses, it has been shown that the direction of the incoming waves and wind is important for the system's response, as it affects the magnitude of the induced motions, forces and moments. In this section, different load cases have been investigated and the behaviour of the system under the combined loading was analysed. Firstly, the effect of the wind speed magnitude for a given sea state was investigated. Secondly, an investigation in seeing the effect of varying the wave peak period and significant wave height was done, and the results are presented. In both these investigations, the wind and wave directions were aligned. For the third investigation, the effect of misaligning the wind and waves was looked at to determine how the system response changes in the case when the wind and waves are not exactly aligned, as those conditions yield more realistic physical wind and wave conditions.

Additionally, in the wind analysis, it has been determined that the chosen wind speeds of 10 m/s and 12 m/s yield tower bottom motions that exceed the pre-determined operational limit of 1.5 m. This operational limit was further investigated to find the limiting environmental conditions for a combined wind and wave loading.

4.3.1. Wind speed effect

The wind speed effect analysis was done to see the importance of the wave loading on the overall system behaviour, as essentially it is the same analysis as for the wind-only case, however also with an incoming wave field ($H_S = 1$ m, $T_P = 6$ s), and only considering one wind and wave direction (180 degrees). The yaw moment from this investigation can be compared to see if there is a large change compared to the wind-only case.

A TurbSim wind field input using 5, 10 and 12 m/s was used for the investigation, with the waves as defined before. Figure 4.13 shows the main statistical parameters (minimum, maximum, mean and standard deviation) represented as box plot diagrams for the different load cases considered. The data presented is the tower connection forces and moments. Just like for the wind-only case, it can clearly be seen that the larger the magnitude of the incoming wind, the greater the maximum force/moment. Furthermore, looking at the exact values of the Z-moment, shown in Table 4.4, it can be seen that for all the wind speeds, the moment is slightly larger when there is also an additional wave loading applied, compared to a wind-only case. However, that difference is very minimal, and therefore, from this particular investigation, it can be concluded that the wind has the biggest effect on the yaw moment of the tower. This is again due to the wind turbine blades being designed to harness as much wind as possible, even when pitched to an angle where the aerodynamic forces are minimised. The Thialf is in this case positioned so that head sea waves are encountered, which as already previously determined, yield the most favourable conditions for WTG motions.

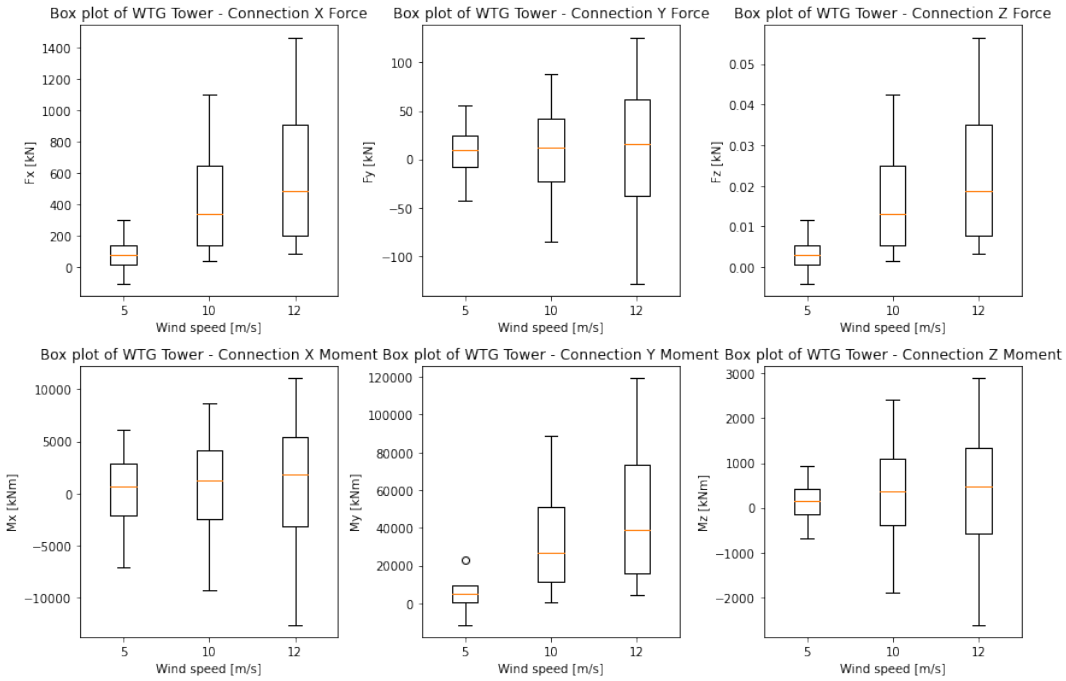

Figure 4.13: Box plots showing the difference in the tower connection forces and moments for various incoming mean wind speeds. The wind and waves are coming from 180 degrees, $H_s = 1$ m, and $T_p = 6$ s. The red line represents the median value, while the box represents the first and third quartile values. The maximum and minimum values are represented by the whiskers (ends of the lines connected to the box).

Table 4.4: Maximum Z-moment of the tower for the combined wind and wave loading. Wind and wave direction is 180 degrees, H_s = 1 m, T_p = 6 s, the wind speed is varied.

	Z- moment [kNm]	
Wind speed [m/s]	Wind-only	Wind and waves
5	894.63	939.45
10	2319.92	2408.78
12	2870.88	2894.43

One of the main limiting parameters, as stated in Table 3.3, is the horizontal motion of the bottom of the tower (XY tip). Figure 4.14 shows the magnitude of the motion of the tower tip in the horizontal plane for the various wind speeds and the given wave conditions. The plot was obtained through $XY = \sqrt{X^2 + Y^2}$, where X and Y represent the displacement of the tower tip from its initial position. It can be seen that when wind and waves are coming from 180 degrees, $H_s = 1$ m, and $T_p = 6$ s, the tower tip motion limit of 1.5 m during the whole 1-hour simulation is only not exceeded for a wind speed of 5 m/s. The limit of 1.5 m, denoted by the red dashed line in the plot, is exceeded for wind speeds of 10 and 12 m/s. This confirms the results of the wind-only analysis, and therefore an additional analysis for the combined wind and wave loading is presented later in this Chapter determining the limiting environmental parameters.

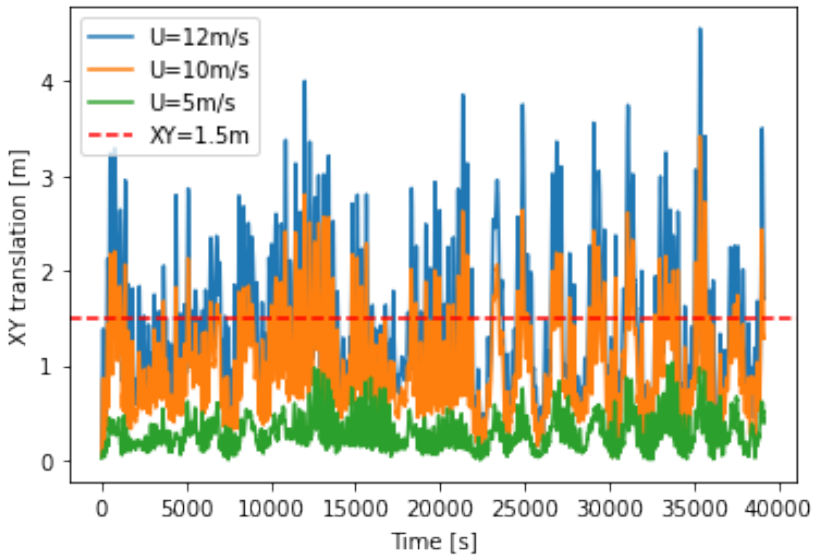

Figure 4.14: Plot showing the magnitude of the tower tip motion in the horizontal plane for various incoming wind speeds. The wind and waves are coming from 180 degrees, $H_s = 1$ m, and $T_p = 6$ s. The red dashed line represents the limiting value of 1.5 m.

4.3.2. Varying the significant wave height and peak period

To see the effect of the significant wave height and peak period on the system, several simulations, with various H_s and T_p combinations, were run. The wind and wave directions were kept at 180 degrees, and the average wind speed at 10 m height for the TurbSim file was set to 10 m/s.

In Figure 4.15 the time series of the Thialf of the 1-hour simulation for the heave, pitch and roll can be seen for two different tests. On the left side, the plots show the effect of varying the peak period, while on the right, the plots show results of varying the significant wave height. The plots of the heave, roll and pitch are presented, as for the other motions there are no significant differences in the motion when the T_p or H_s changes. It can be seen that the Thialf motions get a lot more amplified when the peak period is 12 seconds compared to 4 seconds. This is due to 12 seconds being close to the natural period of the Thialf for those degrees of freedom and hence, can more easily get excited due to resonance. Using the characteristic wavelength formula $\lambda = 1.56T^2$, a wavelength of 224.6 m is obtained for a 12 second period. With such a wavelength and a water depth of 40 m, the Airy deep water criteria, $\frac{d}{\lambda} > 0.5$, is no longer fulfilled, meaning the intermediate water regime needs to be considered (see Figure 2.3). The deep water condition is met up to a period of 7.2 seconds. For periods higher than 7.2 s, the sea bed has an influence on the wave characteristics, according to the theory, and the deep-water dispersion relationship is not valid. The trajectories of the water particles are not circular, like for deep water, but follow an elliptical orbit. The ellipses get more flattened, going further under the water surface. The horizontal excursion of water is approximately the same for all water depths, while the vertical excursion gets smaller with depth. The vertical excursion is also much smaller than the horizontal (Apsley, 2022).

Looking at the results, in Figure 4.15 from varying the significant wave height, the peak period is set to 12 seconds, and it can be observed that the higher the wave height, the greater the response of the vessel in those degrees of freedom. This is clear as only linear wave effects were considered, and the wind did not change in the examined load cases. From this, it can be concluded that the significant wave height and peak period are very relevant parameters and must be closely monitored during the installation, as they can greatly increase the motions of the system and hence impact the installation procedure when only considering linear effects. Operational limits relating to the peak period and significant wave height must be pre-determined and obeyed during the installation to minimise WTG motions and allow for safe operation.

The ellipse plots of the USF, LLT and nacelle motions are depicted in Figure 4.16, for an incoming wind and wave direction of 180 degrees. These plots clearly show that not only the Thialf but the motions of the whole system get amplified with increasing peak period, while the significant wave height remains fixed and that the motions are also greater for higher significant wave heights while the peak period remains constant. However,

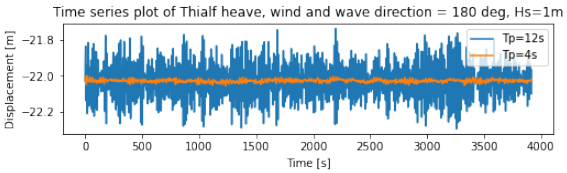

(a) Varying the T_p, Thialf heave

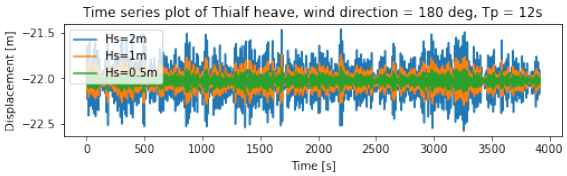

(b) Varying the H_s, Thialf heave

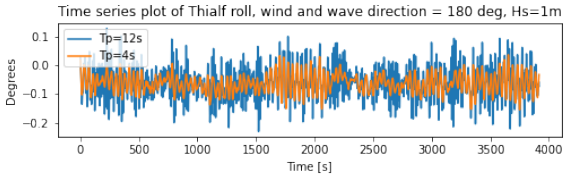

(c) Varying the T_p, Thialf roll

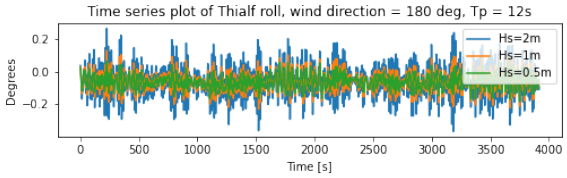

(d) Varying the H_s, Thialf roll

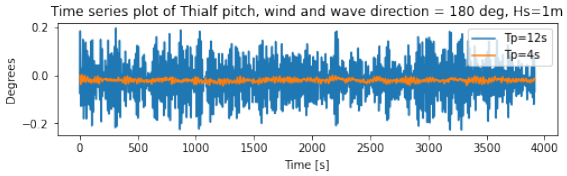

(e) Varying the T_p, Thialf pitch

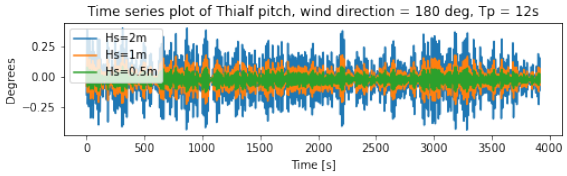

(f) Varying the H_s, Thialf pitch

Figure 4.15: Thialf time series of the heave, roll and pitch motions for different H_s and T_p combinations. Wind and wave direction is 180 degrees, and wind speed is 10 m/s at 10 m height.

for a constant significant wave height and varying peak period (left plots), it can be seen that peak periods of 4, 6 and 8 seconds do not lead to much change in the excitation of motion of the components. Therefore when the limiting environmental conditions for this operation are determined later in this Chapter, 8 seconds has been chosen as the peak period. It is expected that a peak period of 4 seconds would lead to less excitation, however, as mentioned in the modal analysis, done in section 4.1, a pendulum mode is excited at a period of around 4 seconds. This causes the motions of the USF, LLT and nacelle for a peak period of 4 seconds to be similar to the longer peak periods investigated (6 and 8 seconds).

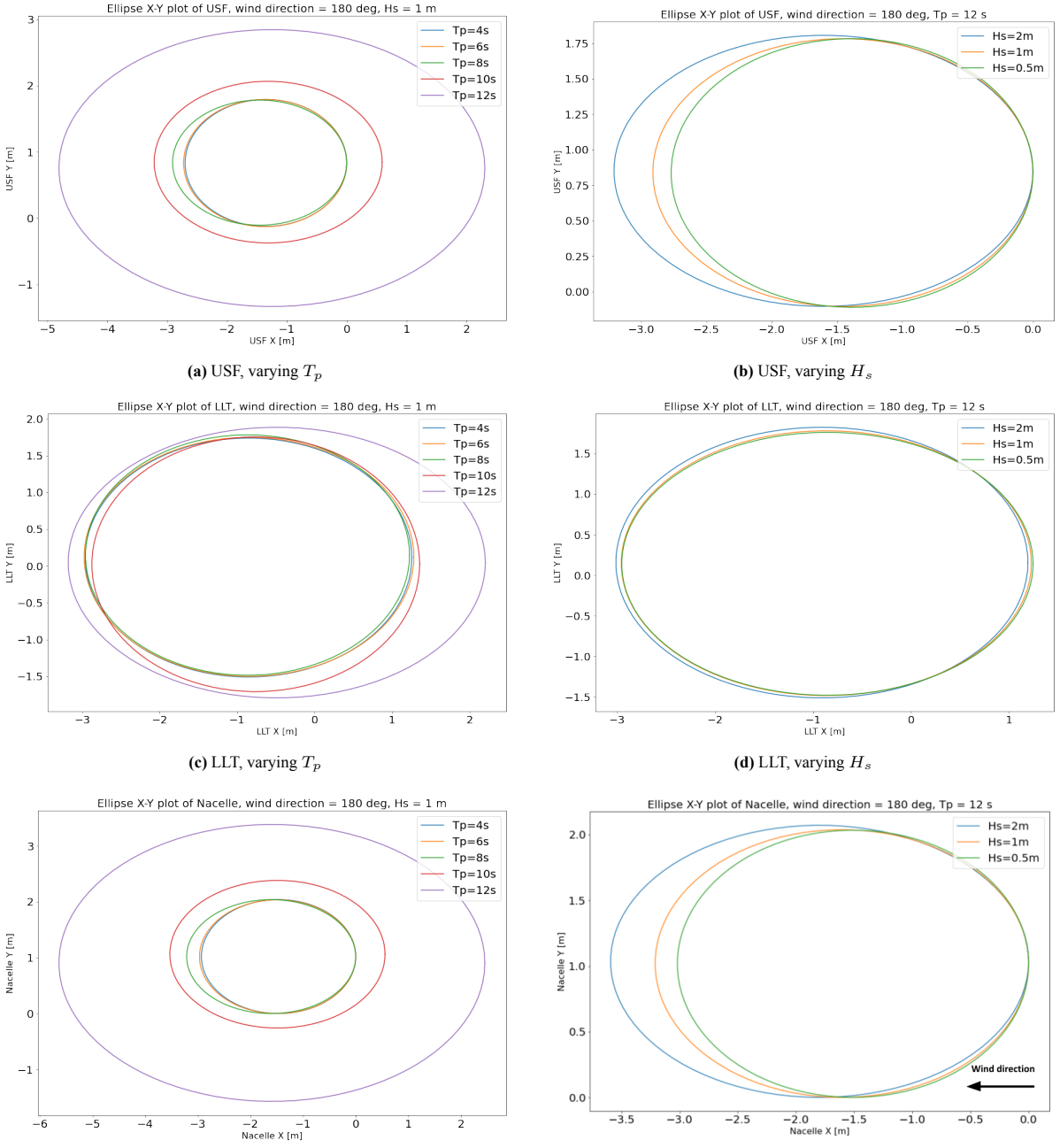

(a) USF, varying T_p

(b) USF, varying H_s

(c) LLT, varying T_p

(d) LLT, varying H_s

(e) Nacelle, varying T_p

(f) Nacelle, varying H_s

Figure 4.16: Ellipse plots of USF, LLT and nacelle motions. In the left column are results from varying the T_p and in the right column are results from varying the H_s. Wind and waves are coming from 180 degrees, as labelled in sub-figure (f).

4.3.3. Misalignment of wind and waves

The third analysis done for the wind and waves investigation considered wind and waves coming from different directions, as all the previous analyses had the wind and waves aligned. In real life, the wind and waves are not always aligned, and therefore complete alignment of the two during a real installation offshore is unrealistic. Through this short investigation, the wind and waves were misaligned by 45 degrees to see if there were any drastic changes in the results. Ellipse plots, showing the maximum amplitude of motion of the USF, LLT and nacelle for the 1-hour simulation are shown in Figure 4.17. It can be seen that while the incoming wind direction is kept at 180 degrees and the wave direction is changed, there are no significant differences in any of the motions of the three components compared to the aligned wind and wave case (both from 180 degrees). However, a difference arises when the incoming wind direction changes to 135 degrees. In this case, the amplitudes of motions increase

and the range of motion is nearly twice as big as for an incoming wind direction of 180 degrees. This again shows that the wind is the leading environmental load when considering WTG motions and therefore needs to be the main parameter when considering the orientation of the whole system during installation. An incoming wind direction of 135 degrees also corresponds to the wind coming perpendicular to the rotor plane, which during the wind-only analysis, has been determined as the direction that yields the largest motions and moments of the WTG.

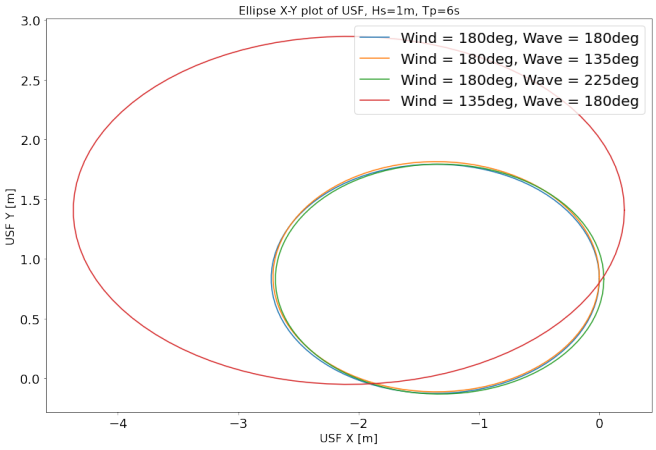

(a) USF

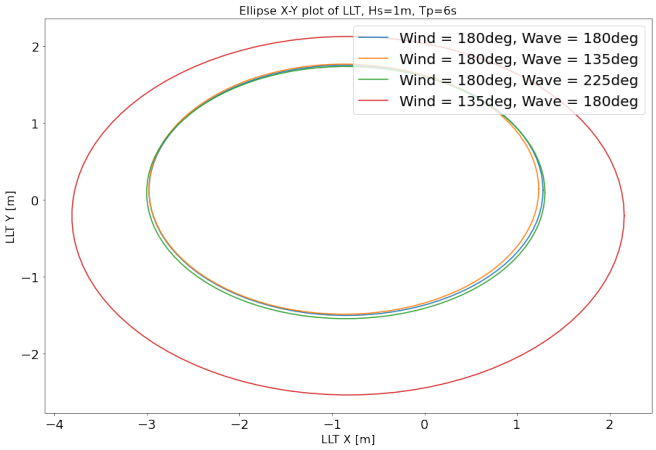

(b) LLT

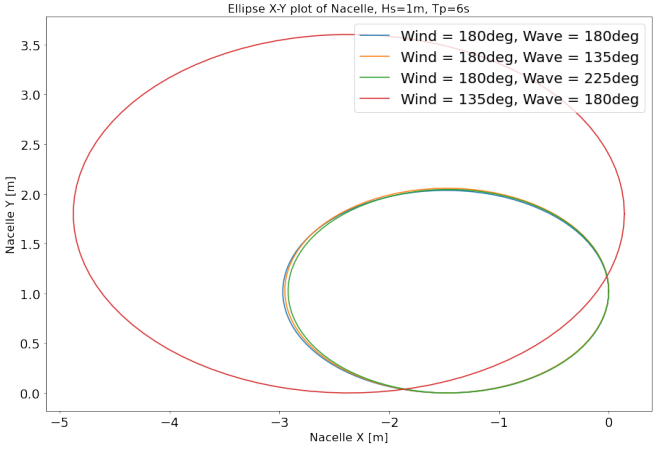

(c) Nacelle

Figure 4.17: Ellipse plots showing the maximum amplitude of motion of the USF, LLT and nacelle during the 1 hr simulation for misaligned wind and waves. H_s = 1 m, T_p = 6 s.

4.3.4. Limiting environmental conditions

It has been shown before in Figure 4.14 that even under an incoming wind and wave direction of 180 degrees, the tower tip motions exceed the allowable limit for mean wind speeds of 10 and 12 m/s. Therefore, it was decided to further investigate the allowable wind speed. Since it has been determined from the previous tests that an incoming wind direction of 135 degrees yields the least favourable conditions, it was decided that the limiting environmental conditions will be determined based on this direction. Further, it was stated that 8 seconds will be used as the peak period, as no larger differences were observed between 4, 6 and 8 seconds and 8 seconds has also already been used for previous offshore operations done by Heerema MC (Table 2.1). Based on previous operations, it has also been decided to use 1.5 m as the limiting significant wave height. With the chosen environmental parameters for the wind direction, wave direction, peak period and significant wave height, the limiting wind speed was investigated. Wind speeds of 6, 7 and 8 m/s were investigated and the results are presented in Figure 4.18 (the initial transient is not shown in the plot). It can be seen that when the wind speed is 7 and 8 m/s, the limit of 1.5 m is exceeded. This results in 6 m/s being the limiting mean wind speed, based on the 1-hour simulation. A wind speed of 6 m/s, $H_s = 1.5$ m, $_p = 8$ s and wind and waves coming from 135 degree heading results in a maximum tower Z-moment magnitude of 2.1×10^3 kNm. This is the necessary moment that the USF must counteract in order to minimize the yaw of the WTG during installation. This value was also used as the moment on which the calculations in section 5.4 were based on. The moments for the other wind speeds for a wind and wave direction of 135 degrees and a wind and wave direction of 180 degrees are presented in Table 4.5. It can be seen that the moments for the load cases where the wind and waves are coming from 180 degrees are significantly lower than the moments for wind and waves from 135 degrees.

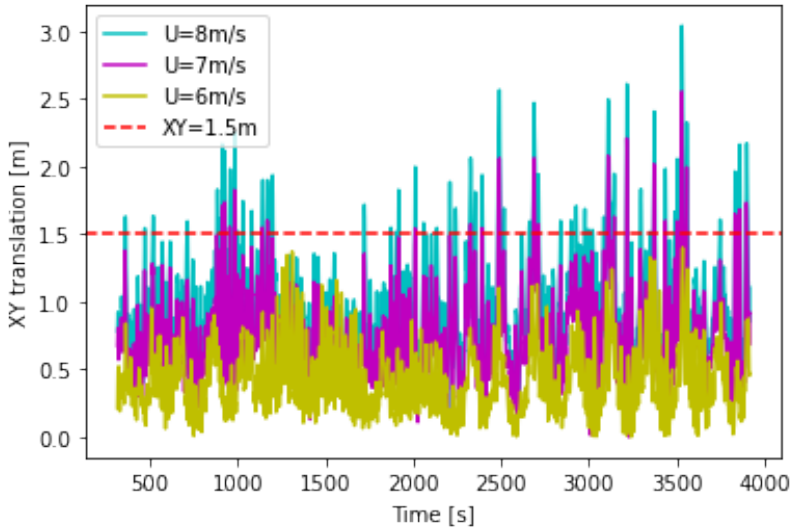

Figure 4.18: Plot showing the magnitude of the tower tip motion in the horizontal plane for various incoming wind speeds. The wind and waves are coming from 135 degrees, $H_s = 1.5$ m, and $T_p = 8$ s. The red dashed line represents the limiting value of 1.5 m.

Table 4.5: Maximum Z-moment of the tower magnitude for combined wind and wave loading for two different wind and wave directions and different wind speeds. $H_s = 1.5$ m, $T_p = 8$ s.

	|Z- moment| [kNm]	
Wind speed [m/s]	180 deg	135 deg
6	1387.09	2101.57
7	1764.28	2617.86
8	2021.78	3103.98

4.3.5. Conclusion wind and waves

Having conducted several different tests for the coupled wind and wave analysis, it has become clear that the wind is the dominant environmental loading between the two based on the tests that have been performed. When the results were compared to the wind-only case, it was seen that the waves do slightly increase the forces and moments acting on the system, however, the effects are very small. Moreover, the outcomes of the combined wind and wave analysis correspond to the previously obtained results of the wind-only and wave-only analyses regarding the best and worst wind and wave directions for this installation strategy.

It was also revealed from the results that a peak period of 12 seconds greatly excites the system in heave, roll and pitch, while peak periods under 10 seconds cause very limited excitation of the system. When misaligning the incoming wind and wave directions, it was again clear that changes in the wind cause significant differences in the results, while changing the wave direction does not yield major changes in the results.

Wind speeds of 10 and 12 m/s resulted in the exceedance of the operational limit for the tower tip motion. When further investigations were done to determine the limiting environmental conditions it was found that a wind speed of 6 m/s, incoming wind and wave direction of 135 degrees, peak period of 8 seconds and significant wave height of 1.5 m resulted in the tower tip motion to stay below the limit of 1.5 m for the duration of the simulation. Under such an environmental loading the maximum magnitude of the tower Z-moment was found to be 2.1×10^3 kNm. In the next Chapter, a safety factor is applied to the moment to ensure that the USF is designed to be able to withstand even larger moments in case that will be necessary.

4.4. Base case results

In this section, the main results of the base case analysis are concluded. One of the most important results that was required for the next step of the investigation was the maximum yaw moment caused by the environmental loading. The yaw moment was measured around the tower Z-axis at the location of the USF. Through this, the maximum rotational restraint capacity of the USF could be determined. This allowed in the next steps, where different concepts were considered for the physical connection at the tower and USF interface, to have a boundary condition for the rotational force that needed to be counteracted between the tower and USF. The maximum yaw moment was found to be 2.1×10^3 kNm, for a design wind speed of 6 m/s, significant wave height of 1.5 m and peak period of 8 seconds. This is the value of the moment without any safety factors applied yet. It was also found that for higher wind speeds, much larger moments were recorded, however, the larger wind speeds led to the exceedance of the limiting parameters and therefore are not representative of the yaw moment that would be encountered during the operation. A wind speed of 6 m/s is very low compared to previous installation operations. The wind speed is based on the tower tip motion limit of 1.5 m. Since the limit is exceeded for wind speeds over 6 m/s, provisions to reduce tower tip motions in order to allow higher wind speeds should be considered in the future. In the recommendations, in section 6.2, the possibility of including an additional tugger system for the LLT is discussed.

It was found from the wave-only analysis that the Thialf motions are least excited in head sea conditions and most excited when waves come from the side. The more the waves excite the Thialf, the more the motions of the crane tip and tower tip bottom get excited as well. In the combined wind and wave analysis it was found that peak periods coinciding with the periods of the critical pendulum mode shapes excite the Thialf motions a lot more than sea states with other peak periods. This was attributed to the resonance of the particular mode shape.

In the wind-only analysis, the blade pitch angle was investigated and found that when the blades are pitched to 0 degrees during the installation, the smallest moments were acting on the turbine, causing less extra motions on the whole system. It was then found that the maximum tower Z-moment occurred when the incoming wind direction was perpendicular to the rotor plane in both models tested (in the rigging configuration and the full model). For both models, the yaw moment was of the same magnitude for the same design wind speeds.

The coupled wind and wave analysis consisted of several tests, which all supported each other's results. It was clear that the wind is the dominant environmental loading when WTG motions are considered, as results from the wind-only analysis and the combined wind and wave analysis did not greatly differ. This is due to the blades being aerodynamic and capturing the incoming wind, while the wave loads do not directly work on the blades and first have to induce vessel motions before the vessel is able to induce WTG motions as a consequence. The

Thialf is a vessel designed with natural periods so that they are outside the incoming wave frequency range to decrease any resonance motions as much as possible. Due to this the motions of the whole system caused by waves are small. However, the waves still have a larger impact on the Thialf than the wind in this investigation, in particular, as the wind loading was not applied on the Thialf. This is most likely the case in real life as well, as due to the stability of the vessel, the wind is not able to cause large motions of the Thialf.

5

Concept Study

In order to obtain solutions to the problem of physically connecting the USF and tower, and to keep the working of the USF as intended, a concept study was done. The concept study concerned possible solutions that could be applied at the interface of the USF and tower. The solutions came from already existing concepts and projects with similar working intentions as the USF, and are presented in section 5.2. The solutions were thought of through research and brainstorming. In the end, based on the required functionalities of the USF, two possible designs were developed from the concepts that have been analysed. Using the designs, some simple calculations were performed to see if the main purposes of the USF can be achieved. A multi-criteria analysis was conducted to asses which design performs better.

5.1. USF functionalities

As mentioned before, several degrees of freedom of the USF are restrained with respect to the WTG during a single lift installation and several are left free (for details see Table B.6). These restrictions all relate to the functionalities of the USF. The functionalities will be further explained in this section. When talking about the different degrees of freedom, Figure 5.1 should be referred to for the local coordinate system of the USF.

A sensitivity analysis regarding the rotation of the WTG with respect to the USF is also done to see how the environmental moment increases with a slight rotation of the WTG, and if the designs, which are presented in section 5.4 can counteract those moments.

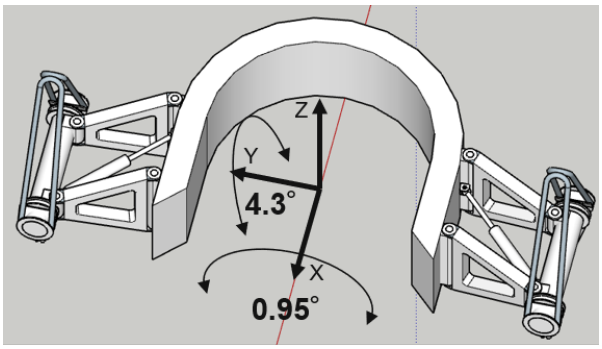

Figure 5.1: Maximum allowable rotations around the X and Y axis of the USF to compensate for uneven sling compensation. 0.95° is allowed around the X axis and 4.3° is allowed around the Y axis.

5.1.1. Functionalities

The Z-rotation is restrained, as otherwise the tuggers are not effective, and the WTG would be free to rotate. Relative rotation of the WTG with respect to the USF is undesired also, as otherwise the clearance between the rigging and the blades of the rotor is reduced. In the case that there was initial friction between the two components, the WTG might not turn back since the static friction would again have to be overcome. The X- and Y-translations are also restrained in order for horizontal loads to be transferred. The horizontal loads are caused

by the sidelead and offlead angle and are calculated in subsection E.2.1. They amount to around 746 kN as a result of the weight of the WTG. Another functionality of the USF requires the Z-translation to be free. This is needed, as the slings used in the rigging are elastic and will therefore, under the WTG load, elongate. The specific elongation of the slings is calculated in subsection E.2.2. A value of 0.30 m is found as the elastic extension of the slings. As for the X- and Y-rotation of the USF, minimal rotations should be possible. The reason for this is again sling extension. However, all the slings will in most cases, most likely not elongate by the same amount, therefore, to accommodate differences in the length of the slings, some rotation along the local X- and Y-axis of the USF needs to be possible. It has been calculated in subsection E.2.2 that 0.95 degrees around the X-axis and 4.3 degrees around the Y-axis should be allowed. The rotations are depicted in Figure 5.1. The X- and Y-rotation functionality greatly increases the complexity of the USF design.

Along with the different degrees of freedom of the USF, there are also other requirements that the USF design should aim to meet. An optional requirement for the USF is to offer vertical support to the tower. A necessary requirement, however, is sufficient stability of the USF during recovery after the WTG has been set down on the foundation. Instabilities can potentially arise during recovery of the USF from the fact that the location of the CoG of the USF does not coincide with the CoG location of the WTG assembly (for reference, see Figure E.2), and therefore the lift point positions need to be considered, or alternative solutions need to be found, which are outside the scope of this investigation, but are briefly discussed in section 6.2.

5.1.2. WTG rotation sensitivity

Using the base case OrcaFlex model of the whole system, a sensitivity analysis was conducted to investigate the WTGs sensitivity to slight misalignment with the USF. For the test, the orientation of the WTG was slightly turned with respect to the USF to simulate real-life conditions in the case that slip occurs between the USF and the tower. In the OrcaFlex model, the LLT and hence the slings connecting the LLT and USF rotated as well due to the rotation of the WTG. This caused the slings to be elongated with respect to the original length when the WTG was facing the initial direction. By providing a slight relative rotation between WTG and USF, the Z-moment of the tower was investigated to see if, with a different orientation between the tower and USF, the moment would increase or not. The results are presented in Figure 5.2. The limiting environmental conditions, determined in subsection 4.3.4 were used for the analysis. The angles of rotation of the WTG tested were -20, -15, -10, -5, 0, 5, 10, 15 and 20 degrees. It can be seen that increasing the relative rotation between the USF and WTG original position increases the maximum tower Z-moment experienced. This could potentially be a problem for the real-life application of the USF, as in the case that the required normal force can no longer be delivered and slip occurs, the moment acting on the WTG will under the same environmental conditions, increase according to the results. The increase of the moment depends on the rotation of the WTG due to the occurrence of slip, however, the more the WTG is rotated, the larger the moment acting on it becomes, as at rotations of -20 and 20 degrees, the maximum moment exceeds 6000 kNm. This could potentially result in the WTG rotating more and more after the initial point of slip.

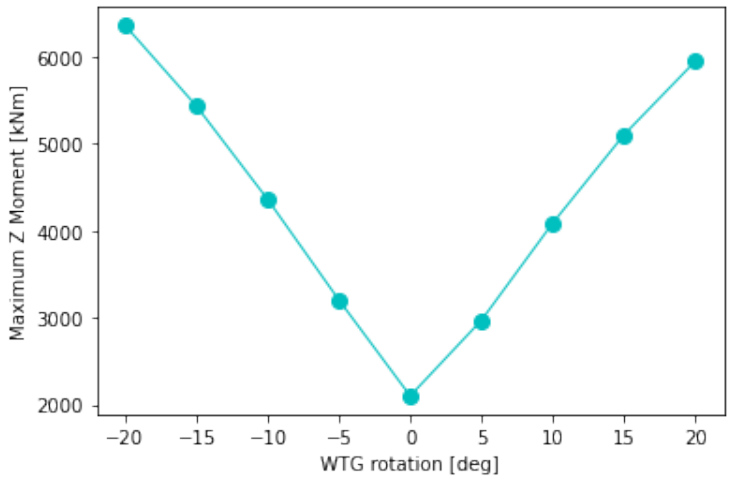

Figure 5.2: Results of the WTG rotation sensitivity analysis. The Y-axis represents the maximum Z-moment magnitude. The X-axis shows the rotation of the WTG relative to its original position.

OrcaFlex cannot model friction between two 6D buoys and therefore these results do not represent the actual dynamic situation that would occur since the tower and USF are rigidly connected to each other. In reality, once the moment becomes too large to be counteracted through friction at the USF and tower interface, once not enough normal force is supplied, slip will occur. As the moment increases, so must the frictional force, and due to an increase of the frictional force, the tangential displacement is slowly increasing as well to a point where macro-sliding can occur between the USF and tower (Deladi, 2006). This point is known as slip. With the occurrence of slip, the friction that occurs between the tower and USF changes from static to dynamic friction. As explained in section 2.4, the coefficient of dynamic friction is much lower than the coefficient of static friction. Due to this, less force is required to overcome dynamic friction. In the case static friction is overcome in the initial position, slip occurs and the WTG starts rotating, there is a possibility for it to continue rotating due to the fact that the moment working on the WTG tower actually increases through slight rotation of the WTG. The tangential force that the moment causes on the WTG could potentially be higher than the maximum frictional force that the USF can deliver. In this case, the WTG would continue rotating as more than enough force is being provided to exceed the dynamic frictional force and sustain the rotation of the WTG. This is a serious problem due to the possibility of the blades striking the crane or other similar disasters happening. It is suggested for future investigations to perform a dynamic analysis of such a situation in appropriate software. This is further discussed in the recommendations in section 6.2.

5.2. Concepts

In this section, possible already existing concepts were investigated and the possibilities of their working principles to be applied to the USF were analysed. Some concepts are specific examples, while others are more general components used for many different engineering applications, such as clamps.

5.2.1. Friction pads

Friction pads offer a simple solution to restraining relative rotation between the USF and tower during the installation of the wind turbines. Friction pads are used in many different industries for various reasons, including the offshore wind industry, where for example they have previously been used for blade installation equipment, lifting frames, and pile grippers. An extended concept analysis with more detailed workings of the specific friction pad-based concepts is given in section E.1.

Blade installation equipment

The installation of blades offshore is a complex procedure, as high accuracy and precision are necessary for the positioning of the blade root with the nacelle. The offshore environment makes this a complicated task. The Guide Root End Positioning (GREP) tool and the Blade Installation Tool (BIT), were required for the RNA method by Heerema MC to install the wind turbines at the Arcadis Ost wind farm. They helped with positioning and steadying of the blade when it was being mounted to the nacelle. The working principles of these tools could potentially be applied to the USF and have therefore been further analysed. The detailed working of both tools is given in section E.1. Both tools are used for something completely different than the purpose of the USF is however, they do share similarities. Both tools need to provide sufficient clamping force while not damaging the component they are holding, which is also the goal of the USF. A diagram of the GREP can be seen in Figure 5.3, where the numbered labels refer to:

1. Tower part;
2. Main frame;
3. Rail frame;
4. X-translation frame;
5. Y-translation frame;
6. Z-rotation frame;
7. Y-rotation frame.

Each given frame allows for motion in the degree of freedom after which it is named. The Y-rotation frame contains 3 rubber friction pads spaced at 120 degrees to ensure equal load distribution. The material of the pads is EPDM 8407 and between the pad material and the material of the blades (mostly fibreglass), the coefficient of friction is 0.5 (Heerema Marine Contractors, 2022a).

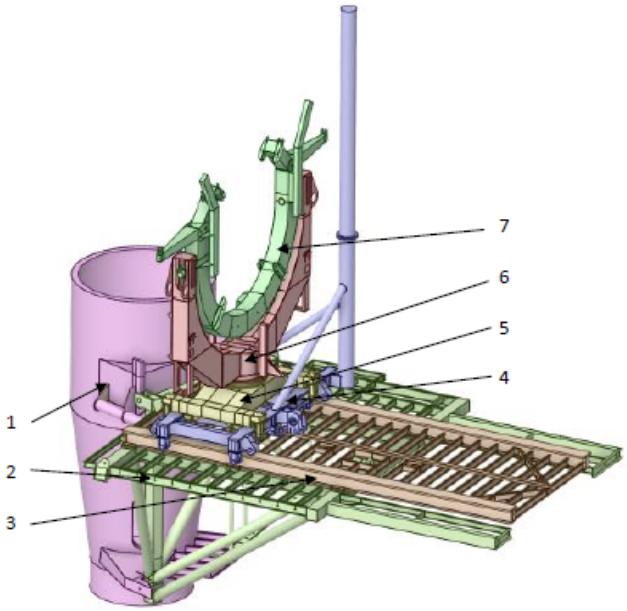

Figure 5.3: GREP tool used for blade installation during the RNA method (Heerema Marine Contractors, 2022a).

The degrees of freedom of the blade that the GREP restrains and allows are different than the degrees of freedom that the USF aims to restrain of the WTG. The GREP makes X-, Y- and Z- translations possible through hydraulic cylinders and chain drives. Such means for translation are unrealistic for the USF, however, the X- and Y-translation are also not necessary for the USF. The most relevant part of the GREP for the USF is the use of friction pads to prevent the rotation of the blade while it is being held. Additionally, hydraulic cylinders are used to provide the necessary clamping force to deliver the required normal force. This can be used for the USF, as rotation between the tower and USF can be prevented through the same mechanism.

The BIT also uses friction pads to prevent the blade from slipping out of it. Very precise details of the BIT are not known, as the BIT was supplied by Vestas for the Arcadis Ost project, who did not make specific information public. The BIT tool allows the rotor to stay in place by holding the blade with two arms. This fixes the blade. The BIT connects the blade to the crane. Pads are located on the arms of the BIT and come in contact with the blade. The material of the pads is EPDM 8407 and between the pad material and the material of the blades (mostly fibreglass), the coefficient of friction is 0.5, which is the same as for the GREP tool. Rotations and other translations of the blade when being held by the BIT are not allowed, and hence other than the friction pads used to generate sufficient friction to restrain motion, the BIT tool does not offer other possible ideas for the USF - tower interface solution.

Lift-frames

Full WTG single lift installation has already been proven possible in the past in a few smaller projects. Some of these projects made use of a similar concept to the USF in the form of stability frames. These projects include the Hywind wind farm, and the Beatrice Demonstrator project, both located off the coast of Scotland.

Hywind was the first ever floating offshore wind farm, installed in 2017. For its installation, it used the integrated approach of the WTG and tower being installed as one assembly onto the floating foundation. It utilised a ”stability frame”, pictured in Figure 5.4 (SAIPEM, 2017). The blue frame was fastened onto the tower during the lift, which was done with both cranes on the heavy lift vessel (HLV) vessel, Saipem 7000. The WTG was installed onto a floating foundation, therefore, weather constraints were tight to avoid unstable floater motions. The frame is attached to the tower by using hydraulic cylinders and making contact with it through four friction pads. Two friction pads were fixed, while two were connected to hydraulic cylinders, acting as arms. The hydraulic cylinders were able to provide enough clamping force so that the frame was able to provide sufficient stability to the whole WTG assembly during the lift (Ribuot, 2019). There is not much information available online regarding the rest of the design considerations, such as which degrees of freedom were constrained. For the USF, hydraulic cylinders could potentially be utilised to provide the necessary clamping force to friction pads, however, more

detailed working of the whole design will have to be considered to account for all the environmental loads. The environmental loads for the lift using the USF will be much greater due to the WTGs for the Hywind project being pre-assembled onshore and mated to the floating spar foundation inshore at a port in Norway. The port of Stord on the West coast of Norway is sheltered by the fjord, which helped to decrease environmental influence. The single lift with the USF is planned to be done offshore at the OWF location, where environmental conditions are harsher.

Figure 5.4: The stability frame (blue) as used for the Hywind project by Saipem (SAIPEM, 2017).

Figure 5.5: The support frame used to hold the wind turbine during installation of the Beatrice project (Scaldis, 2007).

In 2007 the Beatrice Demonstrator Wind Farm Project became the first project in which the turbine, nacelle and blades were assembled together onshore and transported to an offshore location off the coast of Scotland. The water depths in the area were up to 45 m, and the wind turbine used had a capacity of 5 MW. The two cranes of the Rambizin crane ship were used to lift the WTG onto the jacket foundation (Zhang et al., 2013). Just like the Hywind project, this installation made use of the dual crane arrangement, which is not the case for the operation with the USF. The installation process required the use of a support frame for the tower section while being held by the crane for additional stability during transport and lifting. Figure 5.5 shows a close-up of the frame. The support frame, known as the tower interface frame (TIF), is a large steel structure and was built specifically for the Beatrice project by Offshore Heavy Transport, a Norwegian engineering company. The TIF held the tower section at the base while being transported to the offshore location. The TIF was designed so that during the lift, it would be connected to the WTG tower at a height above the combined CoG of the WTG (Seidel and Gosch, 2006).

This allowed for the lifting forces to be applied closer to the base of the tower. Having the lifting forces closer to the base of the tower helped to minimise the loads acting on the tower sections when lifted (minimise stress). The USF is also mounted onto the frame at a height above the combined centre of gravity for the same reason. Along with that, the TIF helped in maintaining the stability of the WTG, as it ensured that the WTG was kept in a vertical position. The TIF had a mass of 230 mT and was designed to be adjustable so that it could accommodate towers of different sizes and weights. To adjust the height of the TIF on the tower to the correct height, hydraulic cylinders were used. The TIF was also equipped with sensors and other equipment used for monitoring, which enabled the installation team to monitor the lifting forces being experienced, and in hand, ensure that the whole procedure was advancing safely (Seidel and Gosch, 2006). Hydraulic cylinders, as utilised for the Beatrice project, could be used for the USF as well. More specific details of the TIF and the lifting procedure are not known. But overall, the TIF was a critical component in the installation of the Beatrice Demonstrator wind farm, as it allowed for the safe and efficient installation of WTGs.

Motion-compensated grippers

There are several concepts of motion-compensated grippers for monopile installations from various contractors. The goal of all these grippers is to aid the installation of monopiles by compensating vessel motions and keeping the monopile vertical. The motion compensation property of such grippers is not relevant for the USF design, however, the way they hold the pile and the relative motion between the pile and gripper could be relevant. A key difference between the grippers and the USF is the type of loads that get induced. USF motions caused by the environment are wind dominated, while the motions of the pile grippers are mostly hydrodynamic forces induced by the waves. TWD and Heerema MC both have concepts of such pile grippers, with slightly different working. For a full description, see section E.1.

5.2.2. Slings

Slings can be attached to the USF, and be used to wrap around the tower to restrain the Z-rotation of the USF via friction. A representation of this idea is shown in Figure 5.6. The slings would have to be under tension, and a sliding system would be required to still allow Z-translation. An advantage of this concept is that the translation in the X- and Y-directions is restrained, but the rotation in these directions is not necessarily. A disadvantage is that the wires used for the slings have a very limited effect on the overall friction as they have a very low coefficient of friction, meaning that adding them to the USF will not greatly improve performance when it comes to restraining the Z-rotation. This means a very large pre-tension would be required to obtain the necessary friction. Removal of the USF after the WTG has been installed also becomes more difficult, as the slings have to be released through some kind of mechanism, further increasing the complexity of the design. Due to this and the high pre-tension requirement, the concept of tensioned slings is not a practical solution to apply to the USF - tower interface.

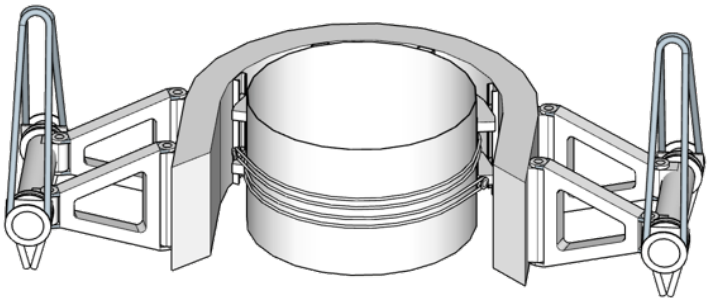

Figure 5.6: Possible design of the USF, using slings.

5.2.3. Band brakes

Band brakes are brakes which work through the use of friction. The application of such braking systems can be found in winch drums and chain saws. A band is wrapped around a rotating drum and when a positive actuating force is applied to the system, the band concentrically tightens around the drum. This causes the two surfaces to become in contact with one another. The drum is forced to decelerate due to friction that has arisen between the surfaces. The brake is a static brake if the drum is prevented from rotating further or a dynamic brake if the drum is just slowed down. The band which gets tightened around the drum is often made from spring steel and has a rectangular cross-section. The inside of the band is lined with a material that will be able to generate friction

when needed. At each end of the band, there are handles so that the band can be held and compressed accordingly. When the band is wrapped around the drum, which is smooth around its outer circumference, the handles of the band can be pulled together to produce the required friction for the drum to stop rotating. The pulling of the band together is often achieved through hydraulics. This way, the band will exert a tangential force on the drum since it will be tightened, and tension will be created.

The torque generated by the band brake varies linearly as a function of the applied force. The force that is applied to tighten the band is, due to the positive servo effect of the break, greatly increased (Downey et al., 2016). Figure 5.7 shows a diagram of the forces working on a band brake.

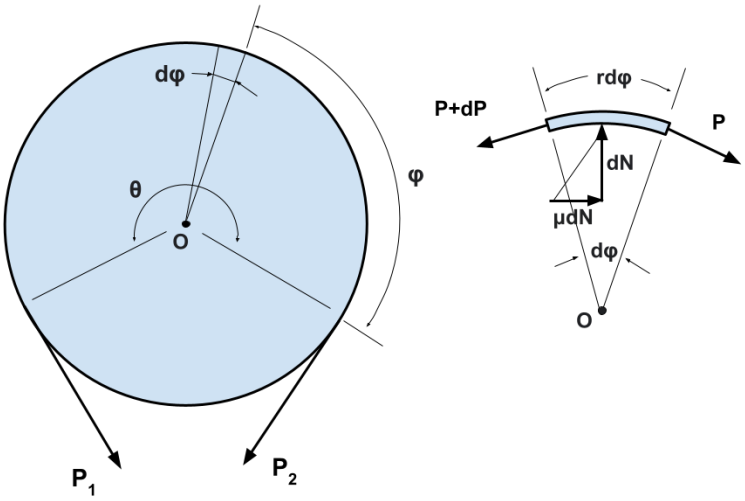

Figure 5.7: Simple band brake diagram with labelled forces.

Due to friction between the band and the drum, in the case, the drum is rotating in the clockwise direction, the reaction force, P_2 is smaller than P_1. If it is rotating in the counter-clockwise direction, the opposite is true. The band can be split into many angular segments, $d\phi$, along the drum, as seen in the figure. Forces acting on each segment must be in equilibrium. The sum of the forces in the vertical direction, when assuming clockwise rotation is:

$$(P + dP)\sin\frac{d\phi}{2} + P\sin\frac{d\phi}{2} - dN = 0 \tag{5.1}$$

$$dN = Pd\theta \tag{5.2}$$

Equation 5.2 is obtained from Equation 5.1, based on the assumption that $\sin(\frac{d\phi}{2}) \approx \frac{d\phi}{2}$ for small angles. In the above equations, P is the tension in the band and N is the normal force. The horizontal forces can also be summed as:

$$(P + dP)\cos\frac{d\phi}{2} - P\cos\frac{d\phi}{2} - \mu dN = 0 \tag{5.3}$$

$$dP = \mu dN \tag{5.4}$$

Equation 5.4 is obtained from Equation 5.3 from the small angle approximation, $\cos\frac{d\phi}{2} \approx 1$. μ is the coefficient of friction. The value for dN from Equation 5.2 can be substituted into Equation 5.4. Integrating the expression yields:

$$\begin{aligned} \int_{P_2}^{P_1}\frac{dP}{P} &= \mu\int_0^{\theta} d\phi \\ \frac{P_1}{P_2} &= e^{\theta\mu} \end{aligned} \tag{5.5}$$

The left side of the equation is integrated between P_2 and P_1, since $P_2 < P_1$ and the right-hand side of the equation is integrated over the angle of wrap, θ, so from 0 to θ. The torque, T can be obtained from:

$$T = (P_1 - P_2)\frac{D}{2} \tag{5.6}$$

The normal force dN acting on a part of the band with width b and length $rd\theta$, where r is the radius of the drum, is given in Equation 5.7.

$$dN = pbrd\theta \tag{5.7}$$

p represents the pressure acting on the length of the segment. If the value for dN from Equation 5.2 is substituted into Equation 5.7, the following is obtained: Equation 5.7.

$$Pd\theta = pbrd\theta \tag{5.8}$$

Rearranging, the equation for pressure can be obtained: Equation 5.7.

$$p = \frac{P}{br} \tag{5.9}$$

Equation 5.9 shows the tension in the band is proportional to the pressure acting on it. The maximum pressure in the band is encountered at the toe (near the pin), where $P = P_1$, therefore the maximum pressure in the band, $p_{b,max}$ is:

$$p_{b,max} = \frac{P_1}{br} \tag{5.10}$$

A more detailed derivation of the above equations can be found in the book 'Mechanical Engineering Design' (2011) by Budynas and Nisbett.

The working principles of band breaks could potentially be implemented into the USF - tower interface to prevent rotation around the Z-axis. The band of the brake would have to be tightened the whole time to produce the necessary friction which would prevent relative rotations of the tower and USF. The two pulling forces on the band would have to provide a torque equal to the moment acting on the tower due to the environment in order to counteract it. Since friction will arise, the environmental moment will be dissipated through heat. In the equations presented above, it can be seen that the working of the brake system will depend on the friction coefficient, but for real applications of the band brake, the brake lining's ability to dissipate heat is also important since the band brake is a very dynamic system (drum rotates at high angular velocities). If heat is produced faster than it can be dissipated, a problem arises. This should however not pose major problems to the USF, as the USF would work as a quasi-static system where the rate of heat production will be much lower than real band brakes. A downside of band brakes is the fact that they are less effective when exposed to moisture and wet environments. In such situations, they are more prone to slip, which decreases their braking effectiveness. However, this is the case for friction pads and similar principles as well.

5.2.4. Tower modification

The previous concepts have all been related to modifications or additions to the USF. However, to improve the connection at the USF-tower interface, the tower can also be slightly modified. Tower modification does add additional complexities to the manufacturing of the tower, especially in regard to production, as many modified towers would need to be created for a whole wind farm. This would increase the costs for the client and could also potentially affect the integrity of it and its fatigue life limits. Another issue is that, often turbine manufacturers are not willing or are hesitant to change anything with regards to the WTG and, therefore if tower modification would be needed at the tower - USF interface, the contractor would have to be involved in the project in the very early stages to make that possible. However, due to tower modification yielding very simple and effective designs, this option is investigated. Tower modification options include the use of multiple hang-off stoppers (trunnions), a flange connection or a collar at a specific elevation of the USF and increasing the tower wall thickness. Some of these will be further elaborated in the following sections.

Wall thickness

One of the tower modifications could affect the wall thickness. The wall thickness at the interface of the USF and tower can be increased in order to increase the maximum allowed clamping force before permanent damage is done to the tower. As will be shown in section 5.3, the tower wall thickness is a relevant variable when determining the maximum allowable stresses working on the tower before a failure mechanism can occur. Higher allowable stresses would allow for more normal force, and in hand, the frictional force would be higher.

Increasing the wall thickness at the interface adds extra weight to the overall assembly that has to be picked

up by the cranes on the vessel and also changes the CoG of the WTG assembly. This then has an influence on the optimal location of the USF on the tower. If the location of the USF with respect to the height of the tower changes, then so does the location at which the tower thickness needs to be increased. An iterative process is required to find the correct USF location on the tower for a given thickness increase.

Multiple stoppers

In the case that tower modification is allowed, the solution of incorporating multiple stoppers at the tower - USF interface is one of the most promising solutions, as it yields a simple and light solution for the USF.

Trunnions should be located around the tower at the height of the USF. They should be located at equally spaced intervals. The stoppers should be appropriately sized so that they are able to fit into vertical slots on the USF. These vertical slots will prevent Z-rotation almost completely (depending on the tolerances). Along with Z-rotation being sufficiently restrained, Z-translation will be possible within the vertical slot. It is important to make the slot long enough so that sufficient sling elongation can be compensated. X- and Y-rotation is also possible due to the slots. An issue with this design is that a release mechanism for the USF is still required.

Separate clamp

A separate clamp as a tower modification refers to the USF keeping its original geometry, but an additional bracelet is added around the tower to which the USF can be attached to. The bracelet is essentially a clamp that can work on the same principles as discussed in subsection 5.2.5. The bracelet gets squeezed by the USF, however, part of the squeezing gets passed on through the bracelet to the tower, which could result in paint damage, which is undesired.

5.2.5. Clamp based

While many ideas that make use of friction have already been discussed, there is also the possibility to use clamping mechanisms based on principles other than friction. This section will discuss the option of hydraulics and bolting to achieve sufficient clamping.

Hydraulic clamping

An option to achieve a sufficient clamping force is to make use of hydraulically pressurized clamps. The hydraulic clamps can be tightened around the tower to provide a secure connection. To make this possible, the clamp should be designed to fit around a tower and be able to apply a clamping force, which would hold the frame in place. The control of the clamp could be done remotely to guarantee that it is tightened to the correct magnitude of force which would prevent rotation around the Z-axis.

Considering Pascal's law, which states that pressure is equally transmitted in every direction when it is applied to a trapped fluid, the explanation behind hydraulic clamping can be given. When a hydraulic clamp is fitted around the tower, the force it exerts is evenly distributed around the surface area. The force, known as the clamping force, can be calculated through Equation 5.11, in which F is the clamping force, P the hydraulic pressure and A is the area of the hydraulic piston.

$$F = P \cdot A \tag{5.11}$$

To control the clamping force, both the hydraulic pressure and the area of the hydraulic piston can be adjusted. The hydraulic pressure can be changed by the pressure relief of a valve.
A design for the USF involving hydraulic clamps, could entail hydraulic cylinders being positioned on the section of the USF that will open and close for hook on and removal. The cylinder would allow the USF to clamp to the tower with sufficient clamping force, which would need to be pre-determined based on the rotational restraint capacity. Different combinations of the hydraulic pressure and area of the hydraulic cylinder can be used. Furthermore, the cylinders could be remotely controlled with a hydraulic power unit and control valves, similar to the way the hydraulic cylinders in the GREP tool are controlled.

Bolted connection

A bolted connection can be utilised to clamp the USF around the tower. In such a connection, the clamping force is achieved by tightening the bolts in the connection to a specified torque.

The design of the connection would involve a collar being connected by a bolted connection. The bolt must

have the correct diameter and length to provide the desired clamping force, and the tightening torque must be well-controlled to ensure the bolt is being tightened to the correct level. The bolted connection is not the best option for the USF- when considering the installation and removal of the USF onto the tower, as the tightening of the bolts to the correct torque and releasing the torque would have to be done manually, which is not possible during such an installation offshore. Damage to the tower is also very likely through such a concept, which is not allowed.

5.2.6. Concept evaluation

The above concepts have been briefly analysed to see which of them yielded realistic and physically possible solutions for creating a connection at the USF and tower interface. The overall focus of this thesis investigation was the Z-restraint of the USF and tower, therefore, it was decided to create a design with a focus on that specific restraint. The other functionalities of the USF that were mentioned in section 5.1, have been omitted in the design phase to reduce complexity.

The USF design is required to provide sufficient torque to prevent rotation. Realistic possibilities for preventing Z-rotation at the USF and tower interface include friction and structural rotational stoppers. Friction is utilised in the friction pad-based designs and the band brake to prevent rotation and other motions. Due to this, generating sufficient friction through a clamping mechanism seems to be the most appropriate option for achieving the rotational restraint around the Z-axis of the USF and tower. Additionally, to aid with the clamping onto the tower without damaging the tower, the closing of the USF, and providing sufficient normal force, hydraulic cylinders can be used, as was the case for the stability frame designed by Saipem. It was decided to steer away from the tower modification option and the use of rotational stoppers, as it is not guaranteed that tower modification will be possible for every project. The use of friction makes the USF more universal and appropriate for several projects. Using friction as the solution to prevent the relative rotation between the WTG and USF can be done in several ways. In the following section section 5.4 these options are further explored and made into designs.

5.3. Load Case

Before a possible design was created, the load case which it had to pass, had to be defined. The most important aspect of the load case is being able to counteract the moment caused by the environmental loading, which will be done through friction. An overview of the load case can be seen in Table 5.1. The load case includes producing sufficient frictional force (tangential force) to counteract the moment and keeping the stress from the clamping force below the maximum permissible stress. How these values were determined is presented in the following sections.

Table 5.1: Load case for the USF designs.

Tangential force [kN]	WSD limit [MPa]	Buckling pressure [MPa]
1200	213	0.95

5.3.1. Minimum tangential force

Based on a maximum moment of 2.1×10^3 kNm from Chapter 4, and a tower radius at the point of the USF - tower interface of 3.5 m, a force of 600 kN can be obtained, as shown in Equation 5.12. This is the tangential force and is also the minimum value the frictional force without any safety factors applied needs to possess.

$$F_t = F_f = \frac{M_z}{r} \tag{5.12}$$

F_t is the tangential force, F_f the frictional force, M_z is the Z tower moment, and r the radius of the tower at the USF location. The value of the frictional force depends on the normal force delivered by the USF and the coefficient of friction between the two surfaces. There are no guidelines for the value of safety factors that should be applied to such lifting equipment. Therefore, to assess the effect of the safety factor and the coefficient of friction on the normal force, a sensitivity analysis was conducted. Both parameters were investigated, as there is a level of uncertainty in both of them. The reasons for uncertainties in the coefficient of friction are explained subsection 5.4.5.

The results of the sensitivity analysis should show how big of an impact the safety factor and coefficient of

friction have on the required normal force. The results of the sensitivity analysis are presented in Figure 5.8. The lines plotted are represented by Equation 5.13.

$$F_N(\mu) = \frac{S.F \cdot F_f}{\mu} \tag{5.13}$$

where F_f is 600 kN, and μ is varied between 0.01 to 1. $S.F$, the safety factor, is constant per plotted line, and takes up values of integers between 1 and 4, each representing one curve on the plot. The X-axis has been plotted using a logarithmic axis to better present the results visually. Values of the coefficient of friction larger than 0.3 do not lead to much change in the normal force. For such values of μ, there is also no great variation when different safety factors are used for the environmental loading. A difference in the normal force can be observed for values of μ smaller than 0.3. For these values, the normal force exponentially increases with decreasing μ and the use of larger safety factors results in a much higher minimal normal force required. This could potentially be a problem if the coefficient of friction is over-estimated for the tower - USF interface. Slipping needs to be prevented between the USF and tower, therefore, it should be aimed to obtain a high coefficient of friction between the two materials when creating the design.

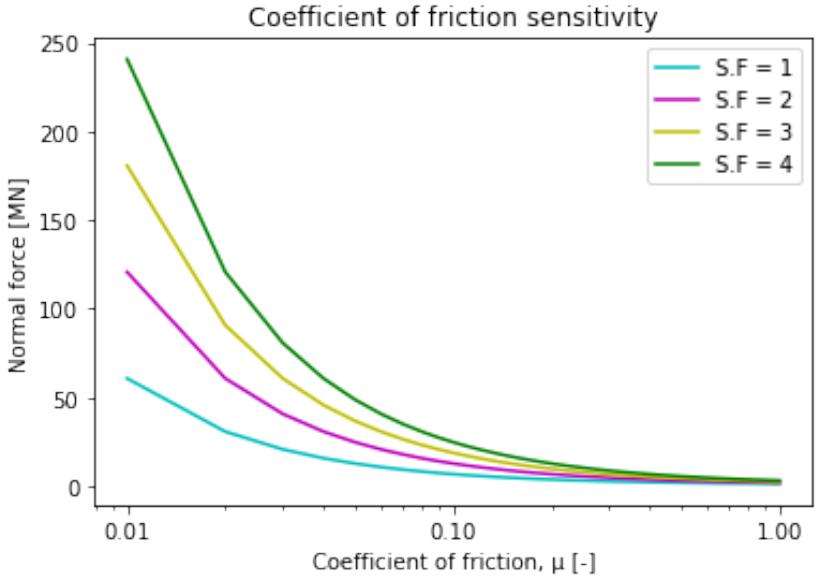

Figure 5.8: Logarithmic plot showing the normal force as a function of the coefficient of friction for a frictional force of 600 kN due to the environmental loading. Different safety factors are considered for the environmental loading.

It has been decided that a safety factor of 2 is sufficient for the purposes of this thesis. So using a tangential frictional force of 600 kN and applying a safety factor of 2 results in a frictional force of 1200 kN, as seen in Equation 5.14.

$$F_f = \text{S.F} \cdot \frac{M_z}{r} = 2 \cdot \frac{2.1 \times 10^3}{3.5} = 1200 \text{ kN} \tag{5.14}$$

Considering the USF as a sort of brake, the force of 1200 kN is the braking force acting in the tangential direction.

5.3.2. Tower yield strength

The tower of the WTG can be considered a thin-walled cylinder due to its diameter-to-wall thickness ratio ($\frac{7}{0.0272} = 257.4 > 100$). Thin-walled cylinders experience different stresses, including circumferential, axial and radial stresses. In addition to the design having to produce enough force to resist the moment induced by the environmental loading, the stress that will be induced on the tower must be smaller than the yield strength of the material of the tower in the circumferential direction. The material is steel S355 and has a yield strength of 355 MPa. The load on the tower should not exceed the yield strength for thin-walled cylinders in any direction. A higher induced stress will cause damage and deformations of the tower (will cause yielding of the tower). However, to include a safety margin, the Working Stress Method (WSD) can be applied. The WSD can be utilised to find the permissible stress and assumes that materials behave in a linear elastic way. The equation relating

stress and force is $\sigma = \frac{F}{A}$, where σ is the stress, F the force trying to split the cylinder due to pressure, and A the cross-sectional area of the tower where the force is applied.

The stress experienced by the tower is not allowed to be greater than the permissible stress or load (Q). The permissible stress is based on the resistance (R), and a safety factor ($S.F.$). The equation for the permissible stress (Q) can be seen in Equation 5.15.

$$Q \leq \frac{R}{S.F.} \tag{5.15}$$

The resistance in this case is the yield strength (355 MPa). The hoop stress of the tower considers an axial loading situation. For axial loading, a safety factor of 1.67 is used for WSD calculations (API, 2014). So with a safety factor of 1.67 and the resistance being equal to the yield strength of the tower, the permissible load is required to be less than 213 MPa.

$$Q \leq \frac{355}{1.67} = 213 \text{ MPa} \tag{5.16}$$

Disadvantages of the WSD include the fact that the safety factor has no theoretical basis and that no distinction is made between different loads acting on the WTG. For example, the environmental loading might require a different safety factor than the weight of the WTG (API, 2014).

5.3.3. Buckling

Yielding is a possible failure mechanism of the tower due to the clamping, but so is buckling. It needs to be checked which failure mechanism will occur first by seeing which critical stress is lower. During buckling, excessive hoop compression will occur. Since the WTG is confined within the USF, it is not possible for it to deform outwards, but instead an inward lobe will form when the hoop stress exceeds a critical level (Figure 2.6). The clamping force acting on the WTG will be relieved after the buckling happens due to the tower being hollow. This is different when dealing with a hydrostatic force causing buckling, as in that case, the load is still present even after buckling (Vasilikis and Karamanos, 2009).

Analytical solutions for the critical buckling stress and pressure of thin-walled cylinders have been presented in subsection 2.5.2. They all depend on different constraints and boundary conditions. The critical buckling pressure as derived by Glock (1977), is presented in Equation 2.27 and relates to a single lobe buckling mode of a confined cylinder. The equation defines the buckling pressure of a tightly fitted elastic cylinder in a rigid cavity. Substituting for the wall thickness, Young's modulus, Poisson's ratio and diameter of the tower, a buckling pressure of 1.04 MPa is obtained.

$$p_{GL} = \frac{E}{1-\nu^2}(\frac{t}{D})^{2.2} = 1.04 \text{ MPa} \tag{5.17}$$

Although this pressure is quite low, it is still many times higher than the buckling (bifurcation) pressure of a long elastic cylinder that is not confined, as shown in Equation 5.18.

$$p_e = \frac{2E}{1-\nu^2}(\frac{t}{D})^3 = 24.5 \text{ kPa} \tag{5.18}$$

However, as mentioned, Glock's equation is based on elastic cylinders and for buckling due to hydrostatic pressure. The material of the tower is steel, which exhibits elastic-plastic behaviour and the cause for buckling is not completely hydrostatic, which is why this might not be the best approximation of the critical buckling pressure.

Using the methodology proposed by Vasilikis and Karamos (2010) in their study, the ultimate buckling pressure in the inelastic region was calculated as 0.95 MPa.

$$p_{max} = 0.95 \text{ MPa} \tag{5.19}$$

The methodology has already been introduced in subsection 2.5.2 and specific calculation steps are presented in Appendix A. Glocks pressure is slightly higher, however still within a reasonable range to 0.95 MPa. It has been decided to continue the investigation with a maximum buckling pressure of 0.95 MPa.

5.4. Concept design and analysis

Based on the evaluation of the concepts, two potential designs for the USF-tower interface have been designed. One makes use of friction pads and the other utilizes the brake band principle. They both constrain the rotation around the Z-axis through friction. More explanation and some basic calculations regarding their rotational restraining capacities are presented in the following sections. For the purpose of this investigation, the designs are not fully developed, and only the most relevant aspects of the designs for this investigation are presented. The diagrams of the designs are shown in Figure 5.9.

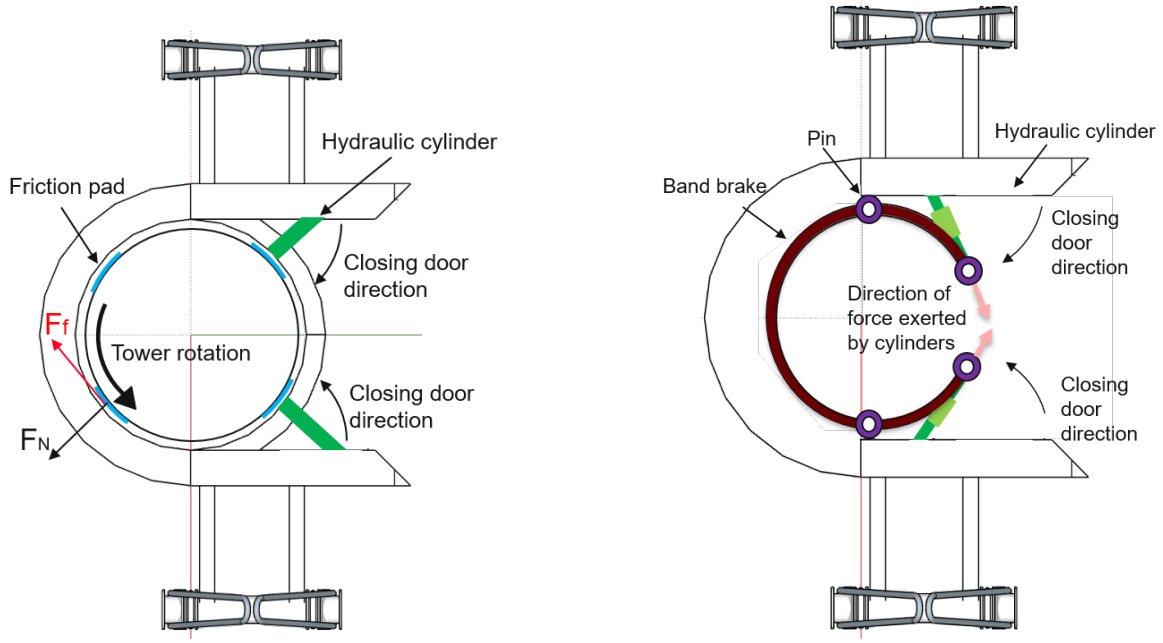

(a) Design 1: Friction pads

(b) Design 2: Band brake

Figure 5.9: Diagrams of the proposed USF designs.

5.4.1. Materials

The two designs that have been thought of for the USF require sufficient friction to be generated in order to fulfil their purpose. An appropriate material is needed for the friction pads and for the brake lining on the band brake. In this section, possible materials are presented with their main properties. The coefficient of friction between the material and the tower is one of the most important parameters but is tricky to predict. It depends on the applied pressure, therefore, there is an uncertainty in the values used, as the applied pressure is not known, and rigorous test results not available. Another important factor to consider during material selection is the materials compatibility with the tower coating and how likely the tower is to be damaged due to physical contact with the frictional material.

Tower coating

The wind turbine used in this thesis is based on the NREL 15 MW wind turbine, which does not have specific coating specifications for the tower. Coatings of specific wind turbines, such as the V174-9.5 MW, as used for the Arcadis project, are also not publicly available. For that reason, it has been decided to assume that the tower is coated with polyurethane (PU) coating, as is commonly seen in literature and is in line with various different ISO standards, such as *ISO 12944-9:2019 -Paints and varnishes - Corrosion protection of steel structures by protective paint systems* (Momber and Marquardt, 2018).

Friction pads

There are many different types of friction pads available and already being used in the industry. They range from rubber pads to pads with serrated steel. The coefficient of friction between the tower and the pad material will depend on the temperature and contact pressure. The temperature dependence is omitted from this thesis. The pad material is also not prohibited to damage the tower structurally or cause any damage to the coating. The

coating is important for protection against corrosion and UV among other factors. At Heerema MC, friction pads are utilised for many different purposes, one of which is for the saddles used to transport monopiles offshore and for clamps used during pipelaying. In Figure 5.10, a diagram of how the pad will look is presented.

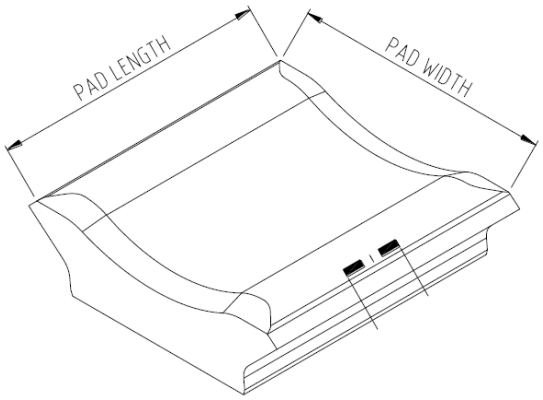

Figure 5.10: Diagram of the friction pad.

Steel pads often have serrations on the surface. The serrations of the surface of serrated pads are ridge shaped. The pads have been used for pipelaying for the tensioner clamps and can be made into V-shaped and curved pads. The ridges press into the outer surface of the pipes, which are specially coated, and so are able to produce enough clamping capacity (Heerema Marine Contractors, 2023). Serrated pads require remedial measures in certain situations and along with that, the load distribution is poor, which could cause tower damage. While the coefficient of friction between steel serrated pads and steel is higher than for rubber pads, they are not fully appropriate to be used for the USF application. The biggest issue with steel pads is the fact that they cause tower and coating damage at the contact pressures involved in this investigation. This is not allowed and hence the serrated pads are not considered.

Rubber pads can be used on any type of coating as long as the coefficient of friction between the two surfaces is able to accommodate sufficient tangential force. In this respect, rubber pads provide a viable option to be used for the USF-tower interface. At Heermea MC, extensive tests have been done with rubber pads for pile transport in wet and dry conditions. The results of the tests showed that with increasing compression stress, the coefficient of friction decreases, however, for low and high compression stresses, the coefficient of friction under dry conditions remains sufficient (Heerema Marine Contractors, 2023). According to *DNVGL-ST-N001: Marine operations and marine warranty*, a friction coefficient of 0.3 can be assumed between steel and rubber (DNV GL, 2018). This is the maximum design friction coefficient.

Another alternative is to use brake lining for the pads. In the past materials which contained asbestos were used as the brake lining, however, for environmental and health reasons, this is no longer allowed, and alternatives must be used. Asbestos was used as it contained suitable frictional properties for the brake lining. Brake lining is a suitable option for the pad material, as it shows good performance in the case of high contact pressure, although there is a possibility that it could lead to surface damage to the tower coating. Specific materials of the brake lining are discussed in the following section, where possible materials for the band brake lining are presented. Within Heerema MC, pads with brake lining have been designed and tested for the installation of fusion-bonded epoxy (FBE) pipes. The brake lining is made from a composite frictional material, which has already been used in other offshore equipment, such as winches and cranes in dynamic conditions. In various tests performed by Heerema MC, the brake liner material had a higher coefficient of friction at high contact pressures (above 3 MPa) compared to rubber and polyurethane pads (Heerema Marine Contractors, 2023).

Band brake

There is a range of options for the brake lining material of the band brake. It is important that the material is flexible to be able to wrap around the tower but also tough and must be heat resistant since the dissipation of the moment caused by the environmental loading through friction releases heat. Additionally, a high dynamic and static coefficient of friction is important, as a higher coefficient results in a larger braking force for the same

applied force on the band brake. Brake lining materials often include ceramic or metallic materials.

Indubal creates woven rolls and blocks that can be used for friction pads and as the material for the brake lining of a band brake. The woven roll, also known as industrial woven material BIN9850, is made up of raw materials and fibreglass yarn together with brass wire. This combination allows for exceptional mechanical strength. Additionally, the rolls are flexible so they can be altered to specific lengths and diameters depending on the requirement. The friction class under normal conditions is F. The woven roll is suitable for applications where high static and dynamic friction levels are needed. The tensile strength of the material is 33.7 N/mm^2 in the warp direction and 17.4 N/mm^2 in the weft direction (according to ISO-4606). The shear strength is 19.0 N/mm^2 in the warp direction and 16.2 N/mm^2 in the weft direction (according to ISO-6311). A coefficient of 0.25 has been assumed between the woven roll brake lining and steel S355 (Indubal, 2018).

An option for the brake lining material, which is used in the tyre industry, involves Twaron fibres and toughened rubber. Twaron alone is a synthetic fibre that shows high performance with regard to its strength, heat resistance and mechanical properties. It is classified as an Aramid. The advantages of utilising brake lining from Twaron fibres include its high tensile strength and excellent resistance to heat and abrasion. A high tensile strength allows for a high loading capacity to be withstood, while heat resistance makes it possible for the brake lining to function properly at high temperatures without substantial performance degradation. Its excellent abrasion properties allow the brake lining to maintain consistent friction characteristics, simultaneously also prolonging the service life of the lining. When in combination with toughened rubber, the Twaron fibre brake lining performance is further improved, as the matrices of toughened rubber allow for flexibility of the lining so that it is better able to conform to the shape of the tower. This way the contact area between the two surfaces is increased, which allows for improved friction. The toughened rubber is also capable of dissipating heat which will arise due to the frictional force, avoiding fade and overheating. A coefficient of friction of 0.31 under dry conditions has been obtained for the interface between Twaron and steel, based on experimental tests done by DSM HPF (Andersson, 2018).

5.4.2. Design 1: Friction pads

Based on the evaluation done in the previous section, a design with friction pads was created. The design consists of 4 friction pads, equally spaced around the USF, as seen in Figure 5.9a. Two of those pads are fixed, while two are connected to the doors of the USF that allow it to be installed and removed from the tower. The doors of the USF work with the help of hydraulic arms. The details of the hydraulic cylinders providing the opening and closing of the USF are not greatly discussed, but only the necessary normal force that they must provide has been calculated and presented.

Sizing and material

The size and material of the friction pads are important with regards to the frictional force that can be generated but also with regards to the stress acting on the tower as a result of the hydraulic cylinders applying a force on the friction pads.

It has been chosen to use 4 pads of sizing 400 $\times$ 400 mm. After the forces acting on the tower due to the pads will be calculated, a sensitivity analysis regarding the number and size of the pads will be presented. It has been decided to use pads made from rubber, as they are compatible with the tower coating and have a low chance of damaging the tower. Further, they have already been proven in the industry and can be made into curved pads. They have a coefficient of friction of around 0.3 when in contact with steel.

The frictional force calculated earlier in section 5.3, is a tangential load. The maximum tangential load that this USF design can withstand before slip occurs will depend on the shear strength of the weakest material involved. The shear strength of the tower is 142 MPa ($\tau = 0.4\sigma_y$), while the shear strength of the pads is 10 MPa (conservative value for shear strength of rubber). This means that the pad is made from the limiting material and the maximum permissible tangential load can be calculated using Equation 5.20, where A_{real} is the real contact area between the two surfaces, as explained in section 2.4, and τ_{min} is the lower value of the shear strength between the two materials. It is assumed that the real surface area is equivalent to the size of the pads. To compensate for this, a reduction factor will be applied to the coefficient of friction of the pad later.

$$F_{t,max} = A_{real}\tau_{min} \tag{5.20}$$

$$F_{t,max} = 4 \times 0.4^2 \times 10 = 6.4\text{MN}$$

In the equation, the area of all the pads is considered. The maximum tangential force obtained from Equation 5.20 is 6.4 MN. This is more than the required frictional force calculated in Equation 5.14, therefore, the shear strength of the materials is not limiting for this design.

Forces

The limiting maximum stress that can work on the tower is equal to the critical buckling pressure, which makes the limiting stress 0.95 MPa. Based on this, it can be verified that when 1200 kN of frictional force needs to be supplied, the design will not buckle.

$$F_f = 1200 \text{ kN}$$

To calculate the normal force, the frictional force is divided by the coefficient of friction between the two materials. It must be noted, however, that for a cylinder and friction pad, the contact pressure is never completely uniform over the whole surface. This has an effect on the coefficient of friction between the two surfaces. In the pipelay industry, a reduction factor of 1.2 is used to account for this issue, regardless of the number of pads used. The reduction factor is also applied in this case, and the friction coefficient is decreased from 0.3 to 0.25.

$$F_N = \frac{F_f}{\mu} = \frac{1200}{0.25} = 4.80 \text{ MN} \tag{5.21}$$

The normal force is equal to the force that the pads exert onto the tower, working in the opposite direction. This force comes as a reaction of the hydraulic cylinders pushing the pads towards the tower radially. The normal force and the radial force of the pads are equal to each other and work in opposite directions. From this, the stress acting on the pads can be calculated by using the combined area of pads of 0.64 m^2:

$$p = \frac{F_N}{A} = \frac{4.80}{0.64} = 7.50 \text{ MPa} \tag{5.22}$$

With the chosen pad area and coefficient of friction between the two surfaces, the critical buckling pressure, $p_{max} = 0.95$ MPa, is exceeded when 1200 kN of frictional force is required to be produced. From the sensitivity analysis done in subsection 5.3.1, it can be seen that lower values of μ greatly affect the magnitude of the normal force. Therefore, in the case that μ was overestimated, drastic consequences could occur to the operation. It was decided to also investigate the area of the pads based on the chosen coefficient of friction. In the sensitivity analysis, the pressure is plotted as a function of a single pad area for n pads. This way, both the size and number of pads were investigated. The results of this analysis are presented in Figure 5.11.

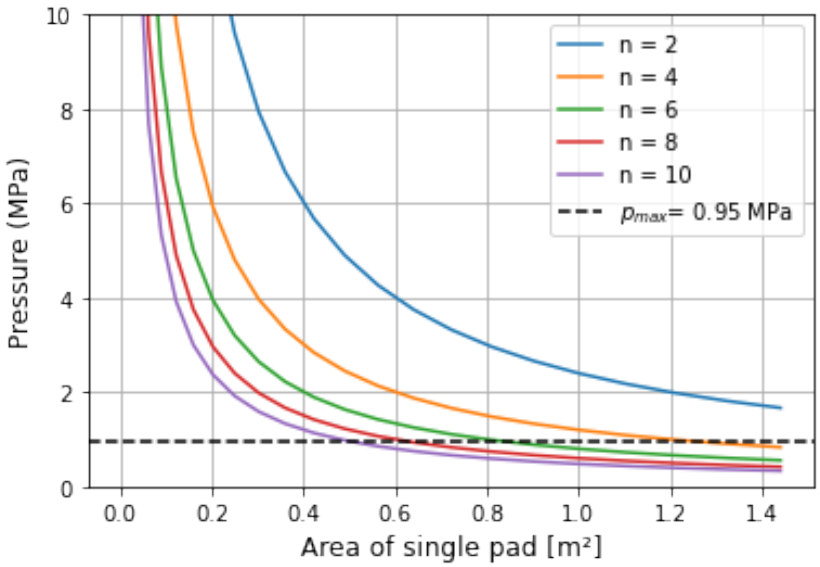

Figure 5.11: Results of the pad area sensitivity analysis. The black dashed line represents the critical buckling pressure p_{max}. The X-axis gives the area of a single pad.

The functions plotted in the plot are based on Equation 5.23.

$$p(A, n) = \frac{F_N}{nA} \tag{5.23}$$

where A is the area of one pad, n the number of pads, F_N is the normal force calculated in Equation 5.21. It can be seen that when 4 pads are used, $p(A, 4)$ exceeds the buckling limit when each pad is smaller than approximately 1.26 m^2. Therefore, for a design with 4 pads, the dimensions of the pads should be at least 1.12 $\times$ 1.12 m, for a total area of the pads of 5.053 m^2.

Since the buckling pressure is exceeded with the original design, new pad dimensions were considered. Due to the sensitivity analysis, it was decided to change not only the pad dimensions but also the number of pads. In the new design, 8 pads are used, as presented in Figure 5.12. It was chosen to work with 8 pads, as in this way the normal force is distributed among more points on the circumference of the tower, hence lower radial loads will act on the tower. For 8 pads to stay below the buckling limit, the area of one pad must be greater than 0.63 m^2. A safety factor of 1.5 will be applied to this value to make the final size of each pad 0.95 m^2. This means the pads will be 0.97 $\times$ 0.97 m, and the total area of the pads is 7.6 m^2. 1.5 was used as a safety factor to obtain a conservative pad size. From Figure 5.11 it can be seen that the pressure is not greatly decreased by increasing the size of the pads in the case of 8 pads and an area of 1 m^2. Accordingly, pads of 0.95 m^2 are acceptable for the purpose, seeing as a safety factor has been incorporated in their size. Making the pads even bigger is not logical as then more material would be required but the change in pressure will not be significant. It also has to do with the costs and handling of the pads. Re-calculating the pressure on the tower with the new pad area leads to 0.63 MPa.

$$p = \frac{F_N}{A} = \frac{4.80}{7.60} = 0.63 \text{ MPa} \tag{5.24}$$

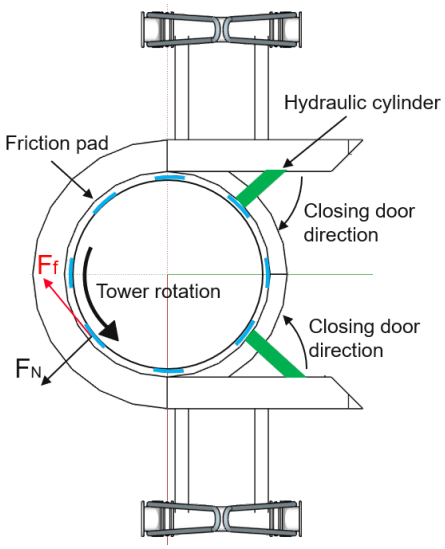

Figure 5.12: Revised USF design with friction pads. Now 8 pads are evenly spaced around the tower circumference.

Strengths and limitations

Many different materials of friction pads are available, as well as shapes, so that the most suitable pad can be chosen for the application. A drawback of friction pads for this specific function in the USF is that the tower will experience nearly radial loads, which can more easily cause buckling of it, compared to a more even distribution of the loading around the tower circumference. Due to this, the pads had to be made very large to keep the pressure on the tower below the buckling pressure. Large pads are more difficult to produce and handle and are also costly. Additionally, due to the roundness of the tower, the coefficient of friction significantly decreases to account for a non-uniform pressure acting over the pad surface. If it could be assured that the whole surface area of the pad is in contact with the tower, a reduction in the coefficient of friction would not be necessary, which would decrease the overall stresses acting on the tower. With the high required stresses to produce sufficient frictional force, it is not certain that the pads will not cause structural damage to the tower or damage to the coating.

5.4.3. Design 2: Band brake

A second possible design for the USF utilizes the band brake principle. For this design, a band brake is wrapped along the USF. The friction lining is in contact with the tower when hooked on. The necessary tension in the band is supplied by hydraulic cylinders. A diagram is presented in Figure 5.9b.

Sizing and material

Based on the available materials for the brake lining, it has been decided that Indubal woven roll would be used for the design. This is due to its strength and ability to conform to the tower. A coefficient of friction of 0.25 has been assumed. The width of the brake lining has been taken as 410 mm, which is the maximum available width of the lining according to the manufacturer (Indubal, 2018). The wrap angle was decided as 270 degrees, which would require a length of 16.5 m of the brake lining when a diameter of 7 m is used. This results in an area of 6.765 m^2, over which the pressure due to the tension in the belt will be evenly distributed. 270 degrees as the angle of the wrap was chosen based on a sensitivity analysis, which is presented in Figure 5.13.

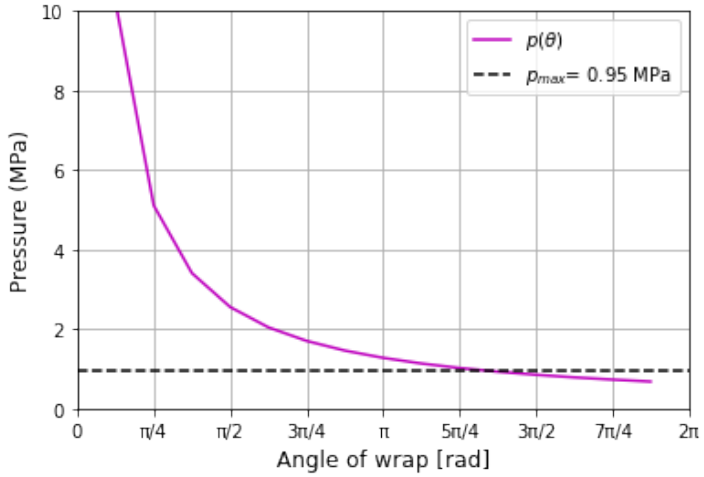

Figure 5.13: Sensitivity analysis investigating the effect of the angle of wrap on the pressure acting on the tower.

In the analysis, pressure as a function of the angle of wrap, θ, is plotted. A reduction factor of 1.2 was applied again to the coefficient of friction to account for the curvature. This resulted in the coefficient of friction used in the calculation being 0.208. The purple curve in the figure represents the following equation:

$$p(\theta) = \frac{F_N}{rb\theta} \tag{5.25}$$

r is the radius of the tower at the location of the USF, b is the width of the band, which has already been chosen as 410 mm, and θ takes up values between 0 and 2π radians as the angle of wrap. The value of the normal force is obtained from Equation 5.26, where the same approach to obtain the normal force was used as for the friction pads:

$$F_N = \frac{F_f}{\mu} = \frac{1200}{0.208} = 5.76 \text{ MN} \tag{5.26}$$

From the plot in Figure 5.13, it can be seen that the angle of wrap based on a width of 410 mm, is required to be at least approximately $\frac{11}{8}\pi$ radians or 240 degrees. For ease, it was decided to use $\frac{3}{2}\pi$ radians or 270 degrees as the angle of wrap. It was decided that an additional safety factor was not required as a safety factor for the coefficient of friction was already applied as a precaution. The reduction factor of 1.2 is intended for the use of rounded friction pads. The brake lining material of Indubal is made to be bent, therefore, such a safety factor is in essence not required, but is still used to make the overall calculations more conservative due to other uncertainties in the chosen approach.

To check if the shear strength of the materials can withstand the tangential loading necessary, the maximum tangential load is calculated. The shear strength of the brake lining is limiting, as it is 16.2 N/mm^2 in the weft

direction (Indubal, 2018). The maximum permissible tangential load can be calculated using Equation 5.4.3. It is again assumed that the real surface area is equivalent to the area of the band.

$$F_{t,max} = 6.765 \times 16.2 = 109.6\text{MN}$$

The maximum tangential force is 109.6 MN. This is more than the required frictional force calculated in Equation 5.14, and therefore the shear strength of the materials is not limiting for this design. The calculation was based on the full area of the band, even though in reality this will not be the case. However, the maximum tangential force calculated is 50 times greater than the required frictional force, so it is still assumed that the shear strength will not be limiting.

Forces

In subsection 5.2.3 many equations for the band brake were introduced. To verify if the design passes the load case, the tension at each end of the band, P_1 and P_2, must be determined. If it is assumed the maximum buckling pressure, p_{max}, is equal to the maximum pressure that occurs in the band, $p_{b,max}$ from Equation 5.10, then the following is obtained for P_1:

$$P_1 = p_{b,max} br = 0.95 \cdot 0.41 \cdot 3.5 = 1.36 \text{ MN} \tag{5.27}$$

Knowing the value of P_1, μ and θ allows the use of Equation 5.4 to be made to obtain P_2:

$$P_2 = \frac{P_1}{e^{\mu\theta}} = \frac{1.36}{e^{0.208 \cdot 1.5\pi}} = 0.511 \text{ MN} \tag{5.28}$$

To check whether the design is capable of dissipating the moment, Equation 5.6 is solved for T and should be greater than $M_z = 2100$ kN.

$$T = (P_1 - P_2)r = 3.5(1.36 - 0.511) = 2.98 \text{ MNm} \tag{5.29}$$

Using the obtained values for P_1 and P_2 yields a torque of 2.98 MNm or 2980 kNm. Since $2980 > 2100$ kNm this design is suitable for the USF.

The chosen angle of wrap provides sufficient surface area for the buckling pressure to not be exceeded but also for the environmental moment to be counteracted. Since the band not only needs to cover an adequate amount of the circumference to provide enough torque to counteract the moment but also needs to keep the tower from slipping out of the USF, it has been decided to keep the angle of wrap set to $\frac{3}{2}\pi$ rad, and see what the maximum pressure is if $T = 2100$ kNm. To do this, Equation 5.30 and Equation 5.31 must be solved simultaneously for P_1 and P_2. The two equations are based on Equation 5.1 and Equation 5.4.

$$P_1 - P_2 = 600 \tag{5.30}$$

$$\frac{P_1}{P_2} = 2.66 \tag{5.31}$$

This results in $P_1 = 0.961$ MN and $P_2 = 0.361$ MN. From the value of P_1, the maximum pressure can be obtained:

$$p_{b,max2} = \frac{P_1}{br} = \frac{0.961}{0.41 \cdot 3.5} = 0.67 \text{ MPa} \tag{5.32}$$

A pressure of 0.67 MPa acts on the tower for the band brake with the chosen dimensions. This is below the critical buckling pressure of 0.95 MPa, as expected from the previous calculations, which means the design should work for the application of the USF.

Strengths and limitations

Using brake lining in the design of the USF to provide friction brings forth certain strengths and limitations in comparison to the design with friction pads. Firstly, the load distribution on the tower is optimised due to the elimination of localised loads. This is preferred as certain failure mechanisms, such as buckling are less likely to occur. Secondly, brake bands usually have better heat dissipation properties. Being able to dissipate heat is slightly important since friction will release heat, however, for the application at the USF-tower interface, it is not one of the most important qualities to have. Compared to friction pads, brake bands are also more durable, but of

course, this depends on the specific coating and materials involved. But due to this, it is not certain that the tower will not get damaged due to the surface roughness of the Indubal material. In that respect, the rubber material of the friction pads is better. Another drawback of band brakes is that the design becomes more complex compared to the design with friction pads. Complexities in the design include the mechanism through which sufficient tension in the band will be provided and also finding the optimal width and angle of wrap. However, since the angle of wrap can be adjusted, the design more easily be changed and adapted to different towers. Additionally, while the width of the band is set by the manufacturing limits, the possibility to place two bands below one another is a possibility as well. A drawback however is several different components are required to achieve proper working. For example, pins that allow the band to open and close, and handles that the hydraulic cylinders can get attached to and provide tension in the band. However, from a practical perspective, the revised design with friction pads needs 8 pads, which makes it in that sense, less practical than the band brake.

5.4.4. Design comparison

The two designs presented in the previous section were compared with each other to see which shows more potential for the USF design. This was judged based on the preliminary calculations performed, how well they meet the functionality for which they were designed, and also their potential to be adapted for future development to fulfil all USF functionalities, as presented in section 5.1. To make the comparison more structured, it was decided to make use of the weighted multi-criteria analysis. This section will present the analysis and the results.

Criteria

For the analysis, a set of criteria were thought of and assigned a weight depending on the criterion's importance to achieving the purpose of the USF. Below the criteria are introduced and a weight is assigned to them. The way the weights were assigned was by first determining the order of importance of the criteria and then assigning the weighing factor. Weights between 1 and 10 were assigned, with 1 being the least important and 10 the most important. More details of this are presented in subsection E.3.1. The criteria used for the analysis are:

1. Moment counteraction: This criterion essentially assesses the design's ability to counteract the moment. It looks at if, with the current calculations, the moment can be counteracted while keeping the structural integrity of the tower and the USF. This is a very important criterion, as essentially if the design is not able to counteract the moment, the goal of the design is not met. Therefore, it has a weight of 10.
2. Integration: The integration criterion looks at how well the design can be integrated into the single lift installation and the actual frame of the USF with the current dimension. The proper integration of the design is vital as otherwise the design cannot be used for the USF. Due to this a weight of 9 has been assigned to it.
3. Loading distribution: This criterion evaluates the type of loading that the USF exerts on the tower. A uniformly distributed loading is the preferred option in order to avoid local stress concentrations and buckling. Radial loads are not desired and score low. This is an important criterion for the overall USF design, as the tower is a thin-walled cylinder and therefore, susceptible to buckling. Any structural damage or potential risks of decreasing structural integrity are unfavourable. Due to this, it has an assigned weight of 7.
4. Material/coefficient of friction: The coefficient of friction between the tower and the material of the USF in contact with the tower needs to be as high as possible so that the minimum required frictional force can be delivered by a smaller normal force. This is an important criterion, as high friction is required for the designs to work. Secondly, the material must also not cause damage to the tower. A weight factor of 5 is assigned to this criterion.
5. Adaptability: This criterion assesses the potential of the design to be adjusted for the other functionalities of the USF in the future. This is an important criterion as if simple modifications without altering the whole design are not possible, then the design is likely not the most suitable option for the USF. However, its potential for future adjustments is not the most important objective of the current designs and the thesis objective, therefore, it has a weight of 4.
6. Practicality: The practicality criterion relates to how simple the design is and how easy it seems to be to manufacture and utilise in practice. Important design specifications include the number of different components, the size of the pads/band, and the complexity of the components. It has a weight of 2 as it is a relevant criterion, however, based on the objective of the thesis, performing better or worse in this particular criterion will not greatly affect the outcome.

Table 5.2 presents the results of the analysis. A score of 1 indicates the design does not perform well in the given criterion, while a 5 means the design fulfils the criteria very well. From the total score, it can be seen that Design 2 scores better overall. This is due to it scoring highly in the three most important criteria. The following sections justify the score of each design for each criterion.

Table 5.2: Results of the multi-criteria analysis.

		Design 1		**Design 2**	
Criteria	Weight	Score	Weighted Score	Score	Weighted Score
Moment counteraction	10	4	40	5	50
Integration	9	5	45	5	45
Loading distribution	7	3	21	5	35
Material	5	5	25	2	10
Adaptability	4	4	16	4	16
Practicality	2	3	6	3	6
		Total	153		162
		Total without material	128		152

Moment counteraction

Seeing if the designs have sufficient rotational restraint capacity to counteract the environmental moment is the most important aspect of the designs as if they cannot do this, then relative rotation between the USF and tower will not be restricted. The initial friction pad design exceeded the critical buckling pressure to deliver sufficient frictional force to do this. The amended design with 8 pads is capable of doing that while keeping within pressure limits, therefore, it was awarded a 4. However, this design still results in 600 kN acting on each pad. The pads would have to be quite rigid in order to be able to transfer a force of 600 kN per pad onto the tower. This would make it more difficult for them to completely conform to the tower surface, especially considering the possibility of the tower out of roundness due to dimension tolerances. This adds a degree of uncertainty to the design's capability of producing sufficient frictional force. On the contrary, the band of Design 2 can much better adhere to the tower shape. Design 2 can prevent rotation under its current configuration and adhere to the buckling limits. Potential problems in the design doing so have not been identified, therefore, it scores a 5 in this criterion.

Integration

Both designs were designed with the purpose to be used as the USF for the single lift WTG installation, therefore should score highly in the integration criterion. For both designs, it has been assumed that there is enough space on the frame and the surrounding areas to accommodate the hydraulic cylinders and allow them to perform as intended and to still allow for easy hook-on and removal of the USF from the WTG. Due to this, both were awarded a 5 for the integration criterion.

Loading distribution

After Design 1 was changed to more friction pads and a larger surface area, both designs stayed within the structural limits. Before the pad size changed, Design 1 exceeded the maximum buckling pressure. With 4 pads, the contact forces were less evenly distributed around the tower circumference, which increased local stress concentrations. High local stress concentrations of thin-walled cylinders are particularly undesired as they may lead to buckling and even yielding. Nevertheless, Design 2 still scored better in this criterion due to a more uniformly distributed loading. Design 1 still leads to localised loads on the tower, however, the pressure is within appropriate limits, therefore, it received a 3.

Material

The rubber material of the friction pads is not very likely to cause damage to the tower and its coating at the pressures involved, however, the effect of the Indubal woven roll on the steel tower coated with PU, is not known. The band brake covers a large area of the tower, and while the pressure acting on this area is relatively low due to it being evenly distributed, it is not certain that the roughness of the material will not cause damage to the tower. Concerning the minimisation of damage to the tower coating, the friction pads show better performance due to the choice of material. The choice of material for the band brake came from already available brake lining materials. An important aspect of brake lining materials is that they must be able to handle high temperatures when used for brake bands. This is because band brakes are used in dynamic situations, with the brake drum

rotating. When the band gets tightened around the drum, the kinetic energy of the drum is transformed into heat, meaning the material has to be very heat resistant. This makes rubber an unfitting material for actual band brakes. However, for the application of a band brake for the USF, a static situation is concerned, where heat dissipation occurs differently (less). In such a situation there is potential to also use rubber as the brake lining material. If this would be possible, the band brake would become an even more adequate solution. Currently, with the Indubal material, design 2 scores poorly, 2. Design 1 scores much better as the rubber has a higher coefficient of friction with steel than the woven roll, and also it does not damage the tower.

Adaptability

With respect to other functionalities not investigated in this thesis, both designs have the potential to be slightly altered to make it possible for the USF to fulfil all its functionalities. Both designs already restrict X- and Y-translation, however, slight rotation along the X- and Y-axis is not yet guaranteed. Z-translation is with the current design configurations also not possible, however, the possibility to install a separate sliding mechanism can be incorporated in both designs. Due to this, they both scored a 4 in this criterion. A 5 would have been awarded if the possibility to include Z-translation would be possible without an external sliding mechanism.

Practicality

With reference to practicality, the original design with 4 friction pads is the most practical in terms of the number of components and size of components. With the revised design with 8 friction pads, more components are involved in the design and the pads become very huge (0.95 m^2) and impractical for the installation and general handling. The circumference of the tower at the height of the USF is 22 m. If 8 pads of 0.97 m in width are placed around the tower, that results in 7.76 m of the circumference occupied and equal gaps of 1.78 m between neighbouring pads. The big pad area is a disadvantage to the revised design with friction pads, therefore, it was awarded a 3 in this criterion. Design 2 was also awarded a 3, as while the size of the band is not problematic, there are several components involved to make the design work, such as pins, handles and hydraulic cylinders. The major issue with the band brake is that the angle of wrap needs to be sufficiently large to keep the pressure on the tower low while also making it possible to open and close a section so that the USF can be hooked on and removed from the tower. The hydraulic cylinders have to be positioned so that they are able to provide the pulling force of the band in the correct direction, as labelled in Figure 5.9b. Only in the direction parallel to the end of the band will the correct pulling force be supplied to provide the necessary pressure of the band. These considerations lead to increased complexity of the design.

Conclusion

Table 5.3 has been made to present an overview of the two designs. For the friction pad design, the values based on the updated design of 8 friction pads are presented. The tower is the same for both designs, however, depending on the type of load (localised load or distributed), different tower limits are presented. The tangential forces are the same in both cases, as the environmental loading does not change, however, the required normal force is different for the two designs due to a different coefficient of friction being used for the materials.

Table 5.3: Comparison of the two proposed USF designs based on calculated parameters. Design 1 includes friction pads, while Design 2 makes use of the brake band principle.

	Design 1: Friction pads (new)	**Design 2: Band brake**
Rotation prevention	Friction	Friction
Material	Rubber	Indubal woven roll
Coefficient of friction	0.30	0.25
Material shear strength[N/mm^2]	10	16.2
Minimum frictional force [kN]	1200	1200
Total normal force [kN]	4800	5760
Normal force per unit	600 kN per pad	21.37 kN per degree
Total area in contact [m^2]	7.6	6.765
Type of loading	Localised	Distributed
Pressure acting on tower [MPa]	0.63	0.67

Based on the totals presented in Table 5.2 it can be seen that Design 2 scores slightly higher overall, which means

it is the better design based on this analysis. This can be attributed to Design 2 scoring better in the three most important criteria according to their weights. The biggest difference was made in the loading distribution criterion, where Design 1 scored a 3 and Design 2 scored a 5. This difference comes from the nature of the type of loading acting on the tower due to the design, which is distributed for Design 2 and localised for Design 1.

Design 2 shows the worst performance for the material criterion. In the justification of the scores of the material criterion, it was mentioned that rubber could potentially also be used for the brake lining material of the band brake. To investigate the case where both designs use the same material, a total is presented in Table 5.2, where that criterion is omitted. In that case, Design 2 scores relatively even better compared to Design 1, than when the material criterion is included.

Through this design comparison, it has been shown that both designs possess distinct strengths and weaknesses that make them more or less suitable for the USF. While there is still some uncertainty regarding the performance of the brake lining material, Design 2 shows better qualities for the USF. The large area of the friction pads, needed to ensure the buckling pressure was not exceeded with a margin of safety, is a critical shortcoming of Design 1. Even with an increased number of pads, the design still exerts localised loads on the tower, which results in poor performance in some of the more important criteria.

5.4.5. Limitations

In this Chapter, a simple analysis of concepts that could be utilised for the USF, and two preliminary designs of the USF were presented. The methods used for validating the designs offered an adequate level of accuracy for their purpose, however, there were some limitations to them, resulting in some uncertainties.

Extensive research was done to find accurate and reliable coefficients of friction for the study, however, it is important to note that predicting the real value of the coefficient of friction between two materials with absolute precision can be a challenging task due to the complex nature of friction. Several factors influence the coefficient including surface conditions (wet or dry), temperature, surface pressure and other things. All these factors introduce some level of uncertainty to the actual value. The values used are more conservative values found in tests done by Heerema MC and standards in literature. Therefore the values are rough but sufficient for the preliminary analysis that was conducted. Due to the uncertainty in the values, a sensitivity analysis to assess the severity of over-predicting or under-predicting the value of the coefficient was also done. From the sensitivity analysis, it was decided that the range of the coefficient of friction which was being handled in the thesis, slightly over or under-estimating, would not greatly affect the final outcome.

The analysis of thin-walled cylinders subject to external pressure involves assessing the critical buckling pressure. A limitation to the methods used for verifying the designs in this Chapter comes from the equations for the critical buckling pressure. The value of p_{max} seems very low, however, the methodology used to obtain it was, based on research, the most applicable. However, to obtain the critical buckling pressure, various methods exist, which include analytical methods, finite element analysis and experimental techniques. Determining the buckling pressure experimentally was not practical or feasible for the thesis, therefore, the analytical and finite element analysis options were better suited. Ideally, both remaining options would have been used in order to verify each other's results however, due to time constraints of the thesis, it was chosen to only make use of analytical solutions.

6

Conclusion & Recommendations

6.1. Conclusion

The investigation presented in this thesis was focused on the single lift installation strategy of a WTG using a single crane of a semi-submersible vessel. The main focus was on the Upper Stabiliser Frame, a Heerema MC concept aimed at restricting WTG motions while being lifted, specifically the yaw motion. The central objective of the thesis was to:

Determine the magnitude of the yaw moment that the Upper Stabiliser Frame is required to counteract, caused by the environmental loading, during a single lift offshore wind turbine installation on a fixed foundation, and investigate how the connection between the tower and Upper Stabiliser Frame can be made physically.

To reach this objective, several research questions were formulated, as well as a coherent and structured research approach. The research included modelling a base case scenario of the installation with the USF, followed by an analysis of this scenario. Based on the results, boundary conditions for a real design of the USF could be determined. Several concepts of possible solutions for the USF to achieve all its functionalities were analysed, and eventually, two potential designs were created, and preliminary calculations regarding their feasibility were conducted. The designs focused on restraining relative rotation around the Z-axis of the USF and tower.

In the base case scenario, a rigid connection was made between the tower and USF. This resulted in the USF motions being the same as the WTG motions. Wave-only, wind-only, and combined wind and wave analyses were done. Several different sensitivity analyses were performed, where different system parameters were changed, and their effect on the system was observed. Parameters such as the blade pitch angle, significant wave height, peak period, wind speed, and incoming wind and wave directions were investigated. It was found that the wind was the dominant environmental loading when it came to inducing motions of the WTG. Additionally, it was found that the WTG motions are largest when the wind is coming from a direction perpendicular to the rotor plane. In the model of the whole system, this was a direction of 135 degrees. Since the least favourable conditions occurred from this direction, it was decided to use this direction to determine the maximum yaw moment acting on the tower. The least favourable conditions needed to be used, as during an offshore installation, the vessel will not be able to weather vane at all moments of the installation, and therefore changes in wind direction should not cause issues during installation. While the wind loading was dominant for the WTG motions, the waves were also relevant for inducing motions at specific peak periods. During the modal analysis, critical modes were identified. These were modes which had natural frequencies within the wave frequency range. Some of the critical modes included pendulum motions of the system, which resulted in enhanced USF and tower tip motions for peak periods of 4 and 12 seconds. Such critical modes should be further investigated, and if possible, their periods adjusted to outside the wave frequency range.

A set of limiting criteria allowing for safe operation were introduced in Table 3.3. The focus of the thesis was on the motions of the WTG, therefore, not all limiting criteria were specifically investigated during every analysis. It was clear from the wave-only analysis that the WTG motions were well within limits when only waves were acting on the system. However, when the wind loading was applied, the WTG motions were greatly increased. The greater the magnitude of the applied wind field, the greater the WTG motions, as was shown in the X-Y

ellipse plots. The operational limit on which the limiting environmental conditions were based on was the horizontal motion of the tower tip. Based on the tested load cases, the WTG motions exceeded allowable limits for all H_s and T_p combinations of wind speeds of 10 and 12 m/s. Due to these unsatisfactory results, it was further investigated what the maximum allowable wind speed could be to keep the tower motions within the limit for $H_s = 1.5$ m and $T_p = 8$ s, for wind and waves coming from 135 degrees. It was found that 6 m/s yielded WTG tower tip motions below 1.5 m for the duration of the whole simulation. For this load case, the maximum tower Z-moment was 2.1×10^3 kNm. This moment was used as the magnitude of the moment that the USF - tower interface had to counteract.

Several concepts with similar working principles as the USF were analysed. The concept study led to the conclusion that a friction-based connection would be most suitable at the USF - tower interface. Two designs based on the friction principle were created.

The first design consisted of four friction pads made of rubber, equally spaced around the circumference of the inner part of the USF. This resulted in the tower and USF coming into contact at four places at the interface and the USF exerting four radial loads at the point of the pads onto the tower. Basic calculations revealed that the four pads with the chosen dimensions exceed the maximum buckling pressure, p_{max} of 0.95 MPa. In light of this, the design was modified to comprise eight pads of larger dimension. The final area of a single pad was 0.95 m^2, which led to a pressure on the tower of 0.63 MPa.

The second design was based on the band brake concept for generating sufficient frictional capacity to prevent rotation. The stress exerted by the band brake is uniformly distributed along the circumference of the tower, and with the chosen dimensions (limited by the brake lining manufacturer), the pressure acting on the tower was 0.67 MPa for an angle of wrap of 270 degrees. Potential further improvement of this design could come from using rubber for the brake lining material, as rubber has been proven to not cause surface damage to the tower from previous projects in the offshore industry. The brake lining material is composed of fibreglass yarn and brass wires, along with other materials, which could definitely damage the tower coating. The band brake is usually used in highly dynamic situations, with the brake drum rotating at high velocities, however, this is not the case for the situation with the USF, where a quasi-static situation is considered. Due to this, the material for the brake lining does not have to possess excellent heat dissipation qualities, and rubber can potentially be used.

To see which design was most fitting for the purpose of the USF, a multi-criteria analysis with weighted factors was conducted, in which the designs were assessed based on six different criteria. The criteria were counteracting the moment, integration, loading distribution, material, adaptability and practicality, in order of importance. The final results were in favour of the band brake design, as it scored better in the more important criteria. Further, if the material criterion, where the band brake design scores poorly, is disregarded, the band brake design performs relatively even better than the friction pad design in comparison to when the material criterion is included. This was done in order to see the scores of the designs if rubber was assumed to be used for both designs.

The single lift installation strategy is a very novel concept in the offshore wind industry but will require further development to become competitive with the current installation methods of offshore wind turbines based on the research presented in this thesis. The installation strategy opens up new possibilities to the offshore industry, but with it brings challenges requiring further exploration and development. Its novelty lies in the refinement of the offshore wind turbine installation procedure, as single lift installations have been used only on limited occasions, for example, the Beatrice and Hywind projects. However, in both cases, two cranes were used for the installation. The Heerema method utilising the USF differs from them as only a single crane is required. The method itself has the potential to revolutionize wind turbine installation by decreasing installation time, increasing operational efficiency, and in general, streamlining the whole process. This thesis's scientific contribution includes the identification of problems that the installation process faces due to the interaction of the whole system with the environment but also suggests innovative solutions that can be applied to the USF to aid in the installation. Through this investigation, the basis for further research within this topic has been formed, more of which is discussed in section 6.2.

Overall the single lift method offers many possibilities for the future of wind turbine installation, and by tackling the challenges the strategy currently poses, the possibility of accelerating wind farm deployment and tackling the world's renewable energy goals is increased.

6.2. Recommendations

In this section, the recommendations for further scientific research involving the USF and the single lift method are presented, as well as recommendations for the improvement of the research done in this investigation.

6.2.1. Analysis

In the investigation, several assumptions and simplifications were made to reach the purpose of the investigation. Additionally, due to the chosen approach, there were some limitations to obtaining results and data. Improvements to the investigation performed in this thesis are given below.

Wind loading

The wind loading in OrcaFlex was only applied to certain components in the system. In real life, the wind acts on all the components in the system above the water level, including the vessel. Shielding effects of any kind were also not taken into consideration. Shielding effects from the crane, or any other components, blocking the wind could potentially have a big impact on the WTG motions depending on the incoming wind direction. In the case of a more extensive investigation into the single lift method, the wind loading should be applied to all the components above the water in the model and shielding effects should be incorporated.

For the wind loading, a TurbSim input file was used to generate a turbulent, spatial varying wind field. For this, an IEC turbulence class C and NTM (normal turbulence model) turbulence type were assumed. Turbulence class C corresponds to the lower turbulence intensity, as it has a mean turbulence intensity characteristic of 0.12 (IEC, 2005). NTM defines turbulence under normal operational conditions, and the parameters used to define NTM are based on some observations. For future investigations, the wind climate in the relevant area can be studied in more detail to determine the most suitable turbulence parameters for the wind encountered in the area.

Wave loading

To generate the wave spectrum, only one seed number was used due to time limitations. More seed numbers could be used in the future to generate different wave fields for the simulation. In this investigation, a stationary process was assumed, however, with the use of more seed numbers, a statistical ensemble of wave realizations can be obtained. With it, a statistical analysis be conducted to get more accurate results. This could better represent the variability of waves encountered offshore.

When modelling the waves, it was chosen to stick to the JONSWAP wave spectrum, this spectrum is not necessarily representative of waves in the Baltic Sea but was deemed as sufficient for the purpose of the analysis. In the future, a different spectrum, more representative of Baltic Sea conditions, can be used, and swell waves could also be taken into consideration, as they have been omitted for this thesis. The effect of swell on the system could be done as an additional analysis due to longer natural periods of the system being identified (>10 seconds). Currently, second-order effects were omitted in the analysis for simplicity and because mild (non-steep) waves were considered. However, due to the given periods of the system, second-order effects could potentially be relevant, as they could excite system resonance. This is a relevant investigation, as it was shown in this thesis that the full WTG installation method is sensitive to long wave periods (>10 seconds).

Safety factors

Some safety factors applied to certain loads and parameters obtained in this investigation were not based on any already existing standard or recommended practice. Therefore, it is difficult to assess whether the application of the chosen safety factors results in a value that is too conservative or if it is realisitic. If a more detailed investigation is conducted, where a more detailed USF is designed, then different safety factors should be considered to see up until what point the operational limits are not exceeded yet (e.g. stress acting on the tower). In this thesis, very conservative safety factors were generally chosen due to the installation strategy's novelty.

USF concept analysis

For the concept analysis, different concepts were analysed, and from there, a preliminary design was created for the USF. Since only some preliminary design dimensions were determined, only simple calculations could be conducted to verify the working of the USF design. This was a limitation, as further analysis of the design was not possible. For future investigations, a FEM analysis could be done for the USF design and, if possible, time

domain analysis using appropriate software. The software should be able to model friction to see how the moments and forces caused by the environment are counteracted at the USF-tower interface. With the FEM analysis, a more accurate representation of the maximum buckling pressure could be obtained, which in this thesis was calculated based on analytical solutions for similar problems.

In the WTG sensitivity analysis, the WTG was slightly rotated with respect to the USF to see if the Z-moment increases under the same environmental loading. This could be better analysed in software that is capable of modelling friction. A time domain analysis of a system that includes friction between the tower and USF could be done to show the point at which slip occurs. This situation can be further investigated to see if the occurrence of slip will cause the WTG to continue rotating or if it will come to a stop again. This will depend on the static and dynamic frictional force. Such an analysis would test the actual working of the proposed USF design.

6.2.2. Single lift installation

Regarding the USF and the specific single lift installation method proposed by Heerema MC, some recommendations have been considered for further research to improve this installation strategy. The recommendations do not only pertain to the free-hanging stage of the installation but also to the set-down and recovery phases.

WTG bottom motions

The bottom of the tower needs a properly designed tugger system that will decrease the bottom tower tip motions, as it was seen in this investigation that the XY tip motion of the tower is an important limiting parameter that is easily exceeded. Through the implementation of a tugger system, the yaw of the WTG should also be decreased, and the possible risk of collision of the tower with the Thialf would be reduced. Damping tuggers can be utilized just like the tuggers connecting the USF to the crane. Through an additional tugger system, the operational limits of the full WTG lift operation would have to be determined again. For future research, different tugger systems could also be investigated to see what system of tuggers would yield the least WTG motions. This would include investigating parameters such as the damping, stiffness, and pretension in the lines, but also the configuration of the tuggers and other types of tugger systems, such as constant tension tuggers.

USF design and functionalities

In this thesis, the USF design focused on fulfilling the Z-rotation restraint. However, as mentioned, there are other functionalities the USF must fulfil for the proper working. For future research, a more detailed design can be made, ensuring the proper working of the USF based on all required functionalities, such as translation in the Z-direction and slight rotation along the X- and Y-axis. The detailed design should also consider specific aspects of the USF, such as the working of the hydraulic cylinders for the closing mechanism and providing sufficient normal force, for example.

Material selection

A brief material analysis was conducted, where possible friction pads and brake lining materials were looked at. The analysis was very limited, as it consisted of materials already used for other offshore industry applications, such as pipelaying. Nonetheless, the USF is a very specific case, and due to this, other materials could be more applicable for its use. For example, rubber is often not used for the application of the brake lining material in band brakes, however, due to the nature of the USF, rubber might be an appropriate option. As for the friction pads, a flexible pad design, which will fully conform to the tower's surface, should also be investigated to increase the pad's surface area in contact with the tower during installation.

Hooking on USF rigging

The hooking on of the USF can be quite a difficult procedure with the current USF design. This is because the rigging is heavy, and since the tower is assembled in the support tower, it has limited access. Optimising the design of the USF by making the attachment of the USF less time-consuming should be considered to decrease overall installation time.

Recovery of USF and LLT

The disconnection and recovery of the USF and LLT should be done as soon as possible after the load transfer is complete. The recovery of the two components is currently done separately, however, options where the USF and LLT are recovered together can potentially also be considered. With this alternative, the bolting scope gets

affected, as a choice has to be made whether or not to keep the rigging slack or tight. A slack rigging would mean the USF is suspended on stoppers. This is not desired, but removing the USF and LLT separately is impractical, as more time is needed. Other options for the recovery procedure should also be considered, such as additional lifting devices.

Another issue with the current design of the USF and the removal procedure relates to the lift points of the frame. The lift points have been designed to be symmetrically placed around the CoG of the WTG. Due to the mass of the nacelle and the rotor, the CoG of the WTG is not exactly in the middle of the tower and therefore does not coincide with the CoG of the USF, as pictured in Figure E.2. This causes a significant problem, as once the WTG is placed onto the foundation and the slings of the rigging are no longer taking up the weight of the WTG, the USF becomes unstable due to the chosen lift points. For future design development, the removal stage and method of removal should be further investigated to avoid this problem from occurring.

Torque release

Another aspect that needs to be considered for the full WTG lift method is the release of the torque in the tower and USF connection during the set down of the WTG onto the foundation. This essentially refers to the moment/torque in the connection at the interface that arises due to loads, for example, from the environment. This torque will have to be released in the clamping connection somehow so that it is not transferred during the set down to the foundation. In the case the torque is not released, the connection between the foundation and tower will contain an unwanted/undesired torque.

Dual crane arrangement

The full WTG lift, as proposed in this thesis, uses one of the cranes available on the Thialf. However, the Thialf is equipped with two cranes. During the concept analysis, two other frames have been analysed, which have already been used for a full WTG installation, and in both cases (for the Hywind project and the Beatrice project), a dual crane arrangement was utilised. An in-depth analysis of the feasibility of a dual crane lift of the whole WTG using the Thialf or another HMC vessel, such as the Sleipnir, should be conducted to see if such a lift would allow for higher limiting environmental conditions than the lift with one of the Thialf cranes. If this is the case, then the method should be further developed and assessed against current methods used in the industry for wind turbine installation to check its competitiveness. Particular attention should be paid to the ship roll during such an installation, as it can lead to uneven load distribution in the crane.

References

About Arcadis Ost 1. (2022). https://www.arcadisost1.com/

Acero, W. G., Gao, Z., & Moan, T. (2017). Methodology for assessment of the allowable sea states during installation of an offshore wind turbine transition piece structure onto a monopile foundation. *Journal of Offshore Mechanics and Arctic Engineering*, *139*(6).

Andersson, C.-H. (2018). DSM High performance fibres.

API. (2014). API-RP2A: Planning, Designing and Constructing Fixed Offshore Platforms - Working Stress Design.

Apsley, D. (2022). Linear wave theory. https://personalpages.manchester.ac.uk/staff/david.d.apsley/lectures/hydraulics3/WavesLinear.pdf

Awrejcewicz, J., & Olejnik, P. (2005). Analysis of dynamic systems with various friction laws. *Applied Mechanics Reviews*, *58*(6), 389–411.

Bai, Y., & Bai, Q. (2010). Installation and vessels. *Subsea engineering handbook*.

Blau, P. J. (2001). The significance and use of the friction coefficient. *Tribology International*, *34*(9), 585–591.

Burton, T., Jenkins, N., Sharpe, D., & Bossanyi, E. (2011). *Wind energy handbook*. John Wiley & Sons.

Bussemakers, P. (2020). *Validation of aero-hydro-servo-elastic load and motion simulation in bhawc/orcaflex for the hywind scotland floating offshore wind farm*.

Chitteth Ramachandran, R., Desmond, C., Judge, F., Serraris, J.-J., & Murphy, J. (2022). Floating wind turbines: Marine operations challenges and opportunities. *Wind Energy Science*, *7*(2), 903–924.

Deladi, E. L. (2006). *Static friction in rubber-metal contacts with application to rubber pad forming processes* (Vol. 68).

Dinh, V. N., & McKeogh, E. (2018). Offshore wind energy: Technology opportunities and challenges. *Vietnam Symposium on Advances in Offshore Engineering*, 3–22.

DNV GL. (2018). DNVGL-ST-N001: Marine operations and marine warranty.

DNV GL. (2021). DNVGL-RP-C205: Environmental conditions and environmental loads.

Downey, A., Cao, L., Laflamme, S., Taylor, D., & Ricles, J. (2016). High capacity variable friction damper based on band brake technology. *Engineering Structures*, *113*, 287–298.

Elisa – elican project. (2017). https://www.esteyco.com/proyectos/elisa-elican-project/

European Standards. (1991). Eurocode 1: Actions on structures.

Faltinsen, O. (1990). *Sea loads on ships and offshore structures* (Vol. 1). Cambridge university press.

Flügge, W. (1960). *Stresses in shells*. Springer Science & Business Media.

Gaertner, E., Rinker, J., Sethuraman, L., Zahle, F., Anderson, B., Barter, G. E., Abbas, N. J., Meng, F., Bortolotti, P., Skrzypinski, W., et al. (2020). *Iea wind tcp task 37: Definition of the iea 15-megawatt offshore reference wind turbine* (tech. rep.). National Renewable Energy Lab.(NREL), Golden, CO (United States).

Glock, D. (1977). Überkritisches verhalten eines starr ummantelten kreisrohres bei wasserdrunck von aussen und temperaturdehnung (post-critical behavior of a rigidly encased circular pipe subject to external water pressure and thermal extension). *Der Stahlbau*, *7*, 212–217.

Guo, Y., Wang, H., & Lian, J. (2022). Review of integrated installation technologies for offshore wind turbines: Current progress and future development trends. *Energy Conversion and Management*, *255*, 115319.

Heerema Marine Contractors. (2018a). LiftDyn Theory Manual.

Heerema Marine Contractors. (2018b). MVOW - WTG installation.

Heerema Marine Contractors. (2019). RNA installation.

Heerema Marine Contractors. (2021a). Lower lifting / latching tool and collar design for full WTG installation rev. 1.

Heerema Marine Contractors. (2021b). WTG Components Accelerations on Thialf.

Heerema Marine Contractors. (2022a). GREP Tool Detailed Design – FEA. *Heerema Engineering Solutions*.

Heerema Marine Contractors. (2022b). Heerema Marine Contractors: Fleet. https://www.heerema.com/heerema-marine-contractors/fleet

Heerema Marine Contractors. (2023). Engineering for Pipelay with Friction Equipment.

IEC. (2005). IEC 614000-1: Design requirements for wind turbines.

Indubal. (2018). Industrial woven material BIN9850.

IRENA, I. (2019). Future of wind: Deployment, investment, technology, grid integration and socio-economic aspects. *Abu Dhabii*.

Iturgaiz Elso, M. (2012). Finite element method studies on the stability behavior of cylindrical shells under axial and radial uniform and non-uniform loads.

Jiang, Z. (2021). Installation of offshore wind turbines: A technical review. *Renewable and Sustainable Energy Reviews*, *139*, 110576.

Journée, J., & Massie, W. (2001). Offshore hydromechanics. *Delft University of Technology*.

Krogstad, H. E., & Arntsen, Ø. A. (2000). Linear wave theory part a. https://folk.ntnu.no/oivarn/hercules_ntnu/LWTcourse/lwt_new_2000_Part_A.pdf

Malekan, M., Budzik, M. K., Jensen, H. M., & Aghababaei, R. (2021). Fracture analyses of surface asperities during sliding contact. *Tribology International*, *159*, 106939.

Miceli, F. (2022). Self-erecting turbines: The elisa / elican project. https://www.windfarmbop.com/self-erecting-turbines-the-elisa-elican-project/

Momber, A., & Marquardt, T. (2018). Protective coatings for offshore wind energy devices (oweas): A review. *Journal of Coatings Technology and Research*, *15*(1), 13–40.

Nybø, A., Nielsen, F. G., Reuder, J., Churchfield, M. J., & Godvik, M. (2020). Evaluation of different wind fields for the investigation of the dynamic response of offshore wind turbines. *Wind Energy*, *23*(9), 1810–1830.

Orcina. (2022). OrcaFlex documentation. https://www.orcina.com/resources/documentation/

Ramachandran, C., Desmond, C., Judge, F., Serraris, J.-J., & Murphy, J. (2021). Floating offshore wind turbines: Installation, operation, maintenance and decommissioning challenges and opportunities. *Wind Energy Science Discussions*, *2021*(1-32), 15.

Rentoulis, Y. (2022). RNA Development – Dynamic Analysis. *Heerema Engineering Solutions*.

Ribuot, J. (2019). Innovative competitive offshore energy production. https://mcedd.com/wp-content/uploads/2019/04/MCEDD-2019-Presentation-SAIPEM-18-March.pdf

Rippel, D., Jathe, N., Becker, M., Lütjen, M., Szczerbicka, H., & Freitag, M. (2019). A review on the planning problem for the installation of offshore wind farms. *IFAC-PapersOnLine*, *52*(13), 1337–1342.

SAIPEM. (2017). Hywind. https://www.saipem.com/en/projects/hywind

Scaldis. (2007). Transport and installation of two 5mw wind turbine generators for the beatrice demonstrator project. https://www.scaldis-smc.com/en/projects/groen-2007-jul-beatrice/

Schreier, S. (2022). Limiting sea state & operability.

Seidel, M., & Gosch, D. (2006). Technical challenges and their solution for the beatrice windfarm demonstrator project in 45m water depth. *Conference Proceedings DEWEK*.

Timoshenko, S. P., & Gere, J. M. (1989). *Theory of elastic stability*. Courier Corporation.

uit het Broek, M. A., Veldman, J., Fazi, S., & Greijdanus, R. (2019). Evaluating resource sharing for offshore wind farm maintenance: The case of jack-up vessels. *Renewable and Sustainable Energy Reviews*, *109*, 619–632.

Vasilikis, D., & Karamanos, S. A. (2009). Stability of confined thin-walled steel cylinders under external pressure. *International Journal of Mechanical Sciences*, *51*(1), 21–32.

Vasilikis, D., & Karamanos, S. A. (2010). Buckling design of confined steel cylinders under external pressure. *Journal of pressure vessel technology*, *133*(1).

Veldkamp, H., & Van Der Tempel, J. (2005). Influence of wave modelling on the prediction of fatigue for offshore wind turbines. *Wind Energy: An International Journal for Progress and Applications in Wind Power Conversion Technology*, *8*(1), 49–65.

Wang, S., Cao, Y., Fu, Q., & Li, H. (2015). Hydrodynamic performance of a novel semi-submersible platform with nonsymmetrical pontoons. *Ocean Engineering*, *110*, 106–115.

WindEurope. (2022). Wind energy in europe: 2021 statistics and the outlook for 2022–2026. *Wind Europe Report: Brussels, Belgium*.

Zhang, P., Ding, H., Le, C., & Huang, X. (2013). Motion analysis on integrated transportation technique for offshore wind turbines. *Journal of Renewable and Sustainable Energy*, *5*(5), 053117.

A

Additional Theory

A.1. Buckling of thin-walled cylinders

The methodology behind the paper by Vasilikis and Karamanos (2010) is presented in this section. The methodology is made for steel cylinders confined in a rigid cavity and can have an imperfection, such as an out-of-roundness of the cylinder or a gap between the cylinder and the cavity. The steps for nondeformable cavities are presented below.

Step 1: The plastic pressure, p_y, Glock's buckling pressure, p_{GL}, and the slenderness parameter, λ, must be calculated. These are presented in Equation A.1, Equation A.2, and Equation A.3, respectively.

$$p_y = 2\frac{\sigma_y}{\sqrt{1-\nu-\nu^2}}(\frac{t}{D}) \tag{A.1}$$

$$p_{GL} = \frac{E}{1-\nu^2}(\frac{t}{D})^{2.2} \tag{A.2}$$

$$\lambda = \sqrt{\frac{p_y}{p_{GL}}} = \sqrt{\frac{2.26\sigma_y(1-nu^2)}{E}(\frac{D}{t})^{1.2}} \tag{A.3}$$

Step 2: The elastic imperfection sensitivity parameter, α, must be calculated and from it, the coefficients β, and η must be determined. Equation A.4 gives the equation for α, in which the δ_0 and g represent the initial out-of-roundness amplitude and initial gap, respectively. β is given in Equation A.5, with λ_p being equal to 2.2 and representing the transition between elastic and inelastic region (plastic limit slenderness). Δ in Equation A.6 for η, is the imperfection parameter, which in the case of no gap between the cylinder and the cavity, and a perfectly round cylinder, is 0.

$$\alpha = \frac{0.15}{[(\frac{\delta_0+3g}{r}\sqrt{\frac{D}{t}}]^{0.7}} \tag{A.4}$$

$$\beta = 1 - \frac{\alpha}{\lambda_p^2} \tag{A.5}$$

$$\eta = 0.6 - 3\Delta \tag{A.6}$$

Step 3: The ultimate pressure for rigid confinement, p_{max}, must be calculated, based on the value of λ. The tower is likely to deform in the inelastic region, for which the equation is given in Equation A.7. It is valid for $\lambda_0 \leq \lambda \leq \lambda_p$

$$p_{max} = p_y(1 - \beta(\frac{\lambda-\lambda_0}{\lambda_p-\lambda_0})^{\eta}) \tag{A.7}$$

B

System parameters

B.1. WTG

Table B.1 shows the geometric properties of the up-scaled NREL 15 MW wind turbine. In the table, the parameters, arc length, chord, thickness ratio, aerodynamic center, and aerodynamic twist can be seen. These parameters are explained in the following bullet point list:

- Chord length: the length between the leading edge and trailing edge of the airfoil. Essentially the length of the airfoil.
- Thickness ratio: this ratio refers to the thickness-to-chord ratio. The maximum thickness of the airfoil is used against the length of the chord.
- Aerodynamic center: the location on the airfoil, at which the lift, drag, and moment are applied.
- Aerodynamic twist: refers to the twist of the airfoil with respect to the root of the blade. Twisting the airfoil at each segment allows for optimal aerodynamic loads during operation to be achieved. This is, because there are differences in the rotational speed along the length of the blade (higher rotational speed at the blade tip than at the blade root), and so the ratio between the rotational speed and the incoming wind velocity, changes at every blade segment.

Table B.2 shows the dimensions and other relevant specifications of the wind turbine that is modelled in the investigation, which represents a 17 MW wind turbine upscaled from a 15 MW NREL WTG. The specifications concern, the nacelle, blades, tower, and the combined WTG specifications.
Additionally, the way the radii of gyration for the WTG elements were obtained is shown in Equation B.1, Equation B.2 and Equation B.3. These show the equations for the calculation of the radii of gyration for the nacelle, rotor, and tower, respectively. W is the width, H is the height, D is the diameter, and L is the length.

- Nacelle

$$R_{xx} = \sqrt{(W^2 + H^2)/12} \qquad R_{yy} = \sqrt{(L^2 + H^2)/12} \qquad R_{zz} = \sqrt{(L^2 + W^2)/12} \tag{B.1}$$

- Rotor

$$R_{xx} = 0.21 D_{rotor} \qquad R_{yy} = 0.15 D_{rotor} \qquad R_{zz} = 0.15 D_{rotor} \tag{B.2}$$

- Tower

$$R_{xx} = \sqrt{L_{tower}^2/12} \qquad R_{yy} = \sqrt{L_{tower}^2/12} \qquad R_{zz} = D_{tower}/2 \tag{B.3}$$

In Table B.2, the radius of gyration of different components is given, however, when defining properties in OrcaFlex, the radius of gyration is not one of the needed input properties. Instead, the mass moment of inertia is required. There is a relationship between the radius of gyration and the mass moment of inertia. The relationship can be seen in Equation B.4. This relationship was used to transform the radii of gyration into mass moments of inertia for the necessary components.

$$I = MK^2 \tag{B.4}$$

In this equation I is the moment of inertia, M is the mass of the component and K is the radius of gyration.

Table B.1: Geometric properties of the upscaled 15 MW NREL wind turbine, as used in the OrcaFlex model.

Segment no.	Arc length [m]	Chord [m]	Thickness [%]	Aerodynamic center [%]		Twist [deg]
				x	y	
1	0.000	4.700	100.000	0.000	50.455	15.595
2	2.538	4.700	100.000	0.000	49.036	15.591
3	4.230	4.800	97.241	0.000	47.345	15.428
4	5.922	4.952	90.201	0.000	45.518	14.987
5	7.614	5.019	80.574	0.000	43.618	14.322
6	9.518	5.097	69.964	0.000	41.740	13.488
7	11.633	5.198	57.869	0.000	39.573	12.291
8	13.495	5.290	49.870	0.000	37.553	11.022
9	15.105	5.347	46.114	0.000	36.113	10.075
10	16.716	5.386	42.681	0.000	34.875	9.194
11	18.326	5.400	39.781	0.000	33.845	8.429
12	19.936	5.389	37.542	0.000	33.037	7.777
13	21.626	5.339	36.063	0.000	32.401	7.182
14	23.396	5.244	35.067	0.000	31.865	6.527
15	25.166	5.115	34.318	0.000	31.443	5.895
16	26.935	4.971	33.700	0.000	31.121	5.294
17	28.754	4.821	33.091	0.000	30.855	4.735
18	30.621	4.673	32.443	0.000	30.618	4.201
19	32.487	4.541	31.846	0.000	30.374	3.726
20	34.354	4.427	31.276	0.000	30.096	3.307
21	36.221	4.312	30.704	0.000	29.801	2.920
22	37.988	4.197	30.100	0.000	29.508	2.561
23	39.654	4.095	29.511	0.000	29.285	2.262
24	41.321	3.996	28.883	0.000	29.099	1.980
25	42.987	3.898	28.238	0.000	28.945	1.714
26	44.654	3.803	27.599	0.000	28.839	1.458
27	46.338	3.711	26.991	0.000	28.782	1.216
28	48.039	3.621	26.388	0.000	28.785	0.988
29	49.740	3.533	25.786	0.000	28.799	0.775
30	51.441	3.447	25.197	0.000	28.876	0.575
31	53.142	3.362	24.633	0.000	28.991	0.380
32	54.799	3.278	24.105	0.000	29.157	0.186
33	56.413	3.198	23.587	0.000	29.342	-0.002
34	58.027	3.117	23.019	0.000	29.557	-0.203
35	59.641	3.035	22.451	0.000	29.798	-0.425
36	61.255	2.954	21.929	0.000	30.060	-0.684
37	62.869	2.874	21.498	0.000	30.341	-0.982
38	64.483	2.794	21.207	0.000	30.632	-1.283
39	66.485	2.713	21.100	0.000	30.931	-1.575
40	68.473	2.592	21.100	0.000	31.364	-1.937
41	70.059	2.509	21.100	0.000	31.680	-2.108
42	71.646	2.423	21.100	0.000	32.036	-2.167
43	73.232	2.335	21.100	0.000	32.441	-2.176
44	74.818	2.245	21.100	0.000	32.881	-2.161
45	76.404	2.152	21.100	0.000	33.352	-2.119
46	77.991	1.614	21.100	0.000	33.847	-2.049
47	79.577	1.565	21.100	0.000	34.375	-1.951
48	81.427	1.481	21.100	0.000	34.950	-1.815
49	83.542	1.326	21.100	0.000	35.827	-1.568
50	84.600	1.032	21.100	0.000	36.818	-1.242

Table B.2: Modelled 17 MW WTG parameters in OrcaFlex.

Item	Parameter	Value	Note
Nacelle	Mass [mT]	818	
	Size [m]	$24 \times 11 \times 12$	Length $\times$ width $\times$ height
	Radii [m]	[4.7, 7.7, 7.6]	[R_{xx} , R_{yy} , R_{zz}]
	Origin [m]	[0, 0, 100]	wrt. to tower origin
Rotor	Mass [mT]	219	
	Diameter [m]	250	
	Radii [m]	[52.5, 37.5, 37.5]	[R_{xx} , R_{yy} , R_{zz}]
	Blade mass [mT]	73	Mass of three blades: 219 mT
	Blade length [m]	122	
Tower	Mass [mT]	813	
	Length [mT]	134	34 m pre-installed
	CoG [m]	[0, 0, 48]	wrt. tower bottom center
	Diameter [m]	6.8-8	Top and bottom diameter
	Radii [m]	[28.9, 28.9, 4]	[R_{xx} , R_{yy} , R_{zz}]
Total	Mass [mT]	1,850	Tower, nacelle and rotor
	CoG [m]	[2.57, 0, 80.51]	wrt. tower bottom center

B.2. Thialf

The Thialf has a DP system in place. In reality, the DP system has stiffness in given degrees of freedom. In OrcaFlex, the DP system is modelled by creating links with the given stiffnesses as input. The surge stiffness is modelled through one link, and the sway stiffness is modelled through two links. One at the midpoint of the ship and one at the stern. Through these links, stiffness in yaw is also achieved. Table B.3 shows the DP data.
The starboard crane properties can be seen in Table B.4.

Table B.3: Thialf DP system data

DoF	DP - Medium gain
11 Surge	2.9×10^2 kN/m
22 Sway	4.4×10^2 kN/m
33 Heave	0 kN/m
44 Roll	0 kNm/rad
55 Pitch	0 kNm/rad
66 Yaw	8.8×10^5 kNm/rad

Table B.4: Input for the starboard crane used in the models (Rentoulis, 2022).

Component	Parameter	Value	Note
Configuration	Slew angle [deg]	315	0 degrees towards stern
	Boom angle [deg]	79.5	90 degrees when pointed to the sky
	Radius [m]	65	Radius of the Jib
Main Boom	Mass [mT]	1,094	
	DOF free	Pitch	wrt. main hinge
	Torsion stiffness [kNm/rad]	950,000	Mimics boom torsion
	Lat. stiffness	110,000,000	Bending in local sway direction
Suspension wire	EA [kN]	5,190,509	For 56 wires including structure flexibility
Delta Jib	Mass [mT]	410	
	DOF free	Pitch	wrt. to Jib hinge
	Axial stiffness [kN/m]	140,000	Mimics axial deformation
	Torsion stiffness [kNm/rad]	450,000	Mimics Jib torsion
	Lat. stiffness	5,800,000	Bending in local sway direction
Backmast	Mass [mT]	90	
	DOF free	Pitch	wrt. to backmast hinge
	Axial stiffness [kN/m]	1,000,000	Mimics axial deformation
	Torsion stiffness [kNm/rad]	1,000,000	Mimics backmast torsion
	Lat. stiffness [kNm/rad]	100,000,000	Bending in local sway direction
Hoist wires	EA [kN]	1,913,552	For 16 wires per fall
Blocks	Mass [mT]	70	Mass per block
	DOF free	Translations	wrt. to the Earth, rotations restricted

B.3. Connections

In the OrcaFlex model, the rigging configuration is simplified so that only the relevant components, such as the USF and LLT, are included, while components, such as the crane masters, which are relevant for WTG set-down on the foundation, are left out.
The parameters for the slings, tuggers, and other connecting winches used in the OrcaFlex model can be seen in Table B.5. Other than winch connections between components in the system, there are also rigid connections.

Some of the system components also have additional constraints placed. These constraints are not objects themselves but limit specific degrees of freedom of the objects connected to them. They do not necessarily completely have to constrain a degree of freedom, but a certain damping or stiffness can be given to chosen rotations and translations. There are several uses for constraints, such as points of connection, the relative positioning of objects, obtaining results at a specific location, sliding mechanisms, and imposed motion. The constraints used in the OrcaFlex model are presented in Table B.6.

Table B.5: Winches used in the OrcaFlex models.

Connection	Type	Parameter	Value
Hook-Crane Blocks	Sling	Stiffness [kN]	1.91×10^6
		Length [m]	32.23
Crane Blocks-Shackle	Sling	Stiffness [kN]	2.57×10^6
		Length [m]	15
Shackle-USF	Sling	Stiffness [kN]	1.57×10^6
		Length [m]	4.7
USF-LLT	Sling	Stiffness [kN]	1.41×10^6
		Length [m]	78.7
USF-Crane	Tugger	Damping [mTs/m]	15
		Length [m]	31.15

Table B.6: Constraints used in the OrcaFlex models.

Restrained component	DoF	Restrained/Free
USF	x	Restrained
	y	Restrained
	z	Free
	Rx	Restrained
	Ry	Restrained
	Rz	Restrained
Shackle	x	Free
	y	Free
	z	Free
	Rx	Restrained
	Ry	Restrained
	Rz	Restrained
Crane blocks	x	Free
	y	Free
	z	Free
	Rx	Restrained
	Ry	Restrained
	Rz	Restrained

B.4. Model

Some additional images of the OrcaFlex model are provided in this section. Figure B.1 shows the tugger configuration used in the model. Figure B.2 shows the model from 4 different directions.

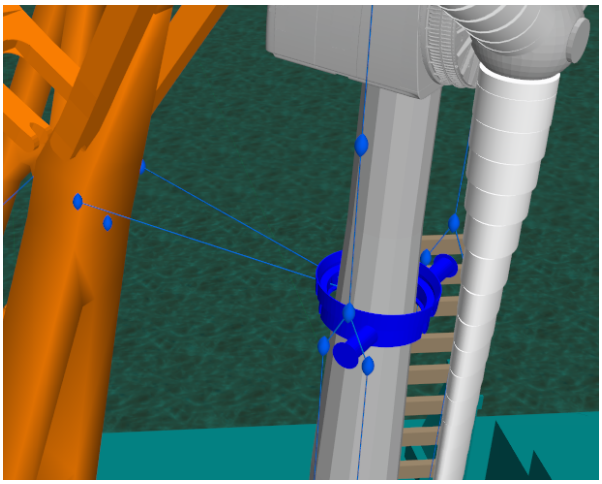

Figure B.1: Configuration of the tuggers used to connect the USF to the PS crane boom.

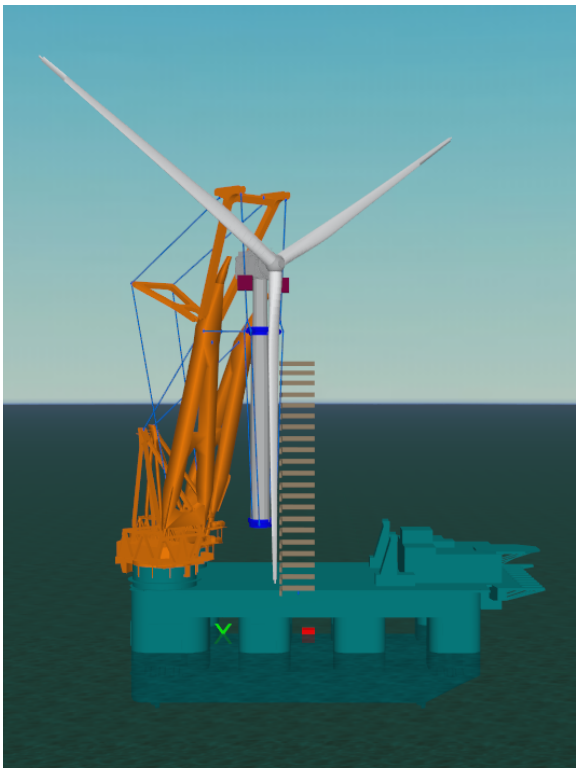

(a) View from SB

(b) View from bow

(c) View from PS

(d) View from stern

Figure B.2: Full system model in OrcaFlex presented from different views.

C

TurbSim

C.1. Input

To generate a 3D spatially varying wind field in OrcaFlex, a TurbSim file with the correct input needed to be created. Below is an example of the TurbSim input file used. The reference wind speed was changed during the simulations to generate stronger/weaker winds.

———TurbSim v2.00.* Input File 10m/s————————
Example input file for TurbSim.
———Runtime Options————————————
False Echo - Echo input data to <RootName>.ech (flag)
2318573 RandSeed1 - First random seed (-2147483648 to 2147483647)
RANLUX RandSeed2 - Second random seed for intrinsic pRNG, or other pRNG: ”RanLux” or ”RNSNLW”
False WrBHHTP - Output HH turbulence parameters in GenPro-binary form? (Generates RootName.bin)
False WrFHHTP - Output HH turbulence parameters in formatted form? (Generates RootName.dat)
False WrADHH - Output hub-height time-series data in AeroDyn form? (Generates RootName.hh)
True WrADFF - Output FF time-series data in TurbSim/AeroDyn form? (Generates Rootname.bts)
False WrBLFF - Output FF time-series data in BLADED/AeroDyn form? (Generates RootName.wnd)
False WrADTWR - Output tower time-series data? (Generates RootName.twr)
False WrFMTFF - Output FF time-series data in formatted (readable) form? (RootName.u, .v, .w)
True WrACT - Output coherent turbulence time steps in AeroDyn form? (Generates RootName.cts)
True Clockwise - Clockwise rotation looking downwind? (Used only for FF binary files w/ BLADED)
0 ScaleIEC - Scale IEC turbulence models to exact target std deviation? [0=none;1=hub;2=all]

———Turbine/Model Specifications———————
32 NumGrid$_Z$ - Vertical grid-point matrix dimension
32 NumGrid$_Y$ - Horizontal grid-point matrix dimension
0.05 TimeStep - Time step [s]
3900 AnalysisTime - Length of analysis time series [s] (program will add time if necessary)
”ALL” UsableTime - Usable length of output time series [s] (GridWidth/MeanHHWS s added if not ”ALL”)
150 HubHt - Hub height [m] (should be > 0.5*GridHeight)
180 GridHeight - Grid height [m]
270 GridWidth - Grid width [m] (should be >= 2*(RotorRadius+ShaftLength))
0 VFlowAng - Vertical mean flow (uptilt) angle [degrees]
0 HFlowAng - Horizontal mean flow (skew) angle [degrees]

———Meteorological Boundary Conditions————————-
”IECKAI” TurbModel - Turbulence model (see Table 4 for valid codes)
”unused” UserFile - Name secondary input file for user-defined spectra or time series inputs
”3” IECstandard - Number of the IEC standard (61400-x, x=1,2,3) with optional 61400-1 ed. number

```
"C"        IECturbc        - IEC turbulence characteristic ("A", "B", "C" or TI in %) or KHTEST
"NTM"      IEC WindType    - IEC turbulence type ("NTM", "xETM", "xEWM1", or "xEWM50" for x=class
1, 2, or 3) default        ETMc        - IEC Extreme turbulence model "c" parameter [m/s] (or "default")
"PL"       ProfileType     - Wind profile type (see Table 6 for valid codes)
"unused"   ProfileFile     - Name of the file that contains user-defined input profiles
10         RefHt           - Height of the reference wind speed [m]
10         URef            - Mean wind speed at the reference height [m/s] [must be 1-hr mean for API model]
450        ZJetMax         - Height of the low-level jet [m] (70-490 m or "default", only for "JET" profile)
0.14       PLExp           - Power law exponent (or "default")
0.0003     Z0              - Surface roughness length [m] (or "default")

---------Non-IEC Meteorological Boundary Conditions---------
default    Latitude        - Site latitude [degrees] (or "default")
0.05       RICH NO         - Gradient Richardson number [-]
default    UStar           - Friction or shear velocity [m/s] (or "default")
default    ZI              - Mixing layer depth [m] (or "default")
default    PC UW           - Hub mean u'w' Reynolds stress [m^2/s^2] (or "default" or "none")
default    PC UV           - Hub mean u'v' Reynolds stress [m^2/s^2] (or "default" or "none")
default    PC VW           - Hub mean v'w' Reynolds stress [m^2/s^2] (or "default" or "none")

---------Spatial Coherence Parameters----------
default    SCMod1          - u-component coherence model ("GENERAL","IEC","API","NONE", or "default")
default    SCMod2          - v-component coherence model ("GENERAL","IEC","NONE", or "default")
default    SCMod3          - w-component coherence model ("GENERAL","IEC","NONE", or "default")
default    InCDec1         - u-component coherence parameters [-, m^-1] ("a b" in quotes or "default")
default    InCDec2         - v-component coherence parameters [-, m^-1] ("a b" in quotes or "default")
default    InCDec3         - w-component coherence parameters [-, m^-1] ("a b" in quotes or "default")
default    CohExp          - Coherence exponent for general model [-] (or "default")

---------Coherent Turbulence Scaling Parameters----------
"path/to/coh events/eventdata"   CTEventPath     - Name of the path where event data files are located
"Random"   CTEventFile     - Type of event files ("LES", "DNS", or "RANDOM")
True       Randomize       - Randomize the disturbance scale and locations? (true/false)
1.0        DistScl         - Disturbance scale (ratio of wave height to rotor disk).
0.5        CTLy            - Fractional location of tower center from right to L of dataset looking downwind
0.5        CTLz            - Fractional location of hub height from the bottom of the dataset
30.0       CTStartTime     - Minimum start time for coherent structures in RootName.cts [s]
```

C.2. Output

In this investigation, three different reference wind speeds were used for the base case load cases, and TurbSim files for them were generated. The wind speeds were 5 m/s, 10 m/s, and 12 m/s. Figure C.1 shows the wind time series throughout the duration of the simulation for the different reference wind speeds.

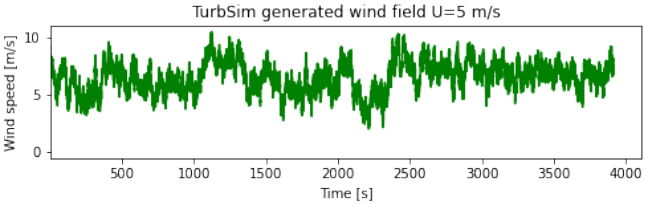

(a) U=5 m/s

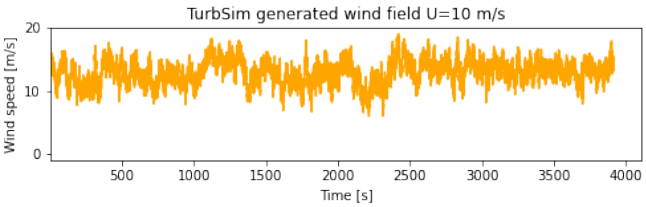

(b) U=10 m/s

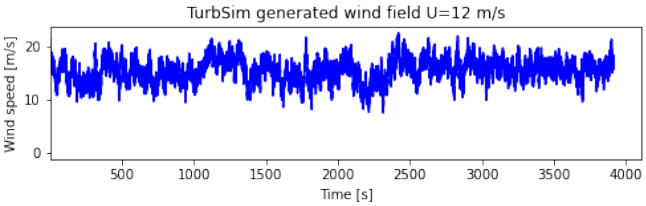

(c) U=12 m/s

Figure C.1: Time series of the wind speed for a 3D spatially varying turbulent wind field generated through TurbSim.

D

Base Case Results

D.1. Load cases

In Table D.1 all the simulated load cases for the base case analysis can be seen. For the final analysis presented in Chapter 4, not all the simulated cases are presented, but only the relevant ones for the investigation. The other cases were used to assess and validate the dynamic behaviour of the system. For each load case, the model used, the type of test done, the sea state, and any other particularities are described.

Table D.1: Load cases considered for the base case analysis.

Case	Model	Test	Hs [m]	Tp [s]	Wave direction [deg]	Type of wind	Wind speed [m/s]	Wind direction	Other parameters	Number of load cases
Wave Only	Full model	Vary wave direction	1	6	0:315, bins: 45	-	-	-	Pitch: 0	8
Wind Only	WTG only	Pitch	-	-	-	Constant	10	0:315, bins: 45	Pitch: 0:90	7x8
Wind Only	WTG + rigging	Vary wind direction	-	-	-	TurbSim	[5, 10, 12]	0:315, bins: 45	Pitch: 0	3x8
Wind Only	Full model	Vary wind direction	-	-	-	TurbSim	[5, 10, 12]	0:315, bins: 45	Pitch: 0	3x8
Wind & Wave	Full model	Vary Hs, Tp	[0.5, 1, 2]	[4, 6, 8, 10, 12]	[90, 135, 180]	TurbSim	10	[90, 135, 180]	Pitch: 0	3x5x3
Wind & Wave	Full model	Misalignment wind and waves	1	6	[90, 135, 180]	TurbSim	10	[90, 135, 180]	Pitch: 0	4
Wind & Wave	Full model	Wind effect	1	6	180	TurbSim	[5, 10, 12]	180	Pitch: 0	3

D.2. Wave-only analysis

In this section, supplementary results of the wave-only analysis are presented.

D.2.1. Frequency domain analysis

For the frequency domain analysis, LiftDyn was used. The environmental condition limits are based on *DNVGL-RP-C205*. From this recommended practice, three curves were obtained from section 3.4, which form the basis of the H_s-T_p combinations presented in Figure 4.2. The first curve represents the maximum significant wave height for wave periods up to $T_p^2/13$. This is based on the wave-breaking limit. The second curve considers the wave periods where the limiting significant wave height can occur in a wind developing sea state. Lastly, the last curve considers swell sea states, which are represented by longer wave periods. Peak periods between 3 and 15 seconds in intervals of 0.5 are considered.

A JONSWAP spectrum was used, with γ equal to 3.3. Additionally, a spreading factor of 10 was used, which is the standard setting in LiftDyn. A value of 10 makes it possible to represent high wind sea states, as well as swell sea states, as described in section 3.5.8 of *DNVGL-RP-C205*.

On the following page, the operability curves from different directions between 0 and 315 degrees in bins of 45 degrees are given for a series of limiting criteria, which have already been defined in section 4.1. The operability curves show that for many directions, especially at lower significant wave height (<1 m) and larger periods, the first parameter that is expected to reach critical limits is the nacelle clearance and also the sidelead angle. The vessel roll and pitch limits require larger significant wave heights to be excited past safe operable limits.

Operability - All criteria

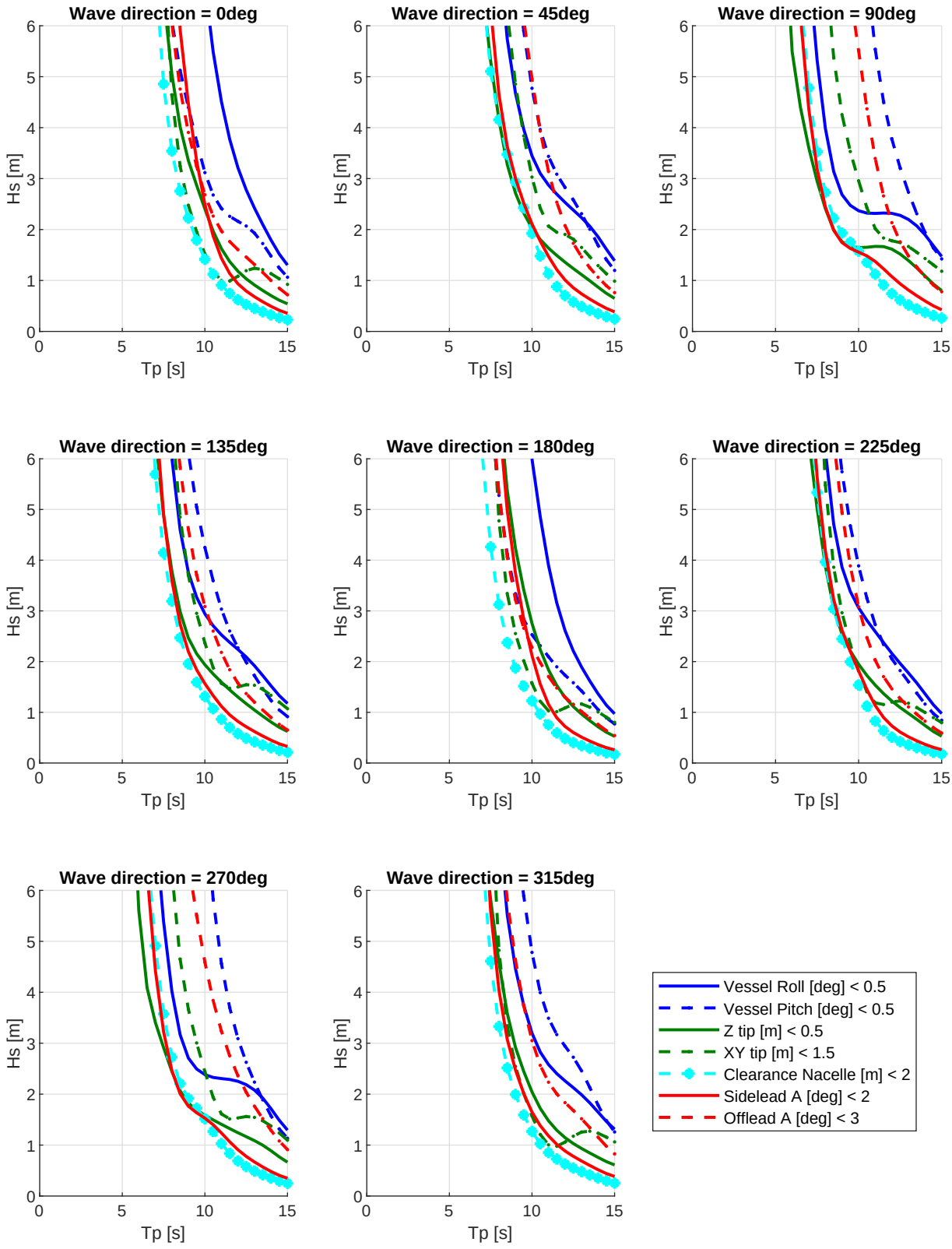

		Wind direction [deg]							
		0	**45**	**90**	**135**	**180**	**225**	**270**	**315**
Thialf surge	**min**	-0.0328	-0.0211	-0.0130	-0.0240	-0.0579	-0.0176	-0.0166	-0.0137
	max	0.0546	0.0313	0.0269	0.0319	0.0612	0.0210	0.0243	0.0239
	mean	0.0050	0.0052	0.0052	0.0051	0.0047	0.0051	0.0051	0.0052
	STD	0.0097	0.0066	0.0056	0.0060	0.0150	0.0050	0.0056	0.0052
Thialf sway	**min**	0.7922	0.7340	0.7208	0.7476	0.7870	0.7400	0.7503	0.7002
	max	0.8500	0.9018	0.9034	0.9089	0.8515	0.8990	0.8983	0.9303
	mean	0.8211	0.8215	0.8214	0.8215	0.8210	0.8209	0.8213	0.8206
	STD	0.0069	0.0183	0.0237	0.0202	0.0099	0.0166	0.0214	0.0259
Thialf heave	**min**	-22.0402	-22.0330	-22.0443	-22.0232	-22.0182	-22.0237	-22.0426	-22.0354
	max	-21.9640	-21.9699	-21.9607	-21.9818	-21.9866	-21.9828	-21.9605	-21.9686
	mean	-22.0023	-22.0023	-22.0023	-22.0023	-22.0023	-22.0023	-22.0023	-22.0023
	STD	0.0109	0.0101	0.0125	0.0053	0.0047	0.0057	0.0125	0.0094
Thialf roll	**min**	0.0100	0.0034	-0.0111	-0.0001	0.0113	0.0013	-0.0152	0.0026
	max	0.0331	0.0395	0.0530	0.0417	0.0310	0.0410	0.0564	0.0402
	mean	0.0211	0.0211	0.0211	0.0211	0.0211	0.0211	0.0211	0.0211
	STD	0.0027	0.0048	0.0098	0.0060	0.0030	0.0057	0.0109	0.0053
Thialf pitch	**min**	-0.0215	-0.0199	-0.0195	-0.0192	-0.0174	-0.0212	-0.0207	-0.0202
	max	-0.0130	-0.0143	-0.0129	-0.0122	-0.0145	-0.0117	-0.0138	-0.0125
	mean	-0.0172	-0.0172	-0.0172	-0.0172	-0.0172	-0.0172	-0.0172	-0.0172
	STD	0.0017	0.0017	0.0016	0.0015	0.0016	0.0015	0.0016	0.0016

Table D.2: Summary statistics of Thialf vessel motions.

D.2.2. Time domain analysis

Table D.2, Table D.3 and Table D.4 show an overview of the Thialf, crane tip and WTG tower bottom motion statistics, respectively. These include the maximum, minimum, mean and standard deviation (STD) values for different incoming wave directions. The values for the standard deviation were used to create the bar charts presented in Figure 4.5.

		Wind direction [deg]							
		0	**45**	**90**	**135**	**180**	**225**	**270**	**315**
Crane tip surge	min	50.5020	50.4868	50.4747	50.4797	50.4822	50.4888	50.4851	50.4677
	max	50.6541	50.7046	50.6822	50.6798	50.6709	50.6687	50.6683	50.7163
	mean	50.5826	50.5824	50.5825	50.5822	50.5823	50.5829	50.5825	50.5831
	STD	0.0213	0.0286	0.0238	0.0278	0.0256	0.0235	0.0279	0.0289
Crane tip sway	min	-84.2313	-84.2596	-84.3320	-84.2801	-84.2301	-84.2858	-84.3320	-84.2881
	max	-84.1576	-84.1380	-84.0587	-84.1073	-84.1690	-84.1094	-84.0680	-84.1131
	mean	-84.1995	-84.1993	-84.1994	-84.1993	-84.1995	-84.1995	-84.1995	-84.1998
	STD	0.0088	0.0182	0.0399	0.0228	0.0093	0.0220	0.0406	0.0235
Crane tip heave	min	192.7010	192.6903	192.6617	192.6953	192.7115	192.6984	192.6638	192.6970
	max	192.7613	192.7728	192.8044	192.7667	192.7502	192.7649	192.8007	192.7636
	mean	192.7308	192.7308	192.7308	192.7308	192.7308	192.7308	192.7308	192.7308
	STD	0.0079	0.0105	0.0207	0.0104	0.0054	0.0097	0.0208	0.0096
Crane tip roll	min	0.0115	0.0043	-0.0117	0.0025	0.0136	0.0037	-0.0142	0.0049
	max	0.0400	0.0476	0.0613	0.0485	0.0376	0.0477	0.0636	0.0473
	mean	0.0257	0.0257	0.0257	0.0257	0.0257	0.0257	0.0257	0.0257
	STD	0.0033	0.0056	0.0113	0.0067	0.0036	0.0064	0.0123	0.0060
Crane tip pitch	min	-0.0158	-0.0153	-0.0192	-0.0158	-0.0139	-0.0150	-0.0198	-0.0157
	max	0.0228	0.0226	0.0262	0.0237	0.0220	0.0235	0.0276	0.0234
	mean	0.0040	0.0040	0.0040	0.0040	0.0040	0.0040	0.0040	0.0040
	STD	0.0052	0.0056	0.0067	0.0055	0.0057	0.0055	0.0064	0.0055
Crane tip yaw	min	-0.4130	-0.4441	-0.4559	-0.4420	-0.4099	-0.4383	-0.4251	-0.4633
	max	-0.3680	-0.3455	-0.3520	-0.3442	-0.3725	-0.3519	-0.3583	-0.3061
	mean	-0.3913	-0.3916	-0.3915	-0.3917	-0.3913	-0.3912	-0.3915	-0.3911
	STD	0.0061	0.0115	0.0111	0.0127	0.0052	0.0106	0.0104	0.0159

Table D.3: Summary statistics of crane tip motions.

		Wind direction [deg]							
		0	**45**	**90**	**135**	**180**	**225**	**270**	**315**
Tower surge	**min**	57.7198	57.6607	57.7191	57.7011	57.7056	57.7189	57.6981	57.6906
	max	57.8709	57.9155	57.8715	57.9010	57.8716	57.9007	57.8777	57.9629
	mean	57.7955	57.7954	57.7955	57.7953	57.7953	57.7958	57.7955	57.7961
	STD	0.0215	0.0282	0.0230	0.0305	0.0244	0.0224	0.0250	0.0274
Tower sway	**min**	-73.7416	-73.7669	-73.7504	-73.7721	-73.7445	-73.7587	-73.7539	-73.7758
	max	-73.5949	-73.5763	-73.5994	-73.5630	-73.6009	-73.5803	-73.5869	-73.5681
	mean	-73.6716	-73.6715	-73.6716	-73.6716	-73.6716	-73.6716	-73.6717	-73.6720
	STD	0.0213	0.0267	0.0222	0.0293	0.0201	0.0214	0.0250	0.0270
Tower heave	**min**	60.1925	60.1798	60.1495	60.1865	60.2008	60.1882	60.1547	60.1877
	max	60.2488	60.2628	60.2959	60.2565	60.2403	60.2538	60.2901	60.2516
	mean	60.2206	60.2206	60.2206	60.2206	60.2206	60.2206	60.2206	60.2205
	STD	0.0073	0.0101	0.0209	0.0103	0.0055	0.0096	0.0207	0.0091
Tower roll	**min**	0.0814	0.0626	0.0691	0.0661	0.0799	0.0798	0.0629	0.0651
	max	0.1781	0.1898	0.1902	0.1952	0.1713	0.1753	0.1999	0.1839
	mean	0.1275	0.1275	0.1275	0.1274	0.1275	0.1275	0.1275	0.1275
	STD	0.0143	0.0181	0.0175	0.0195	0.0136	0.0139	0.0190	0.0158
Tower pitch	**min**	0.0482	0.0300	0.0425	0.0326	0.0468	0.0449	0.0395	0.0429
	max	0.1530	0.1671	0.1545	0.1665	0.1505	0.1413	0.1576	0.1574
	mean	0.0973	0.0972	0.0973	0.0972	0.0973	0.0973	0.0973	0.0972
	STD	0.0154	0.0186	0.0155	0.0199	0.0147	0.0139	0.0176	0.0163
Tower yaw	**min**	-45.4693	-45.5295	-45.4841	-45.5034	-45.4636	-45.4908	-45.4752	-45.5234
	max	-45.3145	-45.2833	-45.3031	-45.2745	-45.3165	-45.2918	-45.3084	-45.2422
	mean	-45.3913	-45.3916	-45.3918	-45.3916	-45.3914	-45.3912	-45.3915	-45.3910
	STD	0.0236	0.0331	0.0285	0.0345	0.0203	0.0401	0.0236	0.0324

Table D.4: Summary statistics of tower bottom motions.

D.3. Wind-only analysis

In this section, supplementary results of the wind-only analysis are presented.

D.3.1. Blade pitch analysis

Figure D.1 shows the plots for all nacelle connection forces and moments in the local nacelle reference frame, as labelled in Figure 4.8b. The plot showing the yaw moment for the different blade pitch angles and wind directions has already been discussed in subsection 4.2.1.

In Figure D.1a it can be seen that the plot is symmetrical about 180 degrees. This is due to the symmetry of the WTG. Furthermore, comparing 180 degrees and 0 (=360) degrees, it can be seen that the magnitude of the force is the same, however, for 0 degrees the value is negative, while for 180 degrees the value is positive. It can also be seen that when the blade pitch angle is 0 degrees, the force is much larger than for 90 degrees. This is because 0 degree pitch angle results in the sides of the blades with the most surface area being perpendicular to the X-axis. This causes a larger surface area in the Y-Z plane, causing greater X forces.

Figure D.1c shows the Y-force. For this force, the forces for 90 degree pitch show the greatest variation between wind directions. This is explained by the fact that for 90 degree blade pitch the length of the blade from the leading to the trailing edge is parallel to the X-axis or perpendicular to the Y-axis. Due to this when the wind is coming from 45, 90, 135, 225, 270 and 315 degrees, large Y-forces are experienced. Much smaller Y-forces are experienced for 0 degree blade pitch, as the surface area of the blade perpendicular to the Y-direction is small.

The Z-force plot, Figure D.1e, shows a constant Z-force for all wind directions and all pitch angles. The value of the Z-force is relatively large (10252 kN), which is due to the weight of the whole assembly. There is no effect of the constant wind or the blade pitch angle on the Z-force.

Figure D.1b shows that the X-moment for 0 degree pitch and 90 degree pitch remain close to 0 for all wind directions. The moment is much larger for other blade pitch angles which have been investigated. The Y-moment, Figure D.1d again shows other blade pitch angles having higher Y-moments than 0 and 90 degree pitch angles.

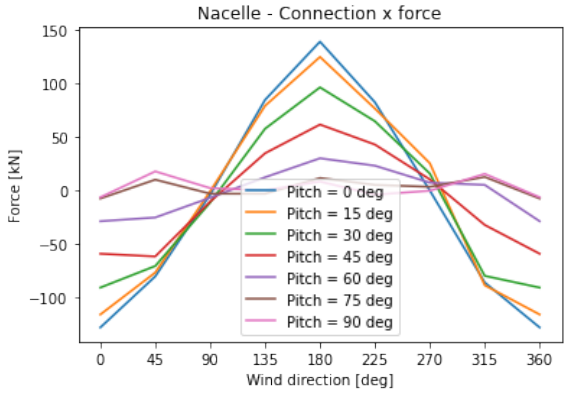

(a) Nacelle - Connection X-force

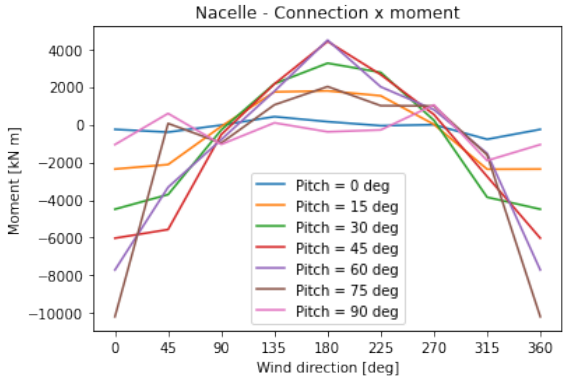

(b) Nacelle - Connection X-moment

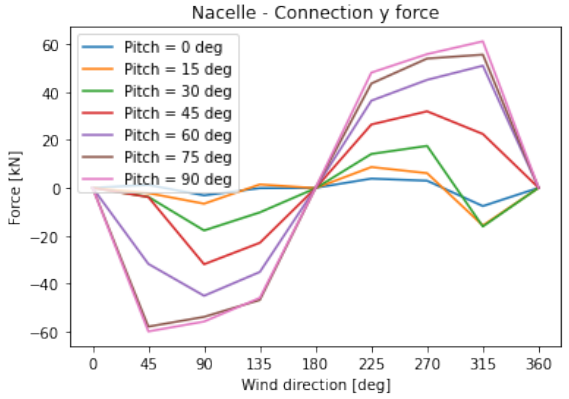

(c) Nacelle - Connection Y-force

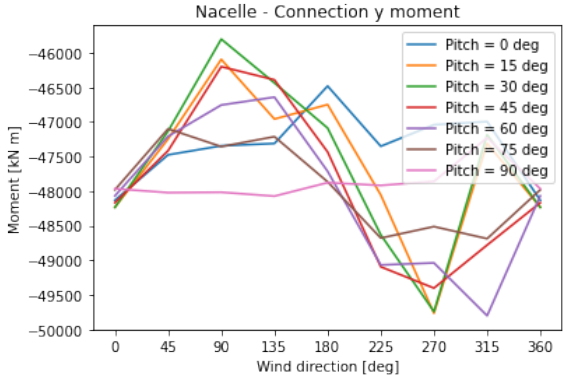

(d) Nacelle - Connection Y-moment

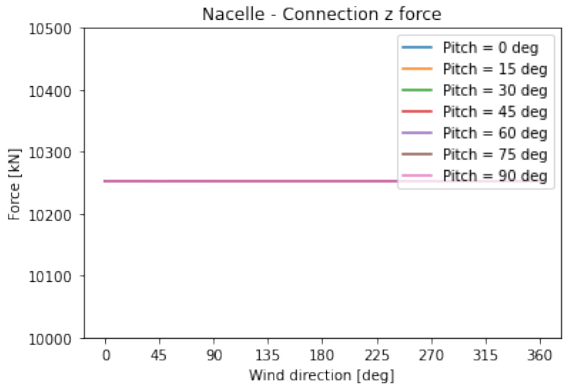

(e) Nacelle - Connection Z-force

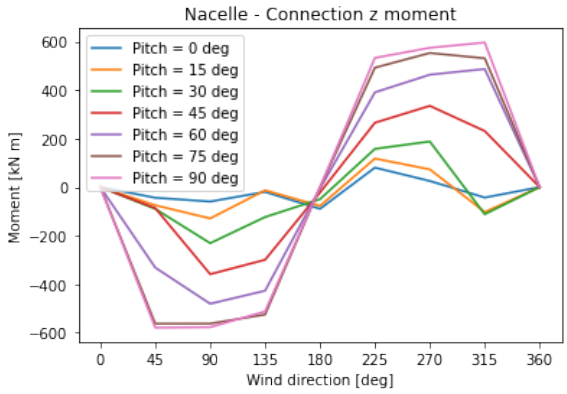

(f) Nacelle - Connection Z-moment

Figure D.1: Nacelle - Connection force/moment plotted as a function of the blade pitch angle against the incoming wind direction.

Figure D.2 shows the mean forces and moments of the tower connection for the model with just the rigging and WTG. Figure D.3 shows the mean forces and moments of the tower connection for the whole system model. It can be seen that the mean values for the Y-force, Z-force and Z-moment remain close to 0 compared to the maximum recorded values, which were presented in section 4.2.

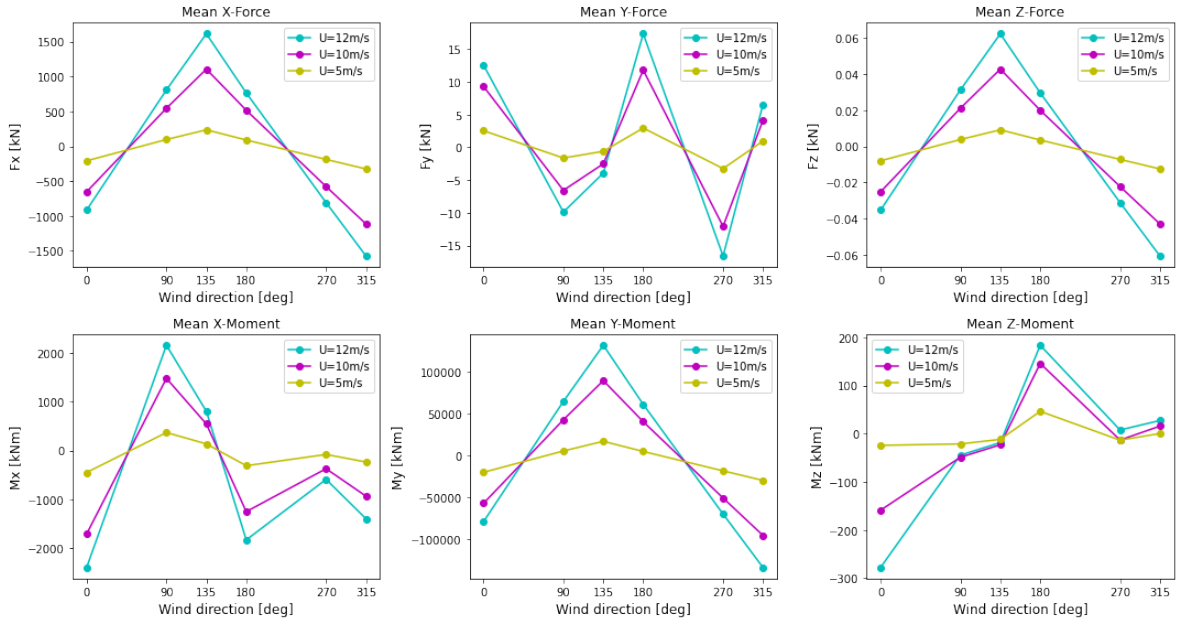

Figure D.2: Mean force and moment plots of the tower connection for different incoming wind directions for the model with the rigging and WTG. Mean wind speeds of 5, 10, and 12 m/s were used as the TurbSim input values.

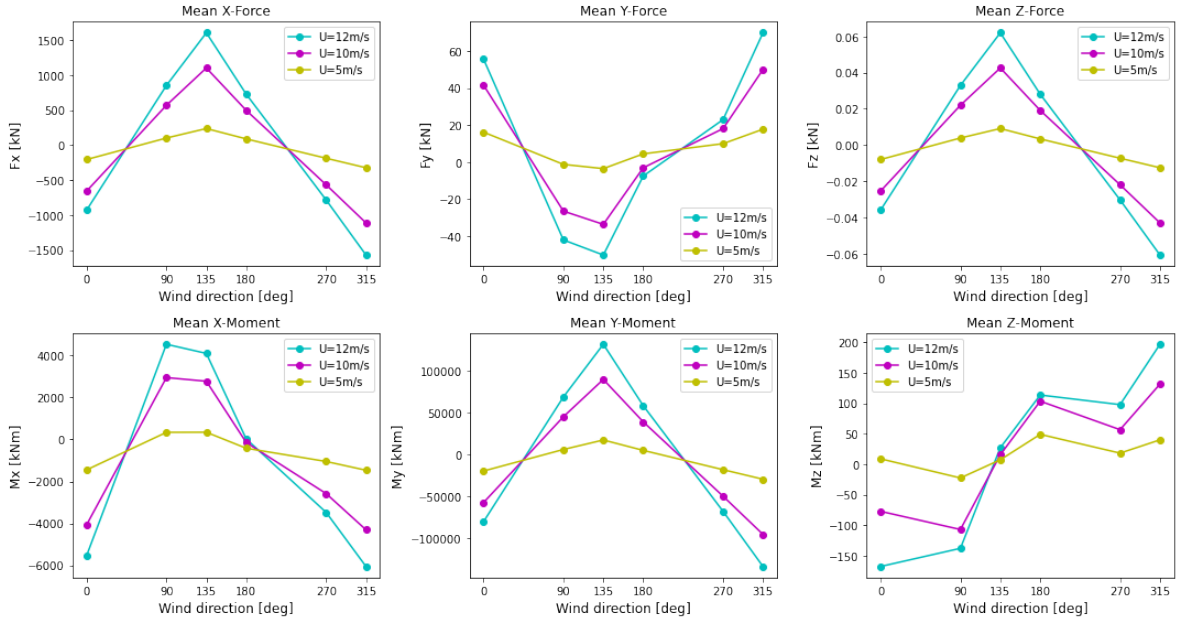

Figure D.3: Mean force and moment plots of the tower connection for different incoming wind directions for the full model. Mean wind speeds of 5, 10, and 12 m/s were used as the TurbSim input values.

E

Concept study

E.1. Concepts

In this section, an additional description is given for the friction pad-based concepts, which have already been analysed in section 5.2. This includes blade installation equipment, lift frames and motion-compensated grippers.

E.1.1. Concept 1: Blade installation equipment

The installation of blades offshore is a complex procedure, as high accuracy and precision are necessary for the positioning of the blade root with the nacelle. The offshore environment makes this a complicated task. The RNA method as described in subsection 1.2.2, makes use of the Heerema designed GREP tool and Vestas designed BIT tool to help with positioning and steadying of the blade when it is being mounted to the nacelle. The working principles of these tools could potentially be applied to the USF and have therefore been further analysed.

GREP Tool

The Guide root end positioning tool is used for mounting of blades to the nacelle during the RNA installation method. The use of the GREP is intended for something completely different than what the goal of the USF is, however, there are some common goals of both tools, such as both tools need to provide sufficient clamping force while not damaging the component they are holding. A diagram of the GREP can be seen in Figure 5.3, where the numbered labels refer to:

1. Tower part;
2. Main frame;
3. Rail frame;
4. X-translation frame;
5. Y-translation frame;
6. Z-rotation frame;
7. Y-rotation frame.

Each given frame allows for motion in the degree of freedom after which it is named. The Y-rotation frame contains 3 rubber friction pads spaced at 120 degrees to ensure equal load distribution. The material of the pads is EPDM 8407 and between the pad material and the material of the blades (mostly fibreglass), the coefficient of friction is 0.5.

The GREP is able to clamp onto the blade through two hydraulically operated clamps, which are able to generate enough clamping force to stop the blade from slipping out of the GREP during the line-up of the blade root with the nacelle. The hydraulic cylinders, which are used as clamps, are powered by an electric-driven Hydraulic Power Unit on the GREP. The blade is supported from underneath and therefore, the GREP does not need to generate friction or clamping force to act against the weight of the blade (Heerema Marine Contractors, 2022a). The same is true for the USF, where the tower weight is being taken by the lift wires, and heave motion between USF and the tower should be possible.

In the GREP tool, X, Y and Z translations are possible through hydraulic cylinders and chain drives. Such means for translation are unrealistic for the USF, however, the X and Y translation are also not necessary for the USF. In the GREP, the Y and Z rotation frames can rotate to prevent high moments on the blade. Pre-tensioned, anti-rotation springs are utilised to keep the frame steady and in position when no blade is placed in the GREP and the stiffness of these springs is very low so that when the frames are forced to rotate by the blade, the moment that arises is very low.

The clamping force of the USF needs to prevent rotation of the tower inside the USF, which should be possible with a similar principle to the GREP tool. However, with the friction pads, the heave motion between the tower and USF would also mostly be restrained, which could cause issues with regards to sling elongation during the tensioning of the rigging. If the GREP tool concept solution was to be applied, an additional mechanism would have to be added, which would allow heave motion. This could be possible through the utilisation of rollers or something similar.

BIT Tool

The blade installation tool was used for the Arcadis Ost wind farm to help with the mounting of blades to the nacelle on board the Thialf, together with the GREP tool. The blade installation tool is supplied by Vestas, and therefore, much information regarding it is not publicly known. The BIT tool allows the rotor to stay in place by holding the blade with two arms. This fixes the blade. The BIT connects the blade to the crane. Pads are located on the arms of the BIT and come in contact with the blade. The material of the pads is EPDM 8407 and between the pad material and the material of the blades (mostly fibreglass), the coefficient of friction is 0.5, which is the same as for the GREP tool.

Rotations and other translations of the blade when being held by the BIT are not allowed, and hence other than the friction pads used to generate sufficient friction to restrain motion, the BIT tool does not offer other possible ideas for the USF - tower interface solution.

E.1.2. Concept 2: Lift-frames

Full WTG single lift installation has already been proven possible in the past in a few smaller projects. Some of these projects made use of a similar concept to the USF in the form of stability frames. In the following section, these concepts are introduced and details regarding the working of them given. Key differences between the projects and the specific scenario for this thesis are also identified.

Hywind by Saipem

Hywind was the first ever floating offshore wind farm, installed in 2017. For its installation, it used the integrated approach of the WTG and tower being installed as one assembly onto the floating foundation. Saipem was the contractor responsible for the installation of the tower and wind turbine. For this, they developed and manufactured a ”stability frame” system as pictured in Figure 5.4 (SAIPEM, 2017). In the figure, a blue frame can be seen that is fastened onto the tower section during the lift. The vessel used for this installation was Saipem 7000, which is a heavy lift vessel (HLV). The vessel has high charter rates and hence its costs were a disadvantage of using this specific method for the Hywind project. Additionally, the unstable motion of the floater foundation during the mating of the tower and wind turbine to the foundation also posed an issue, making the weather constraints tight.

The stability frame provided stability to the whole WTG assembly during the lift through hydraulic clamping. Four friction pads were used, two of which were fixed, while two were connected to hydraulic cylinders, acting as arms. The hydraulic cylinders were able to provide enough clamping force so that the frame was able to provide sufficient stability to the whole WTG assembly during the lift (Ribuot, 2019). A challenge Saipem faced when designing the stability frame was correctly positioning the frame onto the tower without any tower modification or appurtenances. The solutions Saipem has thought of include providing visual markings on the tower and supplying cameras onto the stability frame. There is not much information available online regarding the rest of the design considerations, such as which degrees of freedom were constrained. For the USF, hydraulic cylinders could potentially be utilised to provide the necessary clamping force to friction pads, however, a detailed plan of how the correct degrees of freedom will be restrained is required.

With the use of the stability frame, Saipem achieved a similar lift, as being investigated in this thesis. A key difference, however, is that both cranes on the Saipem 7000 HLV were used to make the installation possible, while the lift using the Thialf in this thesis only uses the SB crane. Also, a significant difference is that the WTG was pre-assembled onshore and mated to the floating spar foundation inshore at a port in Norway. The port of Stord on the West coast of Norway is sheltered by the fjord, which helped to decrease environmental influence. The single lift with the USF is planned to be done offshore at the OWF location, where environmental conditions are harsher.

Beatrice Demonstrator Wind Farm Project

In 2007 the Beatrice Demonstrator Wind Farm Project became the first project in which the turbine, nacelle and blades were assembled together onshore and transported to an offshore location off the coast of Scotland. The water depths in the area were up to 45 m, and the wind turbine used had a capacity of 5 MW. The Rambizin crane ship, which has a lifting capacity of 4000 tonnes, was used for the installation. During installation, the Rambizin cranes were used to lift the wind turbine assembly from the floating installation vessel which transported the assembly to the offshore location, onto the offshore foundation, a jacket structure (Zhang et al., 2013).

The installation process required the use of a support frame for the tower section while being held by the crane for additional stability during transport and lifting. Figure 5.5 shows a close-up of the frame. The support frame, known as the tower interface frame (TIF), is a large steel structure and was built specifically for the Beatrice project by Offshore Heavy Transport, a Norwegian engineering company. The TIF held the tower section at the base while being transported to the offshore location. The TIF was designed so that during the lift, it would be connected to the WTG tower at a height above the combined CoG of the WTG (Seidel and Gosch, 2006). This allowed for the lifting forces to be applied closer to the base of the tower, compared to when no such lifting frame would be used. Having the lifting forces closer to the base of the tower helped to minimise the loads acting on the tower sections when lifted (minimise stress). The USF is also mounted onto the frame at a height above the combined centre of gravity for the same reason. Along with that, the TIF helped in maintaining the stability of the WTG, as it ensured that the WTG was kept in a vertical position. The TIF had a mass of 230 mT and was designed to be adjustable so that it could accommodate towers of different sizes and weights. To adjust the height of the TIF on the tower to the correct height, hydraulic cylinders were used. The TIF was also equipped with sensors and other equipment used for monitoring, which enabled the installation team to monitor the lifting forces being experienced, and in hand, ensure that the whole procedure was advancing safely (Seidel and Gosch, 2006). Hydraulic cylinders, as utilised for the Beatrice project, could be used for the USF as well. More specific details of the TIF and the lifting procedure are not known. But overall, the TIF was a critical component in the installation of the Beatrice Demonstrator wind farm, as it allowed for the safe and efficient installation of WTGs. The installation method with the TIF again differs from the lift with the USF, due to two cranes being required. A similarity is that both lifts are performed offshore, unlike for the Hywind project.

E.1.3. Concept 3: Motion compensated grippers

There are several concepts of motion-compensated grippers for monopile installations from various contractors. The goal of all these grippers is to aid the installation of monopiles by compensating vessel motions and keeping the monopile vertical. The motion compensation property of such grippers is not relevant for the USF design, however, the way they hold the pile and the relative motion between the pile and gripper could be relevant. A key difference between the type of loads that induce the USF and pile grippers motions is that USF motions caused by the environmental loads are wind dominated, while the motions of the pile grippers are mostly hydrodynamic forces induced by the waves.

Motion Compensated Gripper Frame

The motion-compensated gripper frame (MCGF), a Heerema MC concept, is able to rotate the monopile about the Z-axis, allowing for relative rotation between the gripper and monopile. This is not wanted for the USF and tower interface, as the Z-rotation between the two should be constrained. However, the gripper consists of a bumper, which makes contact with the monopile. The bumper helps in reducing impact loads by acting as a compression body. This could be a potential solution for avoiding tower damage during installation, however, the issue with the bumper as designed for the MCGF is, that segments of it are likely to get damaged during operations and need to be replaced. This is undesired for the USF, as if the bumper needed replacement after installation of every few WTGs, the overall installation time will be greatly prolonged.

Motion Compensated Pile Gripper

The Motion Compensated Pile Gripper (MCPG) designed by TWD, is used for the installation of large diameter piles. Due to its modular property, it can be adapted to various pile diameters, making it a versatile tool that can be utilised for a variety of offshore projects. Gripping pads can be added or taken away from the gripper to make it suitable for piles of different shapes and sizes. This is a suitable idea in the case that the USF should be made for the installation of towers of different diameters.

To make the gripper work as intended a combination of mechanical and hydraulic systems are utilised. Maximum friction is provided to the pile surface by the gripping system, and hydraulic cylinders are used to exert a clamping force that then holds the pile in place. Contact between the gripper and the pile is made through rollers. This could be a suitable solution for translation in the Z-direction of the USF.

E.2. Calculations

In this section, different calculations are presented that are required for Chapter 4.

E.2.1. USF horizontal loads

In the case that the WTG assembly in the crane does not move in the horizontal plane, and the sidelead and offlead angle remain 0 degrees, there would be no horizontal loads. However, since that is not the case under the combined environmental loading of wind and waves, the horizontal loads in the X and Y direction must be calculated. The horizontal loads will be calculated based on the maximum allowable side lead and offlead angle as stated in Table 3.3. Both limiting angles are 2 degrees. The sidelead and offlead angles of the system are shown in the diagrams in Figure E.1.

If the sidelead and offlead angles are zero, then the vertical force is the weight of the WTG assembly together with the rigging components. For simplification, the total weight will include the WTG assembly, LLT, and USF. Slings and other components are disregarded. The total mass of these components, M_{tot}, is 2180 mT, and multiplying by the gravitational acceleration (9.81 m/s^2), the weight is obtained, as 21385.8 kN. In the case, there is an offlead or sidelead angle, the total weight gets split into a vertical and horizontal weight (force) component. The horizontal component, F_h, can be obtained through simple trigonometry.

$$F_h = M_{tot} \times 9.81 \times \sin(2) = 21385.8 \times \sin(2) = 746 \text{ kN} \tag{E.1}$$

The value of 746 kN is the horizontal load component in the X- and Y-direction when using a sidelead and offlead angle of 2 degrees.

E.2.2. Sling elongation

Since the slings used in the rigging have an elastic stiffness, EA, they will extend under the load of the WTG assembly. The extension of the slings will most likely not be the same for all slings at the same time.

Maximum sling elongation

To properly define the functionality of the USF with regard to the Z translation possibility, the maximum sling elongation must be calculated. With this information, it can be determined how much translation in the Z-direction the USF must accommodate.

The slings relevant to the Z translation are the slings connecting the USF and LLT. They each have a value of 1.41×10^6 kN as their elastic stiffness and a length of 79 m. The elastic stiffness value comes from the Safe Work Load (SWL) of the type of rope used as the sling. The SWL per sling is 850 mT and the safety factor ($S.F.$) needed to calculate the Minimum Breaking Load (MBL) is 3.38 ($MBL = S.F. \times SWL$). This way the MBL becomes 2873 mT. The elastic stiffness is calculated according to SC-294, and it is also assumed that an elongation of 2% occurs at the MBL. This is applicable for Bexco Rope Sling. The calculation for the elastic stiffness is presented in Equation E.2.

$$EA = \frac{S.F. \times SWL \times 9.81}{0.02} = \frac{MBL \times 9.81}{0.02} = \frac{2873 \times 9.81}{0.02} = 1.41 \times 10^6 \text{ kN} \tag{E.2}$$

The static load of the WTG is the total mass of the WTG assembly, which has previously been calculated as 2180 mT. Since there are 4 slings connecting the LLT and USF, and it is assumed that the loading is equally distributed

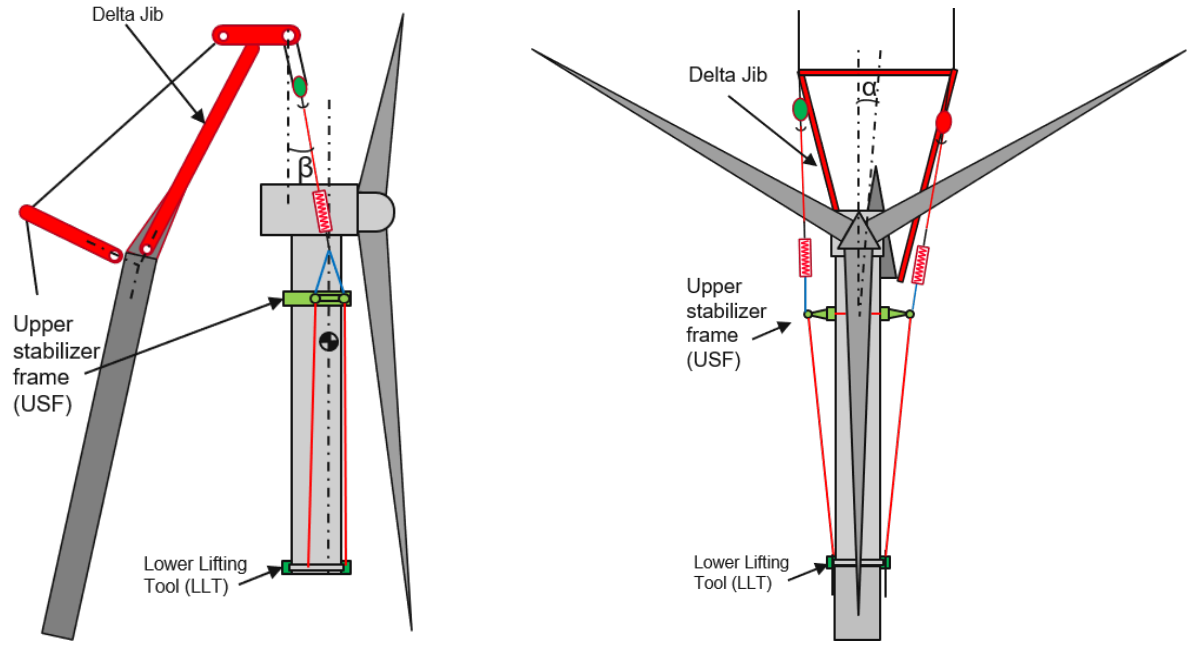

(a) Offlead angle denoted by β.

(b) Sidelead angle denoted by α.

Figure E.1: Left: diagram showing the offlead angle. Right: diagram showing the sidelead angle.

between all four slings, the static load each sling must carry is 545 mT, which is 5346 kN. The axial stiffness of the slings is:

$$k = \frac{EA}{L} = \frac{1.41 \times 10^6}{79} = 17838 \text{ kN/m} \tag{E.3}$$

Using the axial stiffness and the load being taken by each sling, the extension of the slings under the loading can be obtained:

$$\delta L = \frac{\text{Static load}}{k} = \frac{4346}{17838} = 0.30 \text{ m} \tag{E.4}$$

Uneven sling elongation

As mentioned before, the slings will most likely not elongate the same amount at the same time, and therefore through slight rotation along the X- and Y-axes of the USF, these elongations can be compensated. The maximum rotations along the X- and Y-axes will occur when one sling is elongated to its maximum length (79+0.30 m). Figure E.2 shows the basic dimensions of the USF. The slings are connected at the locations marked with a blue dot. Based on those locations and basic trigonometry, the maximum X- and Y-rotations can be determined. The angles required are labelled in Figure E.3 with θ_X and θ_Y for the maximum allowable rotation around the X- and Y-axes, respectively.

$$\theta_X = \sin^{-1}(\frac{0.3}{18}) = 0.95° \tag{E.5}$$

$$\theta_Y = \sin^{-1}(\frac{0.3}{4}) = 4.3° \tag{E.6}$$

The X- and Y-rotations needed to allow for sling elongation of 0.30 m, are 0.95 degrees around the X-axis of the USF and 4.3 degrees around the Y-axis of the USF.

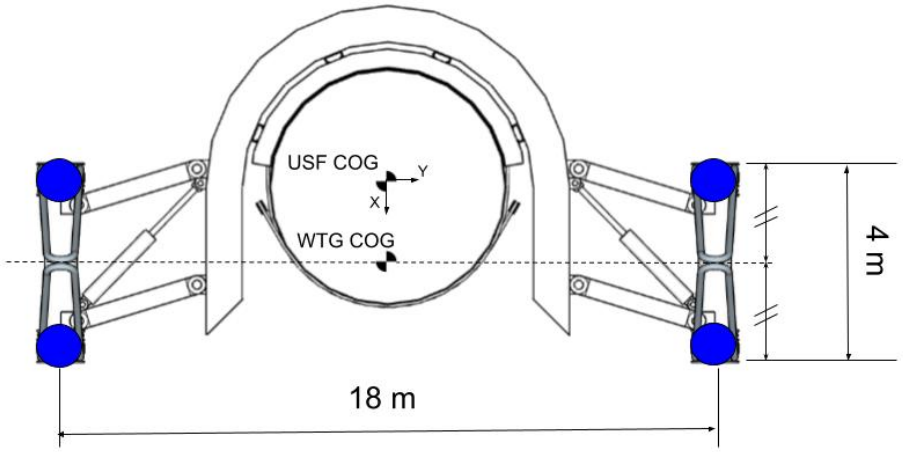

Figure E.2: Cross-section of the USF, with basic dimensions, COG of the WTG, and USF labelled. The blue dots represent the location where the slings are connected (the USF lift points).

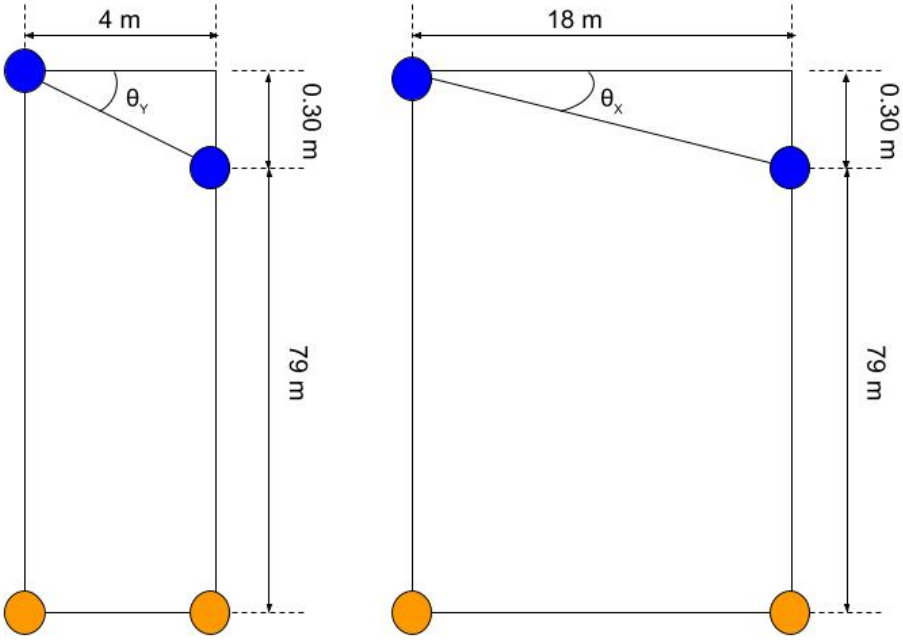

Figure E.3: Simplified diagram used for calculating the rotation along the X- and Y-axis of the USF due to sling elongation. The blue dots represent the sling connection points on the USF, and the orange dots the connection points on the LLT.

E.3. Weighted Multi-Criteria Analysis

In this section additional aspects of the weighted multi-criteria analysis are presented.

E.3.1. Assigning of weights

Table E.1 shows how the order of importance of the criteria was determined. From this, the weights could be assigned. The weight factors take values between 1 to 5, with 5 being the most important.

	Loading distribution	Practicality	Material	Moment counteraction	Adaptability	Integration	Ranking	Weight
Loading distribution							3	7
Practicality							6	2
Material							4	5
Moment counteraction							1	10
Adaptability							5	4
Integration							2	9

Table E.1: Ranking criteria and assigning weights for the weighted criteria analysis.